JOHANNES GUTENBERG UNIVERSITÄT MAINZ

Engineering Dual Dynamic Polymer Networks with Tunable Elasticity and Diffusive Permeability

Dissertation
zur Erlangung des Grades
"Doktor der Naturwissenschaften"
im Promotionsfach Chemie

am Fachbereich Chemie, Pharmazie, Geographie und Geowissenschaften
der Johannes Gutenberg-Universität Mainz

Paola Nicolella

geboren in Rom (Italien)

Mainz, 2022

Die vorliegende Dissertation wurde im Zeitraum von September 2018 bis März 2022 in der Arbeitsgruppe von Herrn Prof. Dr. [redacted] im Department Chemie der Johannes Gutenberg-Universität Mainz angefertigt.

Dekanin: Prof. Dr. [redacted]

1. Berichterstatter: Prof. Dr. [redacted]

2. Berichterstatter: PD Dr. [redacted]

Datum der mündlichen Prüfung: _____

Eigenständigkeitserklärung

Ich, Paola Nicolella, versichere, dass ich die vorliegende Arbeit selbstständig verfasst habe und keine anderen als die angegebenen schriftlichen und elektronischen Quellen sowie andere Hilfsmittel benutzt habe. Alle Ausführungen, die anderen Schriften wörtlich oder sinngemäß entnommen wurden, habe ich kenntlich gemacht.

Mainz, _____ _____

(Ort, Datum) (Unterschrift)

Acknowledgments

First of all, I would like to express all my gratitude to Prof. Dr. [redacted] for having welcomed me in his group and for his supervision during the PhD. Thank you for giving me the opportunity to challenge myself with ambitious research projects allowing me to always improve myself and grow. I would also like to thank PD Dr. [redacted] for being a reference person in this period and Prof. Dr. [redacted] for having promptly accepted to be part of the exam committee.

Grateful thanks go to all the Professors in the DoDyNet project for having shared their knowledge and precious advices with me. In particular, I would like to thank Prof. Dr. [redacted], Prof. Dr. [redacted], Dr. [redacted], and Prof. Dr. [redacted]. My recognition goes likewise to Dr. [redacted] and Dr. [redacted] for being my mentors during the industrial secondment at DSM and to [redacted] for his collaboration. A special thanks also to [redacted] for constant support with the administrative aspects of the PhD.

I gratefully acknowledge H2020-MARIE SKŁODOWSKA-CURIE ACTIONS of the European Commission's Innovative Training Networks for funding my PhD.

Special acknowledgments go to Prof. Dr. [redacted] and Dr. [redacted] for all the rich discussions and collaborations. I would like to acknowledge also Prof. Dr. [redacted] and [redacted] for successful and interesting collaboration on DQ-NMR analysis.

I would like to thank all the past and current members of the [redacted] group for the time together and the support during this PhD. In particular, [redacted] for synthesis guidance and for revision of this thesis, [redacted] for the exchange of ideas and collaboration, [redacted] for consultations and valuable advices on this thesis, [redacted] for support, and of course thanks also to [redacted], [redacted], and [redacted]. Moreover, I would like to thank all the students who collaborated with me, in particular [redacted], [redacted], [redacted], and [redacted]. A big thank you also to [redacted] for technical support with FRAP, and thanks to [redacted], [redacted], [redacted], [redacted], and [redacted], for their assistance.

Likewise, I am grateful to all the DoDyNet PhD students, and in particular to [redacted] and [redacted], for having shared this path with me and for the enjoyable moments together. In addition, I would like to thank [redacted] for her advices on rheology, [redacted] for consultation on synthesis, and [redacted] for collaboration on samples and for joining together the DoDyNet board meetings.

I would also like to thank [redacted] for sustain in the first part of this journey. A special thank you goes to [redacted] for valuable advices, encouragements, and for driving me always forward. Finally, I would like to thank my family for all their constant love and support. Thank you.

Paola

General remarks

This work comprises my PhD research project performed at the Johannes Gutenberg-Universität Mainz, under the supervision of Prof. Dr. [redacted] in the period September 2018 – March 2022 and was financially supported by funding from the H2020 Programme (MARIE SKŁODOWSKA-CURIE ACTIONS) of the European Commission's Innovative Training Networks (H2020-MSCA-ITN-2017) under DoDyNet REA Grant Agreement N°.765811.

The following document includes first a theoretical introduction to guide the reader through the main research topics with related bibliography. Afterwards, the motivation and scientific goals are delineated. Subsequentially, the core research topics are highlighted in the following chapters, which have been previously published or accepted in peer-reviewed journals:

Chapter 3:

Reversible hydrogels with switchable diffusive permeability

Paola Nicolella, Daniel Lauxen, Mostafa Ahmadi, Sebastian Seiffert

Published in: *Macromolecular Chemistry and Physics*, 2021, 222: 2100076

DOI: 10.1002/macp.202100076

Chapter 4:

Mechanical switching of a comb-like dual dynamic polymer network

Paola Nicolella and Sebastian Seiffert

Accepted in: *Journal of Rheology*, 2022, *Special Issue for Double Dynamics Polymeric Networks*

DOI: 10.1122/8.0000388

Chapter 5:

Defect-controlled softness, diffusive permeability, and mesh-topology of metallo-supramolecular hydrogels

Paola Nicolella, Martha Franziska Koziol, Lucas Löser, Kay Saalwächter, Mostafa Ahmadi, Sebastian Seiffert

Published in: *Soft Matter*, 2022, 18, 1071-1081

DOI: D1SM01456K

These papers are reproduced with permission of the journal and coauthors without modifications. The supplementary material of each paper is provided in the Appendix. Each chapter begins with a summary of the research project contextualized in the global scientific goals. In addition, the contribution of each author and acknowledgments are given. Finally, the main results are summarized in the conclusions and future perspectives are suggested.

Abstract

Hydrogels are employed in everyday life products such as contact lenses, diapers, and cosmetic creams. In addition, their aqueous composition, soft mechanics, and high permeability, makes them appealing materials in the biomedical field. However, these diverse applications have specific requirements in terms of mechanics and functionality that can often not be fulfilled by a single polymer. To overcome this limitation, multiple crosslinking types can be embedded in the same polymer matrix, thereby, realizing a dual dynamic network (DDN). However, the determination of structure–property relationships for these multi-component systems is often not straightforward and therefore, comprehensive studies are needed for a rational materials design. This thesis aims to contribute to this field with the development and methodological exploration of elasticity and permeability of a novel DDN as well as the investigation of the effect of defects on the targeted properties.

The synthesis of this novel dual dynamic network is presented in **Chapter 3.** To a model 4-arm poly(ethylene glycol) (pEG) main network, two dynamic motifs are attached. The first dynamic motif is a terpyridine ligand which is capable of forming bis-terpyridine coordination complexes with different metal ions, whereas the second dynamic motif is a linear poly(*N*-isopropylacrylamide) (pNIPAAm) chain. The combination of these dynamic motifs makes it possible to customize the properties of the DDN such as elasticity and diffusive permeability by changing the metal ion or the molar mass of the thermo-responsive polymer. In this work, it is particularly shown, by oscillatory shear rheology and fluorescence recovery after photobleaching, how the elasticity and permeability of the DDN can be switched on demand upon change of the temperature. Furthermore, this system is reversibly degradable due to the supramolecular nature of the bonds, allowing the recyclability of the DDN.

Chapter 4, constitutes a methodological follow-up study of this tunable dual dynamic network. Starting from the different building blocks that constitute the system, it is shown how the elastic properties of the hydrogel can be optimized by adjusting the molar mass of the pEG and pNIPAAm blocks and with the choice of a different metal ion. This systematic investigation constitutes an excellent toolkit for dual dynamic networks and allows to tailor the properties of these networks on demand thereby, enlarging the applicability spectrum of these multi-responsive hydrogels.

In the engineering of new materials, the role of defects cannot be underestimated as in supramolecular systems especially connectivity defects can always occur. It is thus crucial to understand their impact on the properties of hydrogels starting from model systems with the perspective of transferring the knowledge on more complex systems such as DDN. This issue is tackled in **Chapter 5**, where connectivity defects are systematically introduced into a 4-arm pEG-terpyridine model network by doping such network with different amounts of 8-arm pEG-terpyridine precursors. The origin and effect of this connectivity mismatch on the hydrogel's properties, such as elasticity and permeability, are then investigated by DQ-NMR, rheological and fluorescence recovery after photobleaching experiments.

Zusammenfassung

Hydrogele sind Polymernetzwerke, die in Wasser gequollen sind. Sie werden in einer Vielzahl verschiedener Alltagsprodukte wie z.B. Kontaktlinsen, Windeln und kosmetische Cremes eingesetzt. Zusätzlich eignen sie sich aufgrund ihres hohen Wassergehaltes, ihrer weichen mechanischen Festigkeit sowie der hohen Permeabilität auch für bio-medizinischen Anwendungen. Dieses breite Anwendungsspektrum macht es erforderlich, dass moderne Hydrogel-Plattformen verschiedene, gezielt variierbare Eigenschaften in sich vereinen. Das kann beispielweise durch doppelt-dynamische Netzwerke (DDN) realisiert werden. Für das rationale Design von DDN-basierten Materialen stellt ein detailliertes und fundamentales Verständnis ihrer Struktur–Eigenschafts–Beziehungen den Grundstein dar. Ziel dieser Arbeit ist es, durch systematische Untersuchungen an zwei supramolekularen und Stimuli-responsiven Modellsystemen, zu diesem Verständnis beizutragen.

In **Kapitel 3** wird hierfür ein neuartiges DDN vorgestellt, das auf einem 4-Arm Poly(ethylenglykol) (pEG) Modell-Netzwerk basiert, und in dem jedes pEG Kettenende mit zwei dynamischen Bindungsmotiven funktionalisiert ist. Das Erste ist ein Terpyridin-Ligand, der Komplexe mit verschiedenen Metallionen bilden kann. Das zweite ist eine lineare Poly(*N*-isopropylacrylamid) (pNIPAAm) Kette. Die Kombination dieser beiden Funktionalisierungen erlaubt eine gezielte Variation der Elastizität und Permeabilität der Hydrogele durch den Austausch des verwendeten Metallions oder durch die Änderung der molaren Masse der thermoresponsiven Seitenkette. Ein besonderer Fokus dieser Arbeit liegt auf der Untersuchung der Temperaturabhängigkeit von Permeabilität und Elastizität. Es wird außerdem gezeigt, dass dieses System recyclebar ist.

In **Kapitel 4** wird dieses System detaillierter untergesucht, indem weitere Bauteile des Systems systematisch variiert werden. Es wird gezeigt, dass die makroskopischen Eigenschaften der Hydrogele sowohl von der molaren Masse des pEG-Sterns und der pNIPAAm-Seitenketten als auch vom Metallion abhängen. Diese systematische Untersuchung stellt somit ein wertvolles Toolkit für das Design von DDNs mit gezielt einstellbaren Eigenschaften dar.

Bei der Untersuchung von Struktur–Eigenschafts–Beziehungen von Polymernetzwerken darf auch die Rolle von Defekten nicht unterschätzt werden. Trotz vielfältiger Anstrengungen ideale Modell-Netzwerke herzustellen, können immer Defekte und insbesondere Konnektivitäts-Defekte auftreten. Deswegen ist es wichtig, deren Einfluss auf die Hydrogel-Eigenschaften zu verstehen, um die Erkenntnisse auch auf komplexere Systeme, wie beispielsweise DDNs, übertragen zu können. Dieser Aspekt wird in **Kapitel 5** untersucht, indem gezielt Konnektivitäts-Defekte in ein 4-Arm pEG-Terpyridin Modell-System eingeführt werden. Dies erfolgt durch den Einbau von 8-Arm pEG-Terpyridin Polymeren. Der Einfluss der so erzeugten Konnektivitäts-Defekte auf die Elastizität und Permeabilität der Polymernetzwerke wird dann mittels Rheologie und ‚fluorescence recovery after photobleaching' untersucht.

Table of contents

1. Introduction

1.1 Hydrogels

Hydrogels are three-dimensional assemblies of crosslinked polymer chains swollen in water. [1], [2] They constitute a form of shape-stable water, where the solvent is held in place by the polymer network. [3] This composition makes hydrogels permeable and with soft mechanics, and suitable for a wide range of applications, as shown in **Figure 1**. [3]–[5] In addition, they have the capability to absorb large amount of water. This property makes them suitable for applications such as superabsorbers. For example, they are used in diapers or in agriculture for controlled fertilizer release. [6]–[8] They have also a niche in cosmetics, such as body creams. [9] In addition, they are often used as membranes and as separation media, [10]–[12] for removal of heavy metal ions from water, for water desalination, [13], [14] and lately, also in the field of wearable electronics. [15]–[19]

Figure 1. Hydrogels are water-based materials that are used in multiple application fields, from agriculture, to the biomedical field as drug delivers or substituted tissue to wound healing, to everyday applications such as contact lenses or disposable diapers. (Reproduced with permission from Ref. [5], © 2018 Springer Science Business Media)

Their permeability makes it possible for small molecules to pass through. This makes them suitable for example for contact lenses, where the exchange of oxygen with the eye is crucial. [4], [6], [20], [21] They are permeable not only for small molecules, but also for bigger diffusants such as drugs. [11], [22] In addition to drug delivery, their high water content makes hydrogels the ideal candidates for other

biomedical applications, such as tissue engineering, wound healing, and 3D support for cell growth. [4], [20], [23], [24], [25]

In the context of tissue engineering, they can be used to reproduce natural tissues, such as cartilage, muscles, or organs such as the liver. [4] However, such applications require that synthetic hydrogels resemble the mechanics and functionality of the natural tissues. [24], [26] This achievement still represents a challenge for materials scientists, as the mechanical properties of natural tissues vary from a few Pa to several gPa, as summarized in **Figure 2**. [26]

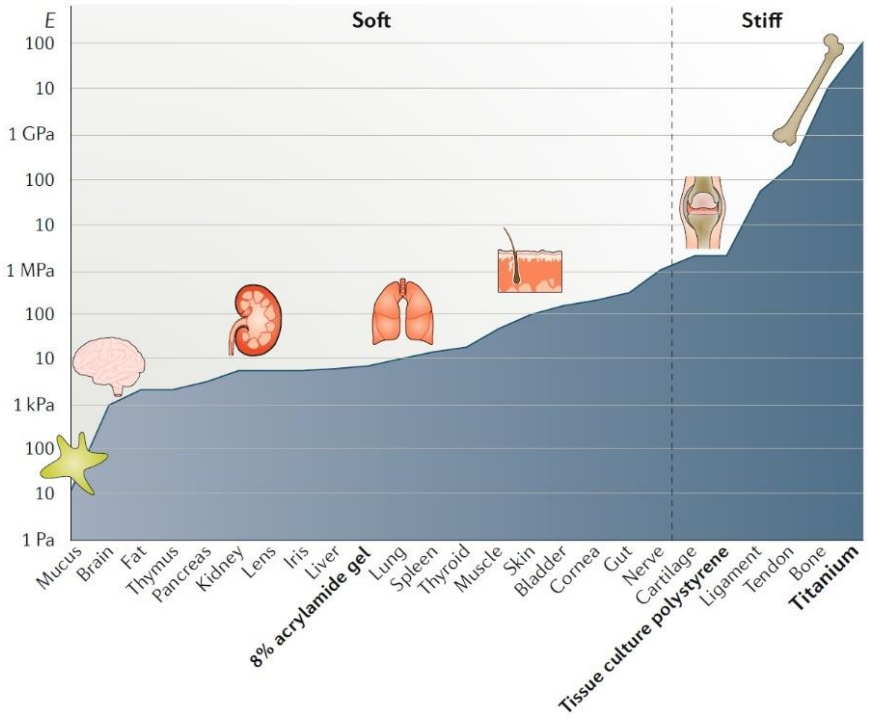

Figure 2. The mechanical properties of the natural tissues vary from a few Pa to GPa. While to imitate stiffer structures like bones, hard scaffolds are used, to imitate softer tissues, hydrogels are the preferred candidates. **(**Reproduced with permission from Ref. [26] © 2020, Springer Nature Limited)

While in tissue engineering, the mechanics of the hydrogel plays a crucial role, in other applications such as drug delivery or contact lenses, the permeability and/or release of small diffusants is of outmost importance. [27] Moreover, it would be useful that the hydrogel would degrade after fulfilling its use. In addition to permeability, in separation techniques it would be desirable that this property would be tunable. Instead, for wound healing applications it would constitute an advantage if the respective hydrogel would be easily processable making it possible to be injected or sprayed.

Therefore, every application has specific requirements and the properties of new hydrogels must be tailored to these. In the following chapters we will see how the structure of hydrogels can be changed in order to have properties like toughness, degradability, and stimuli-responsiveness. In addition, we will see how to combine two properties in one hydrogel. Finally, we will investigate fundamental properties of hydrogels, such as elasticity and permeability, and their characterization.

1.2 Double networks

The soft mechanics of hydrogels constitutes an advantage for some applications, however it is considered a limit for applications that require toughness. [28] The research for tougher hydrogels to expand their applicability range represents still a challenge for materials scientists. However, in the last few years numerous steps forward have been made in this direction.

In 2003 for example, Gong and her group introduced a new tough hydrogel composed of two polymer networks interpenetrated into each other, namely poly(2-acrylamide-2-methylpropane sulfonic acid) (PAMPS) and polyacrylamide (PAM). Even if interpenetrated networks had been used before, the group of Gong was the first to investigate the toughness. [29], [30] Gong showed that the fracture stress of their interpenetrated networks was 20 times higher than the one of the two separate networks. [31] The concept behind interpenetrated double networks is that one densely crosslinked network is interpenetrated with a loosely crosslinked one. [31] Upon application of stress, the first network breaks and the stress is distributed on the second network. [31] Few years after the development of this double network, Brown and Tanaka suggested the dissipation mechanism behind: upon deformation, the highly crosslinked network breaks into clusters, as it can be seen in **Figure 3 (a)**. [1], [32], [33] These clusters not only dissipate energy, but also act as crosslinks for the second loosely crosslinked network. [1], [32], [33]

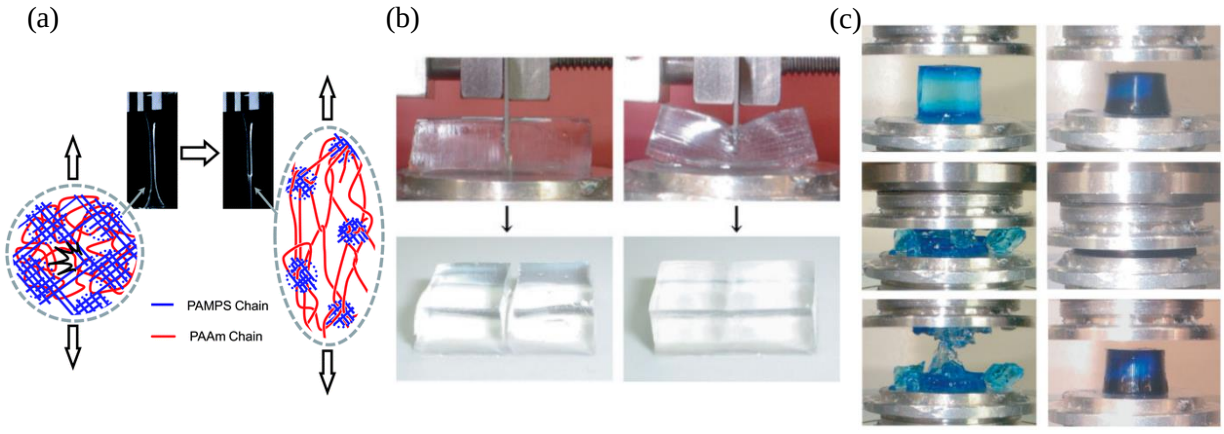

Figure 3. Tough double interpenetrating networks realized by Gong and her group. (a) A highly crosslinked PAMPS network is interpenetrated in a loosely crosslinked PAM network. Upon deformation the densely crosslinked network breaks, thereby releasing energy. (Reproduced from Ref. [34] with permission from the Royal Society of Chemistry) (b) The single PAMPS network withstand a stress of 0.2 MPa (left), whereas the PAMPS/PAM double network withstand a stress of 25 MPa (right). (Reproduced from Ref. [31] with permission of the publishers, © 2003 WILEY-VCH) (c) The single PAMPS network sustains a compression of 0.4 MPa (left), whereas the PAMPS/PAM double network sustain a compression of 17.2 MPa (right). (Reproduced from Ref. [31] with permission of the publishers, © 2003 WILEY-VCH)

Single networks are lacking this dissipation mechanism and therefore, they show weak mechanical properties in comparison. [35] In **Figure 3**, the structure of this double network and the consequences on the properties, such as resistance to cutting and compression are displayed in comparison to a single network.

On this path, Grunlan *et al*. recently developed a cartilage-like double network composed of PAMPS and poly(*N*-isopropylacrylamide)-acrylamide copolymer. Their double network showed a compressive strength of 25 MPa, which is 50 times higher than the one of a single network. [36]

In literature there are numerous other examples of engineered double networks [8], [36]–[46], however, even if these systems show all promising mechanical results, the toughness is lost after the deformation, as the breakage of the sacrificial network is irreversible. [1] Therefore, there is an increasing strategy to replace the highly crosslinked covalent network with a non-covalent network, thereby realizing a hybrid double network. [1]

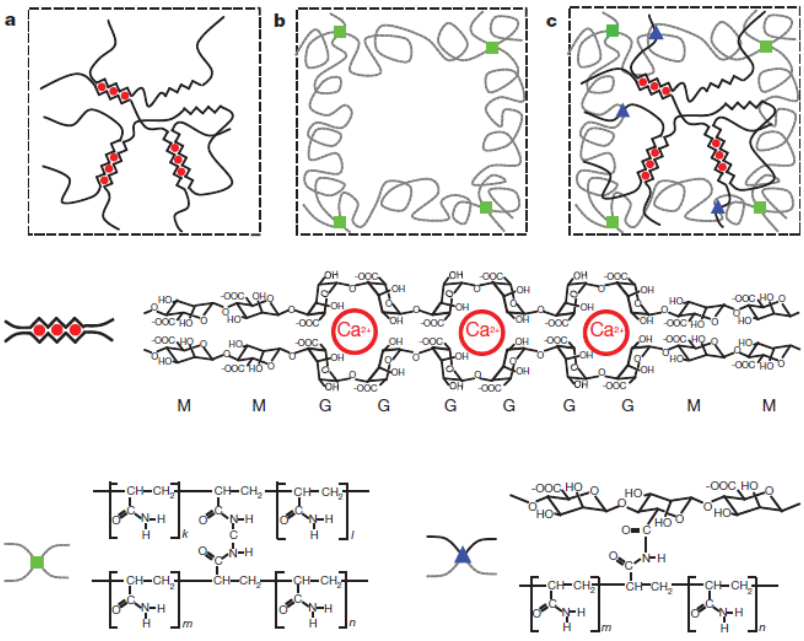

Figure 4. A hybrid double network can be realized combining one covalent and one non-covalent network. Sun *et al*. used calcium-alginate complexes as binding motif of the sacrificial non-covalent network (a) and polyacrylamide as covalent network (b). Their combination (c) is achieved *via* the binding between the amine groups of the polyacrylamide and the carboxyl groups of the alginate. (Reproduced with permission from Ref. [47] © 2012, Nature Publishing Group)

For example, Sun *et al*. realized this strategy by employing a double network (shown in **Figure 4**) with alginate and polyacrylamide, where the sacrificial non-covalent motif is composed of calcium-alginate complexes. [1], [47]

Nevertheless, covalent crosslinked networks have the disadvantage that they cannot be easily processed and recycled. This limitation can be overcome with reversible bonds.

1.3 Supramolecular interactions

Covalent bonds are strong and permanent on long timescales. [48] Therefore, they can give rise to hydrogels with high toughness. However, covalent polymer networks have the remarkable disadvantage that once that the bond is broken, the breakage is irreversible. In addition, their covalent nature sets limits to recyclability and self-healing.

An improvement in such direction would be the use of supramolecular polymer networks held together through non-covalent interactions. [49] These can be based on metal-ligand complexes, hydrogen bonding, van der Waals forces, and others, as represented in **Figure 5** . [49]

Supramolecular interactions offer several advantages such as self-healing, [1], [50]–[59] recyclability, [54], [60]–[62] and easy processability. [54], [60], [63], [64] The extent of it depends on the dynamics and the strength of the reversible bonds. [65]

Supramolecular chemistry is a discipline that developed between the late 1960s and early 1970s, and in 1987, Donald J. Cram, Jean-Marie Lehn, and Charles J. Pedersen won the Nobel Prize in Chemistry for their contribution to the field. [66] This discipline was defined by Jean-Marie Lehn as "the chemistry of molecular assemblies and the intermolecular bond" and often it is referred to as "the chemistry of non-covalent bond". [67]

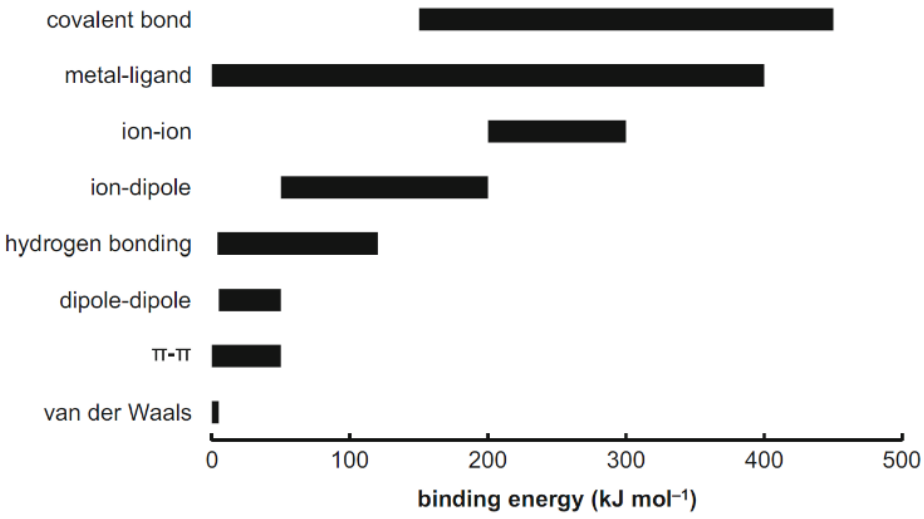

Figure 5. Covalent and non-covalent interactions summarized with the relative binding energy. (Reproduced with permission from Ref. [49])

Among the non-covalent interactions, the metal-ligand complexation is the most interesting one, as it has the largest tunability for the strength, reaching values comparable to covalent bonds. In particular, one of the most used ligands is terpyridine. [49]

Terpyridine was obtained for the first time by Morgan and Burstall in the ’30s. [68] However, the terpyridine-fever exploded only later in the ‘90s, as we can see from the increasing number of publications related to this topic in **Figure 6 a)**. [69]

Terpyridine is a tridentate ligand (as shown in **Figure 6 b)**) [69] that has gained high attention in the last years due to its capability to bind a high number of metals in bis-terpyridine complexes. [49], [68], [70] This allows a high tunability regarding the bond strength [70] and consequently the structure and properties. In addition, these binding motifs can be completely dissociated and reformed again upon change of the pH, as an acid environment protonates the nitrogen atoms of the terpyridine thereby, decreasing the association strength of the ligand. Deprotonation of the ligand in a basic environment restores the metallo-supramolecular connection. [3]

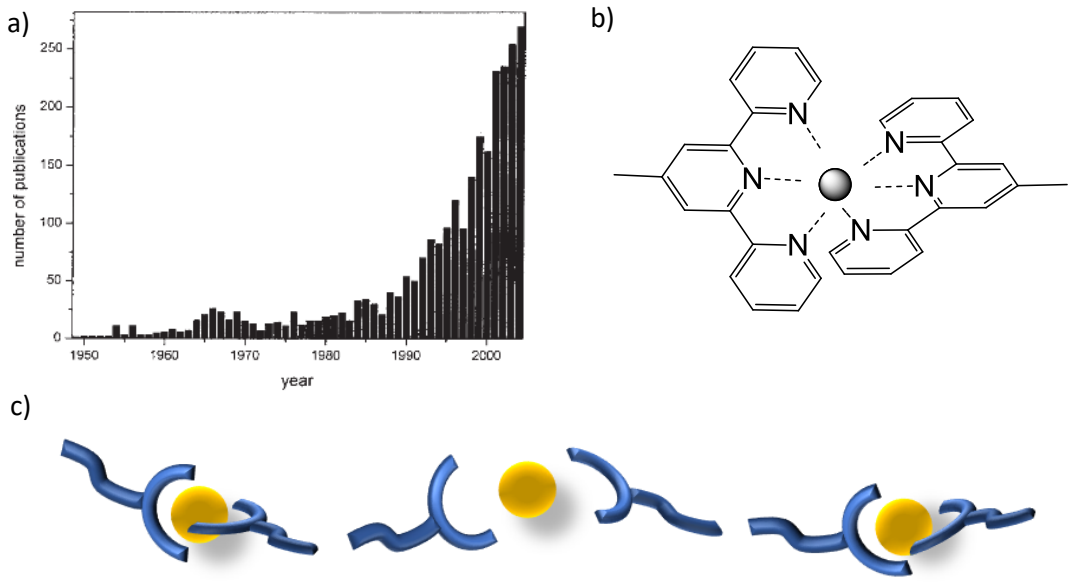

Figure 6. Terpyridine: the increasing interest over the years as demonstrated with the number of publications (a) (Reproduced with permission from Ref. [69] © 2006 Wiley-VCH), structure (b), and reversibility (c).

In the last decades, Schubert *et al*. became pioneers in this field, as they extensively treated synthesis, properties, and applications of terpyridine-metallo-supramolecular polymers. [70] They were also the first to attach a terpyridine moiety to poly(ethylene glycol), [71] which is a widely used hydrophilic polymer. In addition, terpyridine complexes show interesting redox and photophysical properties [69], [72] that can e.g. be used for energy storage applications. [73]

1.4 Stimuli-responsive polymers

For applications such as membranes, separations or controlled release, hydrogels with fixed properties are often not enough and it would be highly desirable to control their properties of diffusion and release on demand. This can be achieved with the incorporation of stimuli-responsive polymers. [74]

Stimuli-responsive or smart polymers are a new class of materials that respond to a stimulus and change their physical and/or chemical status accordingly. [75] Stimuli can be physical, like for example temperature, light, magnetic/electric field, and mechanical force, chemical such as pH, and redox potential or biochemical with the presence of specific bio-molecules, as shown in **Figure 7**. [10], [72], [75]–[86]

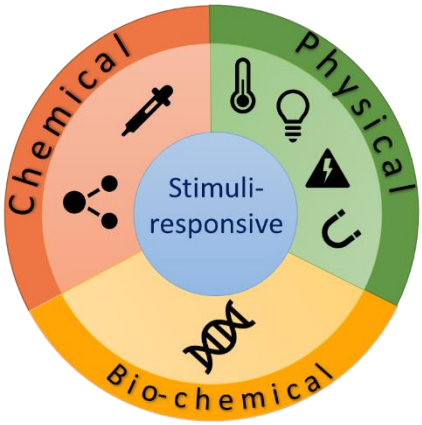

Figure 7. The stimuli can be of different nature: chemical, physical, and bio-chemical.

Stimuli-responsiveness is widely used in nature. For example, all membranes present in our body are stimuli-responsive. [74] Thermo-responsive polymers are often used for drug-delivery, sensors, and thermal separation. [87]–[96] For example, for drug delivery it might be necessary that the drug is first protected and then released in a certain area, at a precise time with a controlled concentration. [4], [88] This can occur when the signal to release the drug is given by an external stimulus. [97] This strategy is often achieved with thermo-responsive polymers.

The majority of thermo-responsive polymers possess a lower critical solution temperature (LCST) whereas only a few possess an upper critical solution temperature (UCST), or both. [98] These critical temperatures delimitate the coil to globule transition and consequent phase-separation of the polymer from the surrounding medium. This transition and consequent decrease in solubility occurs for temperatures above the LCST and below the UCST. [98] In addition, these critical temperatures can occur in any solvent, however, water is the most used one due to its relevance for the intended biomedical applications. [88]

Among the thermo-responsive polymers, poly(*N*-isopropylacrylamide) (pNIPAAm) is the most used one, as its LCST is around 32–33 °C in aqueous medium, thereby making it applicable in the biomedical field. [88], [99] In addition, the LCST of this polymer is independent of concentration and molecular weight. [88] Nevertheless, it can still be tuned by changing the hydrophilic/hydrophobic polymer ratio and water/organic solvent mixture. [99]

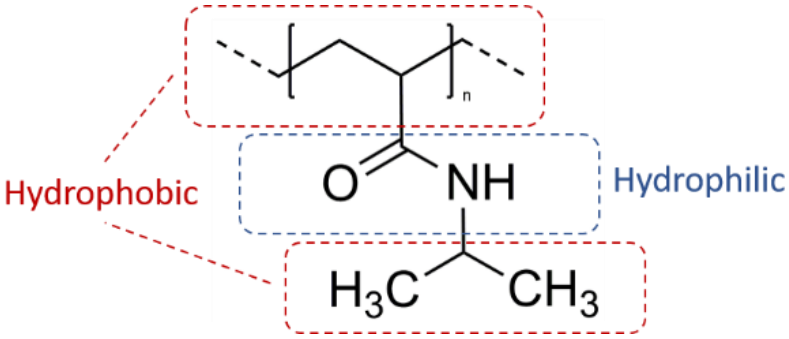

Figure 8. The structure of poly(*N*-isopropylacrylamide) comprises both hydrophilic and hydrophobic groups.

As it can be seen from **Figure 8**, pNIPAAm is an amphiphilic polymer comprised by hydrophobic and hydrophilic groups. [97] Below its LCST it has a random coil configuration where the hydrophilic groups bind through hydrogen bridges with the surrounding aqueous medium. [97] With increasing temperature, the hydrogen bonds between the hydrophilic groups and water become weaker due to increased kinetic energy and are therefore outbalanced by the hydrophobic interactions. [96] When the temperature is raised above the LCST, the hydrophobic interactions predominate and the water bridges break. [100] The polymer phase-separates and its physical configuration changes from a random coil to a globule. [97], [99], [100]

The fact that the LCST of pNIPAAm in water is near the physiological temperature makes this polymer useful for controlled release applications. [13] For example, in combination with pEG, pNIPAAm is used for injectable thermo-responsive hydrogels that can be used for delivering anti-cancer drugs. [87] In addition, pNIPAAm is often used for delivering calcitonin and insulin. They are anchored to the polymer which protects them in the stomach and release them in the intestine. [13]

1.5 Dual dynamic networks

The wide spectrum of binding motifs offers materials scientists great choice for the development of new materials. In addition, as we have seen, when stimuli-responsive motifs are incorporated, the materials' properties can be tuned on demand. To increase this tunability even further and to achieve materials with targeted properties, it is possible to combine two or more different binding motifs, thereby realizing a dual dynamic network (DDN). [62] This strategy can be achieved with two interpenetrated networks baring one motif each or by incorporating two types of bonds into one main network.

When the dual network includes one covalent and one supramolecular motif, then it is called hybrid. [101] Hébraud and co-workers have developed such hybrid dual network and their hydrogels showed mechanical properties superior to the supramolecular or chemical network alone, as it can be seen in **Figure 9**. [102]

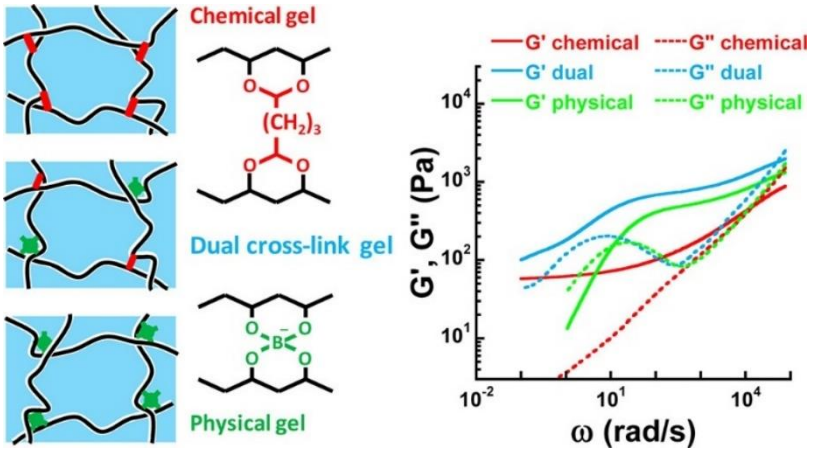

Figure 9. The combination of a chemical and a physical bond in one main network results in a network having mechanical properties that are superior to the ones of the two networks (one physical and one covalent) separately. (Reproduced from Ref. [102] with permission © 2013 American Chemical Society)

Even if hybrid dual/double networks offer more tunability over conventional single or double covalent networks, the presence of the covalent bond still limits its recoverability. On the contrary, when both binding motifs are supramolecular, the network has the great advantage to be fully degradable laying the ground for recyclability.

An exemplary dual dynamic network has been developed by Zheng *et al*. using agar and hydrophobically associated polyacrylamide. In this case, the combination of hydrogen bonds and hydrophobic interactions yielded a gel with rapid self-healing and high toughness. [103]

By incorporating two dynamic bonds in a common *cis*-1,4-polyisoprene network, Zhang and co-workers realized a dual dynamic network that showed high toughness, fast self-healing, and that could recover its mechanical properties of weak and strong bonds. These properties were achieved thanks to the combination of hydrogen bonds and Zn-triazole coordination bonds, as shown in **Figure 10** . [104]

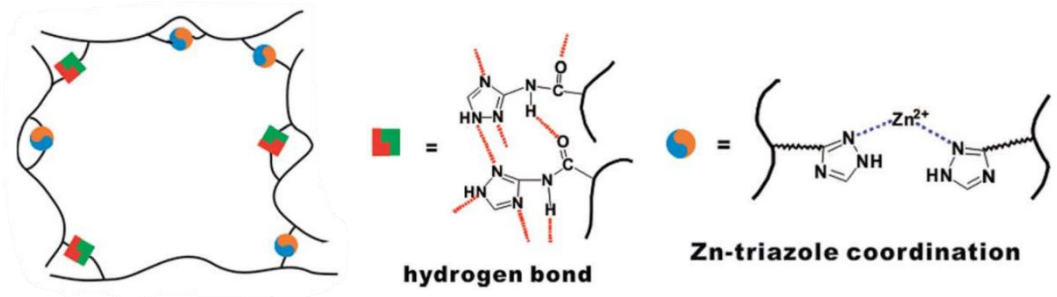

Figure 10. Zhang and co-workers developed a dual dynamic network comprising two supramolecular motifs combined in one main network, namely hydrogen bonding and Zn-triazole coordination. (Adapted and reproduced from Ref. [104] with permission from the Royal Society of Chemistry)

Another example of multi-responsive hydrogel is provided by the Seiffert group. The authors have designed a hydrogel based on linear polyglycerol that bears three dynamic motifs: two motifs can potentially bind with each other through hydrogen bonding (diaminotriazine and cyanurate), whereas the third motif (terpyridine) can potentially bind with an external metal ion through metal-complexation. [105] These two binding types can be activated and deactivated orthogonally and independently from each other or together. [105]

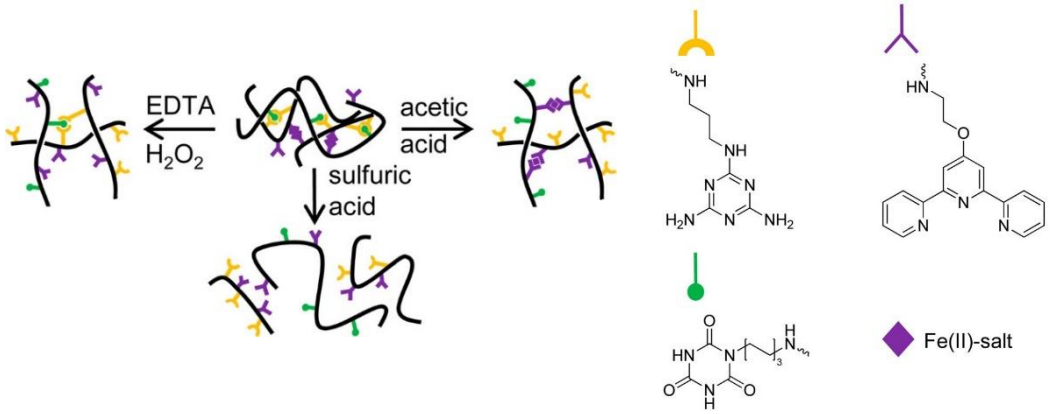

Figure 11. Seiffert *et al*. developed a multi-responsive supramolecular hydrogel where the binding motifs can be activated and deactivated orthogonally. (Adapted and reprinted with permission from Ref. [105] © 2014 American Chemical Society)

Multi dynamic networks are a fascinating and still developing field of research that tries to encounter for the high demand of having ‘multitask’ materials.

1.6 Defects in polymer networks

We have seen that a polymer network can be crosslinked with covalent or supramolecular crosslinks. [106], [107] The crosslinks, however, are often not homogenously distributed within the network. In covalent networks this spatial inhomogeneity originates from uncontrolled crosslinking of the polymer chains, whereas in supramolecular networks it derives from clustering or stacking of the supramolecular crosslinks. [50]

The strands between crosslinks are called meshes and their length determines the mesh-size ξ which is in the order of 1-10 nm. Additionally, the spatial distribution of the crosslinking density Ξ determines spatial heterogeneities on length scales between of 10–100 nm, as schematically shown in **Figure 12**. [106]

On top of that, there are other types of defects that can be encountered in polymer networks. When a building block such as an atom or molecule is locally replaced, then we encounter a doping defect. When the connectivity between building blocks is modified, then the polymer network will have connectivity defects. Finally, when the symmetry is perturbated locally without chemical modification, then the defects are called topological. [108]

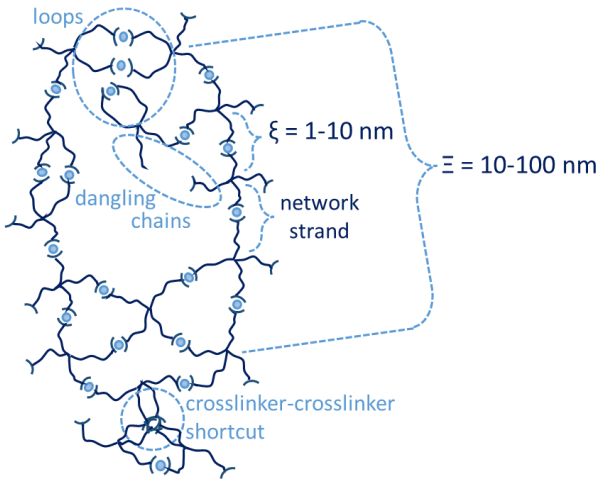

Figure 12. Topological defects that can occur in polymer networks are loops, dangling chains and crosslinker-crosslinker shortcuts. (Reproduced from Ref. [109] with permission from the Royal Society of Chemistry)

These topological defects visualized in **Figure 12** are loops, dangling chains and crosslinker-crosslinker shortcuts. [106] In supramolecular chemistry, a loop is formed when a polymer chain does form a link with itself or another chain of the same polymer. Alternatively, a loop (or higher order loops) can form when two polymer binds through multiple chains, instead of binding with other polymers (meaning that two or more chains of the same polymer binds with two or more chains of another same polymer). A dangling chain has an end that is not crosslinked. This can occur either as temporary non-connected chain, or as a chain that cannot bind at all due to a missing binding motif. Finally, a crosslinker-

crosslinker shortcut occurs when two crosslinks or the same polymer or multiple polymers bind through other interactions than the foreseen ones. In contrast, in covalent polymers, crosslinker-crosslinker shortcuts occur mainly when two crosslinks are close together. [106] In addition, these defects get more pronounced when the polymer network is swollen in a medium, as it can be seen from **Figure 13**. [106], [108]

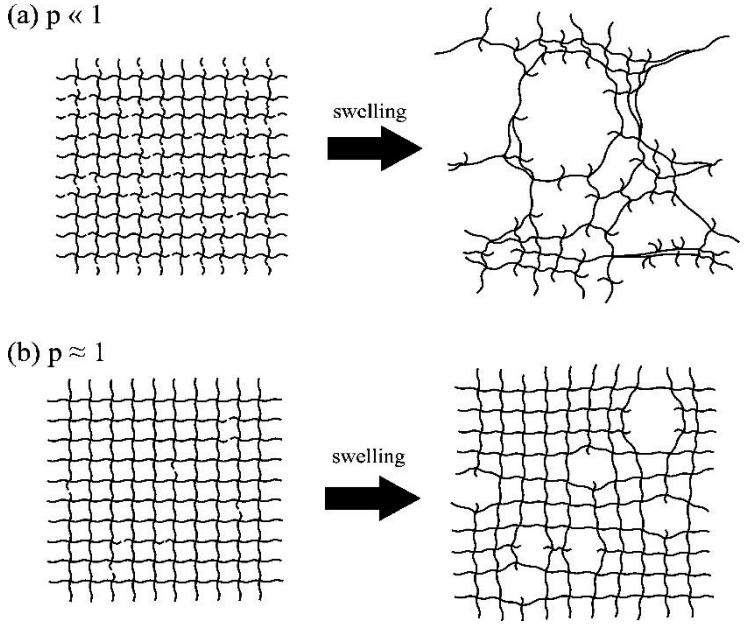

Figure 13. Defects gets more pronounced when the polymer network swells in a solvent. Considering different reaction probability p, the network with higher connectivity defects ($p << 1$) (a) shows more inhomogeneities in the swollen state than a network with less connectivity defects ($p \approx 1$) (b). (Reprinted with permission from Ref. [110] © 2014 American Chemical Society)

To obtain tough networks, not only a dissipation mechanism, but also homogeneity is needed. [29] For example, the presence of defects can initiate a crack and/or increase its propagation speed. [29] Even if homogeneous model structures have been achieved in both covalent [111] as supramolecular [50] networks, natural defects can always occur. [112] Therefore, it is crucial to be conscious of their effects on the properties. In addition, once these effects are known, the materials scientist can even exploit them and use them as additional function givers. Since the different types of defects occur on different length scales, it is necessary to characterize them with multiple techniques. To determine topological defects multiple quantum NMR can be used, whereas scattering methods can be used to characterize the mesh-size and spatial heterogeneities. [106]

The study of defects in soft polymer networks is crucial due to the multiple applications of such materials in our everyday life, from drugs, to detergents and cosmetics, to adhesives and rubbers. [108] However, while there are several studies concerning classical covalent networks, in the supramolecular field there is still a lot to explore.

1.7 Mechanics and dynamics of supramolecular polymer networks

Once that the structure has been determined, and the presence of defects assessed, the following step is the investigation of the properties. Two peculiar properties of polymer networks are viscoelasticity and diffusive permeability. These can be determined with multiple techniques, [113]–[115] but relevant methods for this thesis are respectively oscillatory shear rheology and fluorescence recovery after photobleaching.

Viscoelasticity is a characteristic property of polymer systems and one of the most important reason why polymers are so interesting. [100] Polymers can flow like liquids but can also behave like elastic solids. [100] Solids are characterized by an elastic behavior that can be expressed by Hooke's law

$$\sigma = E \cdot \varepsilon \tag{1}$$

where σ is the applied stress, ε is the strain or deformation, and E is the Young's or elastic modulus. [100] On the contrary, liquids are viscous and follow Newton's law

$$\sigma = \eta \cdot \frac{d\varepsilon}{dt} = \dot{\varepsilon} \tag{2}$$

where η is the viscosity. [100] However, polymer materials show a behavior in between these two extremes and are thus called viscoelastic. [100], [116]

If the pure elastic behavior can be represented with a spring and the pure viscous behavior can be represented with a dashpot, the viscoelasticity can be represented by a combination of a spring and a dashpot. For viscoelastic liquids, these two elements are put in series and the material follows a Maxwell model, whereas for viscoelastic solids, these two elements are put in parallel and the material follows the Kelvin-Voigt model. [117] These two models are schematized in **Figure 14**.

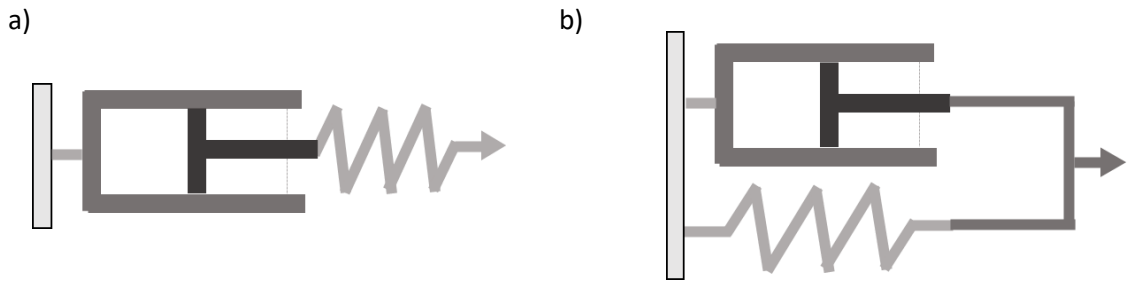

Figure 14. The Maxwell model a) comprises a dashpot and a spring in series, whereas the Kelvin-Voigt model b) comprises these elements in parallel.

In the Maxwell model, where spring and dashpot are in series, the spring firstly shows a deformation upon the application of stress and then, when it is at its maximum extension, the dashpot slowly follows. However, when the solicitation is removed, the spring returns back at its original state, whereas the dashpot stays in the deformed position. [117]

In the Kelvin-Voigt model, the spring and the dashpot are connected in parallel through a solid frame. When a stress is applied, they both deform accordingly, the spring however, is slowed down by the dashpot. When the stress is removed, they go back together to the starting position, but also in this case the dashpot slows down the spring. [117] So, the main difference between these two models is that in the viscoelastic solid the material will recover its original shape completely, but slowly, whereas a viscoelastic liquid will not.

For rational materials design of polymeric systems, the knowledge of the viscoelasticity is fundamental. This mechanical property can be measured and quantified through rheology. [100]

Oscillatory shear rheology is a characterization technique where the sample is placed in between two plates, one is fixed and the other oscillates at a given frequency and shear amplitude. Viscoelasticity can be quantified through the elastic (or storage) and loss moduli. The storage G' and the loss modulus G'', as the name suggests, respectively account for the energy that it is stored or lost during shear. Whereas the ratio $G''/G' = tan\,\delta$ can give an indication on the viscous or elastic portion of the material. [118]

A typical viscoelastic spectrum of a supramolecular gel is shown in **Figure 15**. The elastic modulus is descending from the highest to the lowest frequency, whereas the loss modulus expresses a maximum in the same frequency range. Polymers that show an ideal Maxwell behavior possess a characteristic scaling law relationship with a characteristic slope at low frequency for the elastic and loss modulus, being respectively 2 and 1. [119]

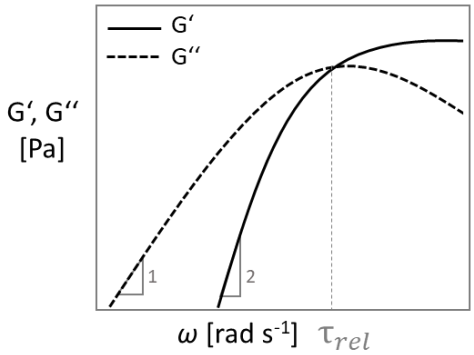

Figure 15. Viscoelastic spectrum that follows the Maxwell model (both axes are in logarithmic scale).

According to the Maxwell model, elastic and loss modulus can be mathematically described by the following expressions

$$G'(\omega) = G_P^{\circ} \frac{{\tau_{rel}}^2 \omega^2}{1 + {\tau_{rel}}^2 \omega^2} \quad (3)$$

and

$$G''(\omega) = G_P^{\circ} \frac{\tau_{rel}\, \omega}{1 + {\tau_{rel}}^2 \omega^2} \quad (4)$$

where G_P° indicates the plateau modulus, τ_{rel} is the relaxation time, and ω is the operational frequency. [120], [121]

The plateau modulus G_P° corresponds to the maximum elastic modulus at the highest frequency. Its value can be estimated theoretically with the affine or phantom model. In the affine model, the plateau modulus is given by

$$G_P^{\circ} = \nu RT \quad (5)$$

where ν is the number of network strands per volume, R the universal gas constant, and T the absolute temperature. The number of network strands per volume can be calculated through the molar concentration of the polymer $\nu = \frac{f\mu}{2}$ where f is the functionality of the polymer and μ is the density of the network crosslinks. [112] In the phantom model, there is a pre-factor and the plateau modulus is consequently given by

$$G_P^{\circ} = \left(1 - {}^{2}/_{f}\right) \nu RT \quad (6)$$

These models are based on the contribution of elastically active chains. [106] However, often the experimental value differs from the theoretical one due to the occurrence of defects, such as loops or dangling chains. [106] For example, a 4-arm polymer precursor is only elastically active when three or four arms are connected to the network. [122] When only two arms are connected, the polymer can form a loop or be a bridging chain, whereas when only one arm is connected, the whole polymer acts as a dangling end. [122] This can be visually seen in **Figure 16**. The presence of these or other defects will therefore cause a deviation of the plateau modulus from the predicted theoretical value. [106]

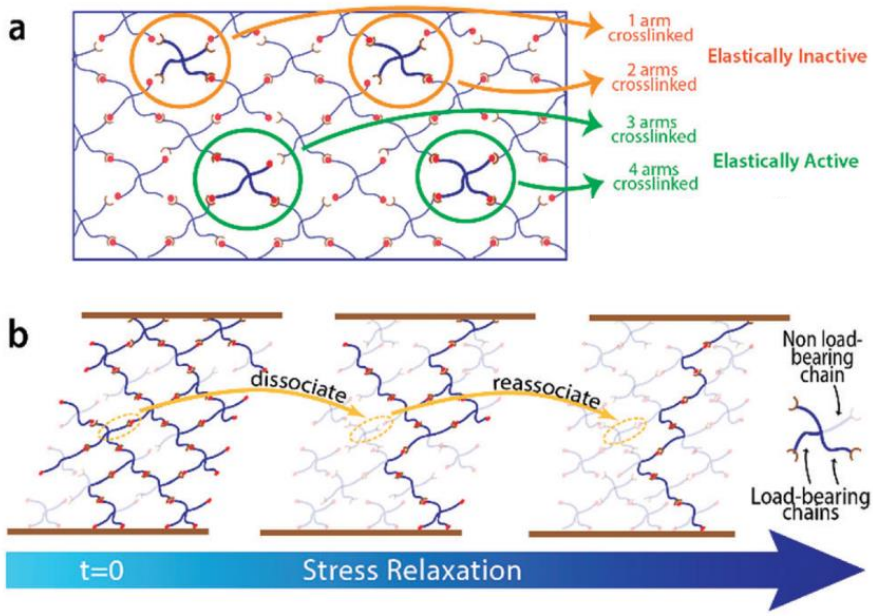

Figure 16. a) In a polymer network not every chain is elastically active. In a 4-arm polymer, only chains that are connected to 3 or 4 chains of different polymers will be elastically active and will therefore be able to store elastic energy. b) Microscopic picture of the behavior of a 4-arm supramolecular polymer during shear. (Reproduced with adaption from Ref. [122] with permission from the American Chemical Society)

In addition, from the elastic modulus and the rheological spectrum, other structural parameters can be extrapolated. It is for example possible to calculate the average mesh-size of the polymer network from the elastic modulus as

$$\xi = \left(\frac{RT}{G_P^{\circ} N_A}\right)^{1/3} \tag{7}$$

with R the universal gas constant, T the absolute temperature, G_P° the measured plateau modulus, and N_A the Avogadro constant.

Oscillatory shear rheology is a useful technique not only for studying the mechanics, but also to unravel the dynamics of supramolecular polymer networks. While the elastic modulus depends on the concentration of crosslinks that are connected, the dissociation time of the connections will determine the relaxation time of the network. [122] The relaxation time can be extracted from the viscoelastic spectrum as the inverse of the crossover frequency of G' and G'', as from the Maxwell model $G'/G'' = \omega\tau$ and $G''/G' = tan\,\delta$. [120], [123]–[125] When $G'' = G'$ and therefore, $tan\,\delta = 1$, then $\tau_{rel} = 1/\omega$. This relaxation time is an indication of the lifetime of the bonds. However, the bonds often can detach and re-attach several times before breaking and moving to another partner. This behavior is denominated bond lifetime renormalization. [126] The exchange of partners can occur via two different mechanisms. In the first case, it can be a simultaneous mechanism where the attachment of a sticker

occurs at the same time as the detachment of another sticker. In the second case, the attachment can follow only after a sticker has detached and therefore is available for a new binding. [126] The availability of a free partner plays a crucial role especially when the overall concentration of the stickers is low due to high association strength of the stickers, a low polymer concentration or high strand length between the individual crosslinks. [126]

In supramolecular polymer networks, the mechanics is strictly related to the dynamics of the supramolecular motifs. Golkaram and Loos individuated four main parameters that influence the elastic behavior of supramolecular polymers, being the number of associations of the stickers, phase separation, the strength of associations, and the position of the stickers. [126]

The number of associations of the stickers depends on the type of sticker and can be tuned through the applied crosslinking motif. For example, a linear polymer that bears ligands at its ends, can form a linear viscous polymer or a percolated network if it forms complexes with a bivalent or trivalent metal respectively. In addition, the number of associations can be tuned by choosing different metal/ligand ratios and pH. [126]

In case of a (micro) phase-separation inside the sample, the relaxation mechanism is different from the one in systems with mainly binary associations. First of all, the dissociation of a single chain or sticker from a cluster requires a significant energy contribution and is therefore energetically not favorable. [126] Therefore, it is more probable that clusters bind/unbind collectively. In the case that two or more smaller clusters meet and form a bigger cluster, they will soon after split again into smaller clusters because small clusters are entropically more favorable. [126] For these reasons, the association time of clusters is less defined and commonly longer than then lifetime of binary associations. [126]

The strength and lifetime of associations in supramolecular polymers can be easily tuned and this is one of the appealing aspects of using this type of chemistry. These parameters can be firstly altered by choosing different motifs from a broad range of possibilities. It is further possible to influence the strength and lifetime with external parameters such as solvent, pH or temperature. Seiffert *et al.* showed for example, how the mechanics of metallo-supramolecular polymer networks can be tuned by the use of solvents with different polarities. [127] At the same time, the properties of metallo-supramolecular complexes change when the oxidation state of the metal changes. For example, polymer networks based on terpyridine-Fe(II) complexes show strong, covalent-like behavior, whereas an oxidation of the central cation to Fe(III) leads to the occurrence of flow at long time-scales. [3]

Lastly, the dynamic of supramolecular polymers can be tuned via the position of the stickers. [126] These can be positioned for example in the main chain, as side or end groups. [126]

1.8 Diffusion mechanisms in polymer networks

In addition to their soft mechanics, another peculiar property of hydrogels is their permeability that allows small diffusants to move inside the network meshes. For some applications, such as contact lenses or drug delivery, the determination and control of the diffusive mechanisms inside the hydrogels plays a crucial role. [27]

Diffusion coefficients can be determined with methods such as light scattering and fluorescence microscopy techniques, where the latter has the advantage, that it can also be used on phase-separated or colored systems, thereby enlarging the applicability range. One of the most common fluorescence microscopy techniques to study the mobility of the diffusants is 'fluorescence recovery after photobleaching' (FRAP). This fluorescence microscopy technique was introduced by Peters and further developed by Axelrod and respective co-workers in the '70s. [128], [129] When fluorophores are excited they emit light, however, this ability can be irreversibly switched off when they are over-excited. [129] Photobleaching is the phenomenon where fluorophores lose their ability to be excited and emit light. [129] For a FRAP measurement, fluorescent tracers are introduced into the hydrogel and then the sample is impinged by a high intensity laser within a defined area. [129] This interaction will bleach the fluorophores on the path of the laser, producing a dark spot in the sample, as visible in **Figure 17 (b)**. With time, the irreversibly photobleached tracers will diffuse out of the bleached spot and at the same time non-bleached ones will diffuse inside (**Figure 17 (c-d)**). This recovery of the initial fluorescence intensity is recorded by taking pictures of the bleached area at regular time intervals for example with a confocal laser scanning microscope. [128]

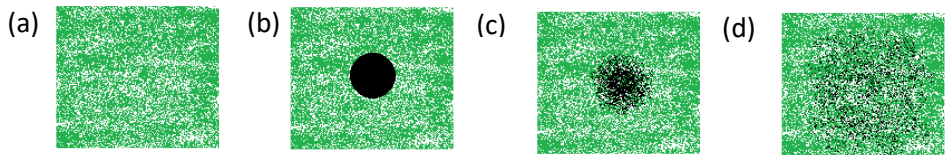

Figure 17. (a) Pre-bleach situation. (b) Bleaching spot produced by a high intensity laser. (c-d) Post-bleach diffusion: after being bleached, the fluorescent tracers diffuse out of the bleaching spot, whereas non-bleached ones diffuse inside.

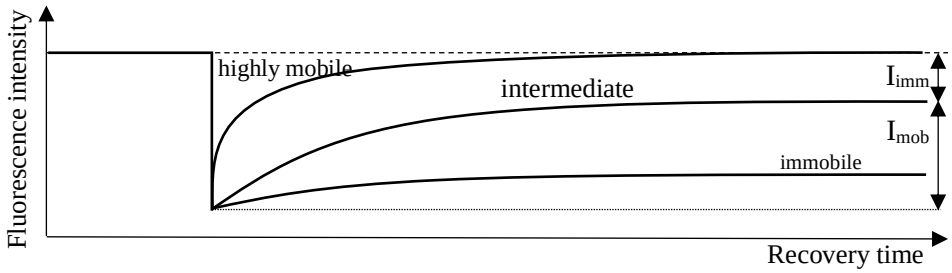

Figure 18. The way the fluorescent intensity recovers in the bleached spot over time gives an indication of the mobility of the tracers. The steeper the slope, the faster the recovery, and the faster the diffusion. The difference between the initial intensity and the recovered portion I_{imm}, gives an indication of the immobile fraction present in the sample, whereas the difference between the recovered intensity and the one right after the bleaching I_{mob}, gives an indication of the mobile fraction in the sample.

After the bleaching, the change in the fluorescence intensity is followed over time with lower laser power. The way the fluorescent intensity is recovered in the bleached spot over time, gives an indication of the mobility, and therefore, diffusion, of the fluorescent tracers inside the polymer network, as it can be seen graphically in **Figure 18**.

The diffusion coefficient can be calculated by fitting the recovery curve with different models. [130] However, this method assumes a pure 2D diffusion, a Gaussian profile of the intensity of the laser beam, the bleaching of fluorophores occurring as a first-order reaction, and that the time for recovery is longer than the bleaching time. [128], [131]

Other analysis methods have been used, which e.g. consider the spatial information of the fluorescence intensity or which rely on performing numerical post-bleach simulations. [132] For example, one of the methods that has been developed, takes into account an arbitrary geometry for the bleaching spot by comparing a simulated diffusion coefficient and the measured one. However, this method takes into consideration only the bleached spot and not the surrounding area. [128], [133] A spatially resolved analysis method has also been developed, however, without taking the dimensionality of the system into consideration. [132] Even if the initial method from Axelrod at least considered an immobile fraction, all other methods do not consider a spatial information at all. [132]

To overcome these limitations, Seiffert *et al*. developed a new method that takes both the temporal and spatial information into account, and in addition does not need an initial calibration of the laser beam. [128] The method is based on four main steps that are implemented in a Matlab algorithm: (1) Normalization of the images, (2) averaging of the intensity, (3) fitting of the intensity, and finally (4) the estimation of the diffusion coefficient and the dimensionality. [128] To start, each FRAP image during the recovery process is normalized by dividing it by an average of pre-bleached images. Afterwards, after that the bleaching spot is precisely localized with a custom algorithm, the intensity profile is generated by averaging the intensity locally. [128] Successively a Gaussian function is fitted to the averaged intensity profile. With time, the bleaching spot spreads radially and therefore its correspondent Gaussian profile smears, as it can be seen in **Figure 19**.

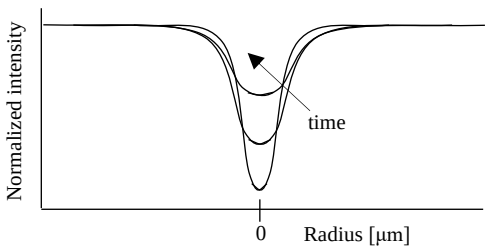

Figure 19. The fitted Gaussian profile is characterized by a deep well at short times and afterwards the profile smears with increasing times.

The temporal and spatial evolution of the concentration C of the fluorescent diffusing species can be extrapolated *via* Fick's second law

$$\frac{\partial C}{\partial t} = D\frac{\partial^2 C}{\partial x^2} \tag{8}$$

$$\frac{\partial C}{\partial t} = D\left(\frac{\partial^2 C}{\partial x^2} + \frac{\partial^2 C}{\partial y^2}\right) \tag{9}$$

$$\frac{\partial C}{\partial t} = D\left(\frac{\partial^2 C}{\partial x^2} + \frac{\partial^2 C}{\partial y^2} + \frac{\partial^2 C}{\partial z^2}\right) \tag{10}$$

that is valid for 1D, 2D, and 3D diffusion mechanism respectively. [128], [132]

Equations (8-10) can be generalized as

$$\frac{\partial C}{\partial t} = div\,(D\ grad\ C) \tag{11}$$

The ideal boundary conditions to solve these equations are that the bleaching occurs in an infinitely short time and with an infinitely narrow laser. [128] The generalized solution to equations (8-11) is then

$$C(r,t) = \frac{M}{(4\pi Dt)^{d/2}} e^{\frac{-r^2}{4Dt}} \tag{12}$$

where d is the dimensionality, r represents the radial coordinate, whereas M represents the total amount of diffusants in the three-dimensional case and the amount of substance per unit length or area for the 1D and 2D case respectively. [128]

In a FRAP experiment, the fluorescence intensity distribution is dependent on the concentration of fluorescent species. [132] For the ideal case the intensity can be written in function of space and time as

$$I(t,r) = I_0 - \frac{M}{(4\pi Dt)^{\frac{d}{2}}} e^{-\frac{2}{4Dt}} = I_0 - A(t)e^{-\frac{r^2}{2w^2}} \tag{13}$$

with t the time, r the spatial coordinate, I_0 the initial intensity, M is the amount of the bleached fluorophores, D the diffusion coefficient, d the dimensionality of the system, A the pre-exponential factor, and w the standard deviation. [128] From this it derives that

$$w^2 = 2\ D\ t \tag{14}$$

Therefore, by plotting w^2 of every Gaussian curve versus the time, the slope of the resulting line equals $2\ D$ and enables the extraction of the diffusion coefficient. [128]

However, the initial ideal conditions are experimentally hardly met, as there is always a time delay for the bleaching and the laser has in fact a finite width. [128] This can be accounted with a time shift t_0 or an initial half-width w_0. [132]

By taking these spatial and temporal deviations into account, equation (14) becomes [128]

$$w^2 = 2\,D\,(t + t_0)\;=\;2Dt + w_0^2 \tag{15}$$

This shift does not affect the diffusion coefficient, as this is calculated through the slope of the line, but it affects the determination of the dimensionality. This can be calculated from the slope of the line plotting $\log\,(A)$ in function of $\log\,(t + t_0)$ as $(-d/2)$. [128]

Considering the spatial and temporal deviations, equation (12) can be adjusted consequently in

$$C(r,t) = \frac{M}{(4\pi D(t + t_0))^{d/2}}\, e^{\frac{-r^2}{4D(t+t_0)}} \tag{16}$$

and

$$C(r,t) = \frac{M}{(4\pi Dt + 2\pi w_0^2)^{d/2}}\, e^{\frac{-r^2}{4Dt+2w_0^2}} \tag{17}$$

where w is the standard deviation assuming a Gaussian profile of the laser beam. [132]

The fluorescence intensity distribution in function of space and time is then accordingly [132]

$$I(t,r) = I_0 - \frac{M}{(4\pi D(t + t_0))^{d/2}}\, e^{\frac{-r^2}{4D(t+t_0)}} \tag{18}$$

and

$$I(t,r) = I_0 - \frac{M}{(4\pi Dt + 2\pi w_0^2)^{d/2}}\, e^{\frac{-r^2}{4Dt+2w_0^2}} \tag{19}$$

Nevertheless, all the aforementioned techniques are based on single-component diffusion process and do not take polydispersity into account. [132] To account for polydispersity as well, Seiffert *et al*. expanded their aforementioned method towards multi-component diffusions. [132] Their method can be applied if the diffusion coefficients of the diffusive species differ at least by a factor of three. [132]

FRAP can not only enable the determination of the diffusion coefficient of fluorescent species that can freely move in the polymer network, but can also reveal precious information on the dynamics of supramolecular bonds. This can occur when the fluorescent dye is attached to a tracer that can interact with the polymer binding motif. The self-diffusion coefficient is then extrapolated with the same method. [134]

For some applications such as contact lenses or drug delivery, it might be necessary to introduce a specific molecule inside the polymer network and control its diffusion and/or release. [4]

The diffusion mechanism is controlled by the ratio of a driving and a dragging force, being respectively thermal energy and friction. [100] These elements can be combined in an alternative formulation of the diffusion coefficient known as Einstein equation

$$D = \frac{k_B T}{F} \tag{20}$$

where k_B is the Boltzmann constant, T is the temperature, and F is the friction acting on the diffusing species. [100]

Assuming a spherical form of the diffusants, the friction can be related with the hydrodynamic radius R_H (Stokes-Einstein equation)

$$D = \frac{k_B T}{6\pi\eta R_H} \tag{21}$$

where k_B is the Boltzmann constant, T is the absolute temperature, and η the viscosity of the solvent. [100], [135]–[137]

Therefore, by looking at the diffusion coefficient under a different perspective it is possible to extract further structural parameters from the diffusion mechanism of the species under investigation. Consequently, once that the diffusion coefficient is known, it is possible to extract the hydrodynamic radius which gives an indication of the size of the diffusing species. [138]

Additionally, the hydrodynamic radius can also give information about the network mesh-size. If in a series of experiments, particles with increasing known R_H are systematically introduced into a hydrogel and the diffusion coefficient is measured for every combination, the critical particle size at which the diffusion gets restricted will give an indication about the average mesh-size of the system. [139] If the particle is smaller than the average mesh-size of the hydrogel, then the diffusion will be fast. If it has a similar size compared to the meshes, then the diffusion will be slow. Finally, if the particle has a larger size than the average mesh-size, then the diffusion will be hindered, as schematized in **Figure 20** for drug delivery applications. [140] In case the drug cannot freely diffuse, its release can still occur, if the network degrades, swells or deforms, and thereby, permits the passage of the drug. [140]

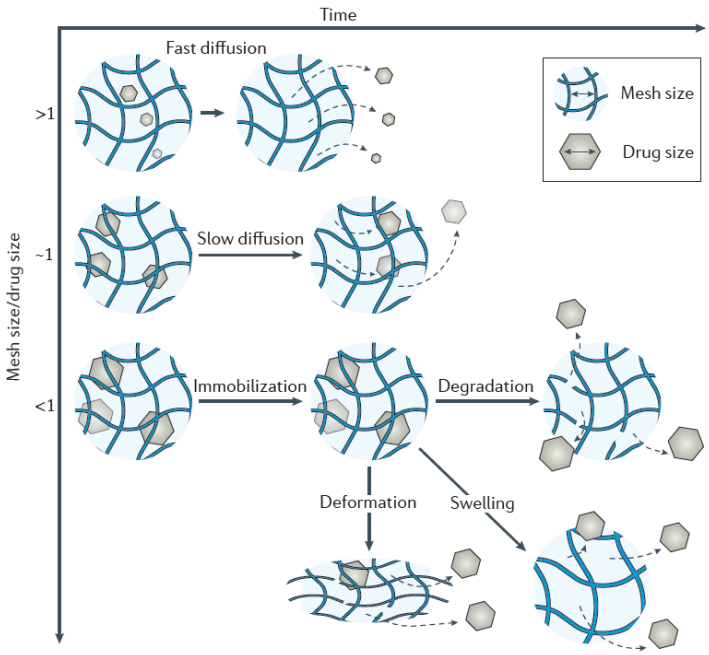

Figure 20. The diffusion in polymer networks depends strongly on their mesh-size. (Reproduced with permission from Ref. [140] © 2016, Macmillan Publishers Limited)

Therefore, the diffusion properties inside hydrogels are strictly connected with the hydrogel's mesh-size, which is a structural parameter. Consequently, by controlling the mesh-size it is possible to tune the diffusion.

There are several ways to control a hydrogels' mesh-size. The most intuitive options are an increase of the polymer concentration or crosslinks density. [27] Another option is to customize the structure. For example, Grunlan *et al*. achieved control over the mesh-size, by adding dangling chains to the first polymer network of a double network. [27] Their double network is composed by a densely crosslinked first network which is negatively charged and bears dangling chains. They interpenetrated this network with a loosely crosslinked, neutral second network. They attached dangling chains to the first network and systematically varied the charge (neutral, positive, and negative), the concentration, and the length of dangling chains. Their findings show that smaller mesh-sizes (<3 nm) are achievable with negatively charged dangling chains, due to the electrostatic repulsion with the first network. That mesh-size has been achievable with all the investigated comb lengths. However, longer chains required a lower concentration. [27]

Grafting polymer chains to a main network seems to be a winning strategy. In multiple studies, Lowman *et al.*, showed that it is possible to control the diffusion of proteins with this polymer network architecture. In particular, this is achieved by grafting poly(ethylene glycol) chains on a poly(methacrylic acid) network that is pH-responsive. In basic conditions the gel is swollen, whereas in acidic conditions it is unswollen. Therefore, by tuning the pH it is possible to control the diffusion rate of the proteins. [141]

Another way to engineer the mesh-size is the use of precursors with different strand length as done by Sakai *et al.* who employed tetra-arm pEGs of two different molar masses. Their findings show that the final mesh-size is an average of the mesh-size of the two polymer precursors. [142]

The tunability of the diffusion through the mesh-size is just one example of how the structure of the polymer network influences the final properties. However, all the aforementioned studies concern covalent systems. For supramolecular systems, less studies are known, and the number decreases even more when moving to more complicated network configurations such as double or dual networks. Therefore, the aim of this thesis is to fill this gap and contribute with systematic insights to the field.

References

[1] W. Wang, R. Narain, and H. Zeng, “Rational design of self-healing tough hydrogels: A mini review,” *Front. Chem.*, vol. 6, no. OCT, pp. 1–9, 2018, doi: 10.3389/fchem.2018.00497.

[2] T. R. Hoare and D. S. Kohane, “Hydrogels in drug delivery: Progress and challenges,” *Polymer (Guildf).*, vol. 49, no. 8, pp. 1993–2007, 2008, doi: 10.1016/j.polymer.2008.01.027.

[3] P. Nicolella, D. Lauxen, M. Ahmadi, and S. Seiffert, “Reversible Hydrogels with Switchable Diffusive Permeability,” *Macromol. Chem. Phys.*, vol. 222, no. 16, p. 2100076, 2021, doi: 10.1002/macp.202100076.

[4] M. Bahram, N. Mohseni, and M. Moghtader, “An Introduction to Hydrogels and Some Recent Applications,” *Emerg. Concepts Anal. Appl. Hydrogels*, no. April 2018, 2016, doi: 10.5772/64301.

[5] R. D. Pyarasani, T. Jayaramudu, and A. John, “Polyaniline-based conducting hydrogels,” *J. Mater. Sci.*, vol. 54, no. 2, pp. 974–996, 2019, doi: 10.1007/s10853-018-2977-x.

[6] E. Caló and V. V. Khutoryanskiy, “Biomedical applications of hydrogels: A review of patents and commercial products,” *Eur. Polym. J.*, vol. 65, pp. 252–267, 2015, doi: 10.1016/j.eurpolymj.2014.11.024.

[7] R. C. Sabadini, M. M. Silva, A. Pawlicka, and J. Kanicki, “Gellan gum–O,O′-bis(2-aminopropyl)-polyethylene glycol hydrogel for controlled fertilizer release,” *J. Appl. Polym. Sci.*, vol. 135, no. 2, pp. 1–7, 2018, doi: 10.1002/app.45636.

[8] B. H. Cipriano *et al.*, “Superabsorbent hydrogels that are robust and highly stretchable,” *Macromolecules*, vol. 47, no. 13, pp. 4445–4452, 2014, doi: 10.1021/ma500882n.

[9] P. Calvert, “Hydrogels for soft machines,” *Adv. Mater.*, vol. 21, no. 7, pp. 743–756, 2009, doi: 10.1002/adma.200800534.

[10] I. Tokarev and S. Minko, “Stimuli-responsive porous hydrogels at interfaces for molecular filtration, separation, controlled release, and gating in capsules and membranes,” *Adv. Mater.*, vol. 22, no. 31, pp. 3446–3462, 2010, doi: 10.1002/adma.201000165.

[11] M. K. Yazdi *et al.*, “Hydrogel membranes: A review,” *Mater. Sci. Eng. C*, vol. 114, no. March, 2020, doi: 10.1016/j.msec.2020.111023.

[12] M. Annaka, T. Matsuura, M. Kasai, T. Nakahira, Y. Hara, and T. Okano, “Preparation of comb-type N-isopropylacrylamide hydrogel beads and their application for size-selective separation media,” *Biomacromolecules*, vol. 4, no. 2, pp. 395–403, 2003, doi: 10.1021/bm025697q.

[13] W. Ali *et al.*, “On the potential of using dual-function hydrogels for brackish water desalination,” *Polymers (Basel).*, vol. 10, no. 6, pp. 1–21, 2018, doi: 10.3390/polym10060567.

[14] A. Jangizehi and S. Seiffert, “Salt partitioning in ionized, thermo-responsive hydrogels: perspective to water desalination,” *J. Chem. Phys.*, vol. 154, no. 14, 2021, doi: 10.1063/5.0044376.

[15] G. Cantarella *et al.*, “Design of Engineered Elastomeric Substrate for Stretchable Active Devices and Sensors,” *Adv. Funct. Mater.*, vol. 28, no. 30, pp. 1–9, 2018, doi: 10.1002/adfm.201705132.

[16] Y. Ma *et al.*, “Soft Elastomers with Ionic Liquid-Filled Cavities as Strain Isolating Substrates for Wearable Electronics,” *Small*, vol. 13, no. 9, pp. 1–10, 2017, doi: 10.1002/smll.201602954.

[17] R. T. Shafranek, S. C. Millik, P. T. Smith, C. U. Lee, A. J. Boydston, and A. Nelson, “Stimuli-responsive materials in additive manufacturing,” *Prog. Polym. Sci.*, vol. 93, pp. 36–67, 2019, doi: 10.1016/j.progpolymsci.2019.03.002.

[18] M. Cai, S. Nie, Y. Du, C. Wang, and J. Song, “Soft Elastomers with Programmable Stiffness as

Strain-Isolating Substrates for Stretchable Electronics," *ACS Appl. Mater. Interfaces*, vol. 11, no. 15, pp. 14340–14346, 2019, doi: 10.1021/acsami.9b01551.

[19] K. Liu, Y. Jiang, Z. Bao, and X. Yan, "Skin-inspired electronics enabled by supramolecular polymeric materials," *CCS Chem.*, vol. 1, no. 4, pp. 431–447, 2019, doi: 10.31635/ccschem.019.20190048.

[20] A. S. Hoffman, "Hydrogels for biomedical applications," *Adv. Drug Deliv. Rev.*, vol. 54, pp. 3–12, 2002, doi: 10.1002/9781119301714.ch9.

[21] X. Zhao, X. Chen, H. Yuk, S. Lin, X. Liu, and G. Parada, "Soft Materials by Design: Unconventional Polymer Networks Give Extreme Properties," *Chem. Rev.*, vol. 121, no. 8, pp. 4309–4372, 2021, doi: 10.1021/acs.chemrev.0c01088.

[22] L. Chu, R. Xie, and X. Ju, "Stimuli-responsive membranes: Smart tools for controllable mass-transfer and separation processes," *Chinese J. Chem. Eng.*, vol. 19, no. 6, pp. 891–903, 2011, doi: 10.1016/S1004-9541(11)60070-0.

[23] R. P. Narayanan, G. Melman, N. J. Letourneau, N. L. Mendelson, and A. Melman, "Photodegradable iron(III) cross-linked alginate gels," *Biomacromolecules*, vol. 13, no. 8, pp. 2465–2471, 2012, doi: 10.1021/bm300707a.

[24] S. Mantha *et al.*, "Smart Hydrogels in Tissue Engineering and Regenerative Medicine," *Materials (Basel).*, vol. 12, no. 20, p. 3323, 2019, [Online]. Available: https://www.ncbi.nlm.nih.gov/pmc/articles/PMC68/.

[25] S. Bernhard and M. W. Tibbitt, "Supramolecular engineering of hydrogels for drug delivery," *Adv. Drug Deliv. Rev.*, vol. 171, pp. 240–256, 2021, doi: 10.1016/j.addr.2021.02.002.

[26] C. F. Guimarães, L. Gasperini, A. P. Marques, and R. L. Reis, "The stiffness of living tissues and its implications for tissue engineering," *Nat. Rev. Mater.*, vol. 5, no. 5, pp. 351–370, 2020, doi: 10.1038/s41578-019-0169-1.

[27] P. Dong, B. J. Schott, A. K. Means, and M. A. Grunlan, "Comb Architecture to Control the Selective Diffusivity of a Double Network Hydrogel," *ACS Appl. Polym. Mater.*, vol. 2, no. 11, pp. 5269–5277, 2020, doi: 10.1021/acsapm.0c00987.

[28] X. Huang, J. Li, J. Luo, Q. Gao, A. Mao, and J. Li, "Research progress on double-network hydrogels," *Mater. Today Commun.*, vol. 29, no. September, p. 102757, 2021, doi: 10.1016/j.mtcomm.2021.102757.

[29] C. Creton, "50th Anniversary Perspective: Networks and Gels: Soft but Dynamic and Tough," *Macromolecules*, vol. 50, no. 21, pp. 8297–8316, 2017, doi: 10.1021/acs.macromol.7b01698.

[30] L. H. Sperling and V. Mishra, "The current status of interpenetrating polymer networks," *Polym. Adv. Technol.*, vol. 7, no. 4, pp. 197–208, 1996, doi: 10.1002/(SICI)1099-1581(199604)7:4<197::AID-PAT514>3.0.CO;2-4.

[31] J. P. Gong, Y. Katsuyama, T. Kurokawa, and Y. Osada, "Double-network hydrogels with extremely high mechanical strength," *Adv. Mater.*, vol. 15, no. 14, pp. 1155–1158, 2003, doi: 10.1002/adma.200304907.

[32] H. R. Brown, "A model of the fracture of double network gels," *Macromolecules*, vol. 40, no. 10, pp. 3815–3818, 2007, doi: 10.1021/ma062642y.

[33] Y. Tanaka, "A local damage model for anomalous high toughness of double-network gels," *Epl*, vol. 78, no. 5, 2007, doi: 10.1209/0295-5075/78/56005.

[34] J. P. Gong, "Why are double network hydrogels so tough?," *Soft Matter*, vol. 6, no. 12, pp. 2583–2590, 2010, doi: 10.1039/b924290b.

[35] Z. Cao *et al.*, "Tough, ultrastretchable and tear-resistant hydrogels enabled by linear macro-

cross-linker," *Polym. Chem.*, vol. 10, no. 25, pp. 3503–3513, 2019, doi: 10.1039/c9py00600a.

[36] A. K. Means, C. S. Shrode, L. V. Whitney, D. A. Ehrhardt, and M. A. Grunlan, "Double Network Hydrogels that Mimic the Modulus, Strength, and Lubricity of Cartilage," *Biomacromolecules*, vol. 20, no. 5, pp. 2034–2042, 2019, doi: 10.1021/acs.biomac.9b00237.

[37] P. Matricardi, C. Di Meo, T. Coviello, W. E. Hennink, and F. Alhaique, "Interpenetrating polymer networks polysaccharide hydrogels for drug delivery and tissue engineering," *Adv. Drug Deliv. Rev.*, vol. 65, no. 9, pp. 1172–1187, 2013, doi: 10.1016/j.addr.2013.04.002.

[38] V. Nigro *et al.*, "Study of network composition in interpenetrating polymer networks of poly(N isopropylacrylamide) microgels: The role of poly(acrylic acid)," *J. Colloid Interface Sci.*, vol. 545, pp. 210–219, 2019, doi: 10.1016/j.jcis.2019.03.004.

[39] D. Myung, D. Waters, M. Wiseman, P. Duhamel, C. N. Ta, and C. W. Frank, "NIH Public Access," vol. 19, no. 6, pp. 647–657, 2009, doi: 10.1002/pat.1134.Progress.

[40] S. Naficy, H. R. Brown, J. M. Razal, G. M. Spinks, and P. G. Whitten, "Progress toward robust polymer hydrogels," *Aust. J. Chem.*, vol. 64, no. 8, pp. 1007–1025, 2011, doi: 10.1071/CH11156.

[41] J. A. Johnson, N. J. Turro, J. T. Koberstein, and J. E. Mark, "Some hydrogels having novel molecular structures," *Prog. Polym. Sci.*, vol. 35, no. 3, pp. 332–337, 2010, doi: 10.1016/j.progpolymsci.2009.12.002.

[42] Q. Chen, H. Chen, L. Zhu, and J. Zheng, "Fundamentals of double network hydrogels," *J. Mater. Chem. B*, vol. 3, no. 18, pp. 3654–3676, 2015, doi: 10.1039/c5tb00123d.

[43] L. Xu, C. Wang, Y. Cui, A. Li, Y. Qiao, and D. Qiu, "Conjoined-network rendered stiff and tough hydrogels from biogenic molecules," *Sci. Adv.*, vol. 5, no. 2, 2019, doi: 10.1126/sciadv.aau3442.

[44] A. Argun, V. Can, U. Altun, and O. Okay, "Nonionic double and triple network hydrogels of high mechanical strength," *Macromolecules*, vol. 47, no. 18, pp. 6430–6440, 2014, doi: 10.1021/ma5014176.

[45] T. M. Fung, C. Gallego Lazo, and A. M. Smith, "Elasticity and energy dissipation in the double network hydrogel adhesive of the slug Arion subfuscus," *Philos. Trans. R. Soc. B Biol. Sci.*, vol. 374, no. 1784, 2019, doi: 10.1098/rstb.2019.0201.

[46] M. A. Haque, T. Kurokawa, and J. P. Gong, "Super tough double network hydrogels and their application as biomaterials," *Polymer (Guildf).*, vol. 53, no. 9, pp. 1805–1822, 2012, doi: 10.1016/j.polymer.2012.03.013.

[47] J. Y. Sun *et al.*, "Highly stretchable and tough hydrogels," *Nature*, vol. 489, no. 7414, pp. 133–136, 2012, doi: 10.1038/nature11409.

[48] S. Seiffert and J. Sprakel, "Physical chemistry of supramolecular polymer networks," *Chem. Soc. Rev.*, vol. 41, no. 2, pp. 909–930, 2012, doi: 10.1039/c1cs15191f.

[49] T. Rossow and S. Seiffert, *Supramolecular polymer networks: Preparation, properties, and potential*, vol. 268. 2015.

[50] T. Rossow, A. Habicht, and S. Seiffert, "Relaxation and dynamics in transient polymer model networks," *Macromolecules*, vol. 47, no. 18, pp. 6473–6482, 2014, doi: 10.1021/ma5013144.

[51] R. Hoogenboom, "Hard autonomous self-healing supramolecular materials-A contradiction in terms?," *Angew. Chemie - Int. Ed.*, vol. 51, no. 48, pp. 11942–11944, 2012, doi: 10.1002/anie.201205226.

[52] J. M. Lehn, "Perspectives in Chemistry - Aspects of Adaptive Chemistry and Materials," *Angew. Chemie - Int. Ed.*, vol. 54, no. 11, pp. 3276–3289, 2015, doi: 10.1002/anie.201409399.

[53] H. Yang *et al.*, “Healable terpyridine-based supramolecular gels and the luminescent properties of the rare earth metal complex,” *New J. Chem.*, vol. 41, no. 24, pp. 15173–15179, 2017, doi: 10.1039/c7nj03175k.

[54] T. Aida, E. W. Meijer, and S. I. Stupp, “Functional supramolecular polymers,” *Science (80-.).*, vol. 335, no. 6070, pp. 813–817, 2012, doi: 10.1126/science.1205962.

[55] Y. Li, C. Zhu, Y. Dong, and D. Liu, “Supramolecular hydrogels: Mechanical strengthening with dynamics,” *Polymer (Guildf).*, vol. 210, no. September, p. 122993, 2020, doi: 10.1016/j.polymer.2020.122993.

[56] X. Xu, V. V. Jerca, and R. Hoogenboom, “Self-Healing Metallo-Supramolecular Hydrogel Based on Specific Ni2+ Coordination Interactions of Poly(ethylene glycol) with Bistriazole Pyridine Ligands in the Main Chain,” *Macromol. Rapid Commun.*, vol. 41, no. 4, pp. 6–11, 2020, doi: 10.1002/marc.201900457.

[57] P. M. Lopez-Perez, R. M. P. Da Silva, I. Strehin, P. H. J. Kouwer, S. C. G. Leeuwenburgh, and P. B. Messersmith, “Self-Healing Hydrogels Formed by Complexation between Calcium Ions and Bisphosphonate-Functionalized Star-Shaped Polymers,” *Macromolecules*, vol. 50, no. 21, pp. 8698–8706, 2017, doi: 10.1021/acs.macromol.7b01417.

[58] A. Campanella, D. Döhler, and W. H. Binder, “Self-Healing in Supramolecular Polymers,” *Macromol. Rapid Commun.*, vol. 39, no. 17, pp. 1–19, 2018, doi: 10.1002/marc.201700739.

[59] E. Su, M. Yurtsever, and O. Okay, “A Self-Healing and Highly Stretchable Polyelectrolyte Hydrogel via Cooperative Hydrogen Bonding as a Superabsorbent Polymer,” *Macromolecules*, vol. 52, no. 9, pp. 3257–3267, 2019, doi: 10.1021/acs.macromol.9b00032.

[60] Y. Deng, Q. Zhang, B. L. Feringa, H. Tian, and D. Qu, “Toughening a Self-Healable Supramolecular Polymer by Ionic Cluster-Enhanced Iron-Carboxylate Complexes,” *Angew. Chemie*, vol. 132, no. 13, pp. 5316–5321, 2020, doi: 10.1002/ange.201913893.

[61] G. Zhou, X. Zhang, and X. L. Ni, “Tuning the amphiphilicity of terpyridine-based fluorescent probe in water: Assembly and disassembly-controlled H g2+ sensing, removal, and adsorption of H2S,” *J. Hazard. Mater.*, vol. 384, no. September, p. 121474, 2020, doi: 10.1016/j.jhazmat.2019.121474.

[62] L. Hammer, N. J. Van Zee, and R. Nicolaÿ, “Dually crosslinked polymer networks incorporating dynamic covalent bonds,” *Polymers (Basel).*, vol. 13, no. 3, pp. 1–34, 2021, doi: 10.3390/polym13030396.

[63] Q. Zhang, C. Y. Shi, D. H. Qu, Y. T. Long, B. L. Feringa, and H. Tian, “Exploring a naturally tailored small molecule for stretchable, self-healing, and adhesive supramolecular polymers,” *Sci. Adv.*, vol. 4, no. 7, pp. 1–9, 2018, doi: 10.1126/sciadv.aat8192.

[64] L. Wang *et al.*, “A Self-Cross-Linking Supramolecular Polymer Network Enabled by Crown-Ether-Based Molecular Recognition,” *J. Am. Chem. Soc.*, vol. 142, no. 4, pp. 2051–2058, 2020, doi: 10.1021/jacs.9b12164.

[65] R. K. Bose, N. Hohlbein, S. J. Garcia, A. M. Schmidt, and S. Van Der Zwaag, “Connecting supramolecular bond lifetime and network mobility for scratch healing in poly(butyl acrylate) ionomers containing sodium, zinc and cobalt,” *Phys. Chem. Chem. Phys.*, vol. 17, no. 3, pp. 1697–1704, 2015, doi: 10.1039/c4cp04015e.

[66] NobelPrize.org, “The Nobel Prize in Chemistry 1987.” https://www.nobelprize.org/prizes/chemistry/1987/press-release/ (accessed Oct. 08, 2020).

[67] J. W. Steed and J. L. Atwood, *Supramolecular Chemistry*, Second. Wiley, 2009.

[68] U. S. Schubert and C. Eschbaumer, “Macromolecules containing bipyridine and terpyridine metal complexes: Towards metallosupramolecular polymers,” *Angew. Chemie - Int. Ed.*, vol. 41,

no. 16, pp. 2892–2926, 2002, doi: 10.1002/1521-3773(20020816)41:16<2892::AID-ANIE2892>3.0.CO;2-6.

[69] U. S. Schubert, H. Hofmeier, and G. R. Newkome, "Introduction," in *Modern Terpyridine Chemistry*, Weinheim: WILEY-VCH, 2006, pp. 1–6.

[70] S. Chakraborty and G. R. Newkome, "Terpyridine-based metallosupramolecular constructs: Tailored monomers to precise 2D-motifs and 3D-metallocages," *Chem. Soc. Rev.*, vol. 47, no. 11, pp. 3991–4016, 2018, doi: 10.1039/c8cs00030a.

[71] B. G. G. Lohmeijer and U. S. Schubert, "Water-soluble building blocks for terpyridine-containing supramolecular polymers: Synthesis, complexation, and pH stability studies of poly(ethylene oxide) moieties," *Macromol. Chem. Phys.*, vol. 204, no. 8, pp. 1072–1078, 2003, doi: 10.1002/macp.200390078.

[72] A. Agosti, E. Kuna, and G. Bergamini, "Divergent Terpyridine-Based Coordination for the Construction of Photoactive Supramolecular Structures," *Eur. J. Inorg. Chem.*, vol. 2019, no. 5, pp. 577–584, 2019, doi: 10.1002/ejic.201801263.

[73] K. H. Wu *et al.*, "A bis(terpyridine)iron network polymer on carbon for a potential energy storage material," *Dalt. Trans.*, vol. 42, no. 45, pp. 15877–15880, 2013, doi: 10.1039/c3dt51186c.

[74] R. Ghosh, "Stimuli-Responsive Membranes for Separations," pp. 491–508, 2019, doi: 10.1007/978-3-319-95990-0_8.

[75] M. Wei, Y. Gao, X. Li, and M. J. Serpe, "Stimuli-responsive polymers and their applications," *Polym. Chem.*, vol. 8, no. 1, pp. 127–143, 2017, doi: 10.1039/c6py01585a.

[76] J. D. Willott, W. M. Nielen, and W. M. De Vos, "Stimuli-Responsive Membranes through Sustainable Aqueous Phase Separation," *ACS Appl. Polym. Mater.*, vol. 2, no. 2, pp. 659–667, 2020, doi: 10.1021/acsapm.9b01006.

[77] X. Zhang, Y. Yin, J. Yan, W. Li, and A. Zhang, "Thermo- and redox-responsive dendronized polymer hydrogels," *Polym. Chem.*, vol. 9, no. 6, pp. 712–721, 2018, doi: 10.1039/c7py01284e.

[78] J. Chen, M. Liu, C. Gao, S. Lü, X. Zhang, and Z. Liu, "Self-assembly behavior of pH- and thermo-responsive hydrophilic ABCBA-type pentablock copolymers synthesized by consecutive RAFT polymerization," *RSC Adv.*, vol. 3, no. 35, pp. 15085–15093, 2013, doi: 10.1039/c3ra41832d.

[79] S. Datta, M. L. Saha, and P. J. Stang, "Hierarchical Assemblies of Supramolecular Coordination Complexes," *Acc. Chem. Res.*, vol. 51, no. 9, pp. 2047–2063, 2018, doi: 10.1021/acs.accounts.8b00233.

[80] X. Sun, S. Agate, K. S. Salem, L. Lucia, and L. Pal, "Hydrogel-Based Sensor Networks: Compositions, Properties, and Applications - A Review," *ACS Appl. Bio Mater.*, vol. 4, no. 1, pp. 140–162, 2021, doi: 10.1021/acsabm.0c01011.

[81] S. B. Lee, D. I. Ha, S. K. Cho, S. J. Kim, and Y. M. Lee, "Temperature / pH-Sensitive Comb-Type Graft Hydrogels Composed of Chitosan and Poly (N -isopropylacrylamide)," 2003.

[82] G. E. Giammanco, C. T. Sosnofsky, and A. D. Ostrowski, "Light-responsive Iron(III)-polysaccharide coordination hydrogels for controlled delivery," *ACS Appl. Mater. Interfaces*, vol. 7, no. 5, pp. 3068–3076, 2015, doi: 10.1021/am506772x.

[83] C. De las Heras Alarcón, S. Pennadam, and C. Alexander, "Stimuli responsive polymers for biomedical applications," *Chem. Soc. Rev.*, vol. 34, no. 3, pp. 276–285, 2005, doi: 10.1039/b406727d.

[84] D. Klinger and K. Landfester, "Stimuli-responsive microgels for the loading and release of functional compounds: Fundamental concepts and applications," *Polymer (Guildf).*, vol. 53, no.

23, pp. 5209–5231, 2012, doi: 10.1016/j.polymer.2012.08.053.

[85] K. Bauri, M. Nandi, and P. De, "Amino acid-derived stimuli-responsive polymers and their applications," *Polym. Chem.*, vol. 9, no. 11, pp. 1257–1287, 2018, doi: 10.1039/c7py02014g.

[86] N. Sood, A. Bhardwaj, S. Mehta, and A. Mehta, "Stimuli-responsive hydrogels in drug delivery and tissue engineering," *Drug Deliv.*, vol. 23, no. 3, pp. 748–770, 2016, doi: 10.3109/10717544.2014.940091.

[87] A. Alexander, Ajazuddin, J. Khan, S. Saraf, and S. Saraf, "Polyethylene glycol (PEG)-Poly(N-isopropylacrylamide) (PNIPAAm) based thermosensitive injectable hydrogels for biomedical applications," *Eur. J. Pharm. Biopharm.*, vol. 88, no. 3, pp. 575–585, 2014, doi: 10.1016/j.ejpb.2014.07.005.

[88] A. Gandhi, A. Paul, S. O. Sen, and K. K. Sen, "Studies on thermoresponsive polymers: Phase behaviour, drug delivery and biomedical applications," *Asian J. Pharm. Sci.*, vol. 10, no. 2, pp. 99–107, 2015, doi: 10.1016/j.ajps.2014.08.010.

[89] Y. J. Oh, I. In, and S. Y. Park, "Temperature-sensitive hydrogel prepared by graft polymerization of N-isopropylacrylamide onto macroradical Pluronic," *J. Ind. Eng. Chem.*, vol. 18, no. 1, pp. 321–324, 2012, doi: 10.1016/j.jiec.2011.11.050.

[90] J. Brassinne, J. P. Bourgeois, C. A. Fustin, and J. F. Gohy, "Thermo-responsive properties of metallo-supramolecular block copolymer micellar hydrogels," *Soft Matter*, vol. 10, no. 17, pp. 3086–3092, 2014, doi: 10.1039/c3sm53013b.

[91] S. Hackelbusch, T. Rossow, D. Steinhilber, D. A. Weitz, and S. Seiffert, "Hybrid Microgels with Thermo-Tunable Elasticity for Controllable Cell Confinement," *Adv. Healthc. Mater.*, vol. 4, no. 12, pp. 1841–1848, 2015, doi: 10.1002/adhm.201500359.

[92] Y. Zhao *et al.*, "Transparent thermo-responsive poly(N -isopropylacrylamide)- l -poly(ethylene glycol)acrylamide conetwork hydrogels with rapid deswelling response," *New J. Chem.*, vol. 43, no. 24, pp. 9507–9515, 2019, doi: 10.1039/c9nj01545k.

[93] H. Sun, J. Chen, X. Han, and H. Liu, "Multi-responsive hydrogels with UCST- and LCST-induced shrinking and controlled release behaviors of rhodamine B," *Mater. Sci. Eng. C*, vol. 82, no. August 2017, pp. 284–290, 2018, doi: 10.1016/j.msec.2017.08.067.

[94] M. Taylor, P. Tomlins, and T. Sahota, "Thermoresponsive Gels," *Gels*, vol. 3, no. 1, p. 4, 2017, doi: 10.3390/gels3010004.

[95] M. A. Ward and T. K. Georgiou, "Thermoresponsive polymers for biomedical applications," *Polymers (Basel).*, vol. 3, no. 3, pp. 1215–1242, 2011, doi: 10.3390/polym3031215.

[96] K. Jain, R. Vedarajan, M. Watanabe, M. Ishikiriyama, and N. Matsumi, "Tunable LCST behavior of poly(N-isopropylacrylamide/ionic liquid) copolymers," *Polym. Chem.*, vol. 6, no. 38, pp. 6819–6825, 2015, doi: 10.1039/c5py00998g.

[97] K. Jain, R. Vedarajan, M. Watanabe, M. Ishikiriyama, and N. Matsumi, "Tunable LCST behavior of poly(N-isopropylacrylamide/ionic liquid) copolymers," *Polym. Chem.*, vol. 6, no. 38, pp. 6819–6825, 2015, doi: 10.1039/c5py00998g.

[98] Y. Zhu, R. Batchelor, A. B. Lowe, and P. J. Roth, "Design of Thermoresponsive Polymers with Aqueous LCST, UCST, or Both: Modification of a Reactive Poly(2-vinyl-4,4-dimethylazlactone) Scaffold," *Macromolecules*, vol. 49, no. 2, pp. 672–680, 2016, doi: 10.1021/acs.macromol.5b02056.

[99] M. Najafi, E. Hebels, W. E. Hennink, and T. Vermonden, "Poly(N-isopropylacrylamide): Physicochemical Properties and Biomedical Applications," in *Temperature-Responsive Polymers: Chemistry, Properties, and Applications*, 1st ed., V. V. Khutoryanskiy and T. K. Georgiou, Eds. John Wiley & Sons Ltd., 2018, pp. 1–34.

[100] S. Seiffert, *Physical Chemistry of Polymers*. Berlin/Boston: Walter de Gruyter, 2020.

[101] Q. Chen, H. Chen, L. Zhu, and J. Zheng, "Engineering of Tough Double Network Hydrogels," *Macromol. Chem. Phys.*, vol. 217, no. 9, pp. 1022–1036, 2016, doi: 10.1002/macp.201600038.

[102] T. Narita, K. Mayumi, G. Ducouret, and P. Hébraud, "Viscoelastic properties of poly(vinyl alcohol) hydrogels having permanent and transient cross-links studied by microrheology, classical rheometry, and dynamic light scattering," *Macromolecules*, vol. 46, no. 10, pp. 4174–4183, 2013, doi: 10.1021/ma400600f.

[103] Q. Chen *et al.*, "A novel design strategy for fully physically linked double network hydrogels with tough, fatigue resistant, and self- Healing properties," *Adv. Funct. Mater.*, vol. 25, no. 10, pp. 1598–1607, 2015, doi: 10.1002/adfm.201404357.

[104] J. Liu *et al.*, "An advanced elastomer with an unprecedented combination of excellent mechanical properties and high self-healing capability," *J. Mater. Chem. A*, vol. 5, no. 48, pp. 25660–25671, 2017, doi: 10.1039/c7ta08255j.

[105] S. Hackelbusch, T. Rossow, H. Becker, and S. Seiffert, "Multiresponsive polymer hydrogels by orthogonal supramolecular chain cross-linking," *Macromolecules*, vol. 47, no. 12, pp. 4028–4036, 2014, doi: 10.1021/ma5008573.

[106] F. Di Lorenzo and S. Seiffert, "Nanostructural heterogeneity in polymer networks and gels," *Polym. Chem.*, vol. 6, no. 31, pp. 5515–5528, 2015, doi: 10.1039/c4py01677g.

[107] M. Rubinstein and R. H. Colby, *Polymer Physics*. Oxford: Oxford University Press, 2003.

[108] A. Jangizehi, F. Schmid, P. Besenius, K. Kremer, and S. Seiffert, "Defects and defect engineering in Soft Matter," *Soft Matter*, vol. 16, pp. 10809–10859, 2020, doi: 10.1039/d0sm01371d.

[109] P. Nicolella, M. F. Koziol, L. Löser, K. Saalwächter, M. Ahmadi, and S. Seiffert, "Defect-controlled softness, diffusive permeability, and mesh-topology of metallo-supramolecular hydrogels," *Soft Matter*, vol. 18, no. 5, pp. 1071–1081, 2022, doi: 10.1039/d1sm01456k.

[110] K. Nishi *et al.*, "Small-angle neutron scattering study on defect-controlled polymer networks," *Macromolecules*, vol. 47, no. 5, pp. 1801–1809, 2014, doi: 10.1021/ma402590n.

[111] M. Shibayama, X. Li, and T. Sakai, "Precision polymer network science with tetra-PEG gels—a decade history and future," *Colloid Polym. Sci.*, vol. 297, no. 1, pp. 1–12, 2019, doi: 10.1007/s00396-018-4423-7.

[112] M. Ahmadi and S. Seiffert, "Thermodynamic control over energy dissipation modes in dual-network hydrogels based on metal-ligand coordination," *Soft Matter*, vol. 16, no. 9, pp. 2332–2341, 2020, doi: 10.1039/c9sm02149c.

[113] F. Di Lorenzo, J. Hellwig, R. Von Klitzing, and S. Seiffert, "Macroscopic and Microscopic Elasticity of Heterogeneous Polymer Gels," *ACS Macro Lett.*, vol. 4, no. 7, pp. 698–703, 2015, doi: 10.1021/acsmacrolett.5b00228.

[114] L. Avram and Y. Cohen, "Diffusion NMR of molecular cages and capsules," *Chem. Soc. Rev.*, vol. 44, no. 2, pp. 586–602, 2015, doi: 10.1039/c4cs00197d.

[115] M. Shibayama and X. Li, "Probe Diffusion Dynamic Light Scattering of Polymer solutions and Gels," *ACS Symp. Ser.*, vol. 1296, pp. 51–69, 2018, doi: 10.1021/bk-2018-1296.ch004.

[116] H. Murata, "Rheology - Theory and Application to Biomaterials," *Polymerization*, 2012, doi: 10.5772/48393.

[117] T. Mezger, *The Rheology Handbook*, 4th ed. Hanover, 2014.

[118] T. Mezger, *The Rheology Handbook*. 2020.

[119] S. Tang and B. D. Olsen, "Relaxation Processes in Supramolecular Metallogels Based on

Histidine-Nickel Coordination Bonds," *Macromolecules*, vol. 49, no. 23, pp. 9163–9175, 2016, doi: 10.1021/acs.macromol.6b01618.

[120] T. Rossow and S. Seiffert, "Supramolecular polymer gels with potential model-network structure," *Polym. Chem.*, vol. 5, no. 8, pp. 3018–3029, 2014, doi: 10.1039/c3py01692g.

[121] C. Verdier, "Rheological properties of living materials. From cells to tissues," *J. Theor. Med.*, vol. 5, no. 2, pp. 67–91, 2003, doi: 10.1080/10273360410001678083.

[122] G. A. Parada and X. Zhao, "Ideal reversible polymer networks," *Soft Matter*, vol. 14, no. 25, pp. 5186–5196, 2018, doi: 10.1039/c8sm00646f.

[123] T. Vermonden *et al.*, "Linear rheology of water-soluble reversible neodymium(III) coordination polymers," *J. Am. Chem. Soc.*, vol. 126, no. 48, pp. 15802–15808, 2004, doi: 10.1021/ja0458928.

[124] F. Van De Manakker, T. Vermonden, N. el Morabit, C. F. Van Nostrum, and W. E. Hennink, "Rheological Behavior of Self-Assembling PEG- -Cyclodextrin / PEG-Cholesterol Hydrogels," *Langmuir*, vol. 24, no. 21, pp. 12559–12567, 2008.

[125] J. Karvinen, T. O. Ihalainen, M. T. Calejo, I. Jönkkäri, and M. Kellomäki, "Characterization of the microstructure of hydrazone crosslinked polysaccharide-based hydrogels through rheological and diffusion studies," *Mater. Sci. Eng. C*, vol. 94, no. April 2018, pp. 1056–1066, 2019, doi: 10.1016/j.msec.2018.10.048.

[126] M. Golkaram and K. Loos, "A Critical Approach to Polymer Dynamics in Supramolecular Polymers," *Macromolecules*, vol. 52, no. 24, pp. 9427–9444, 2019, doi: 10.1021/acs.macromol.9b02085.

[127] T. Rossow and S. Seiffert, "Supramolecular polymer gels with potential model-network structure," *Polym. Chem.*, vol. 5, no. 8, pp. 3018–3029, 2014, doi: 10.1039/c3py01692g.

[128] S. Seiffert and W. Oppermann, "Systematic evaluation of FRAP experiments performed in a confocal laser scanning microscope," *J. Microsc.*, vol. 220, no. 1, pp. 20–30, 2005, doi: 10.1111/j.1365-2818.2005.01512.x.

[129] H. C. Ishikawa-Ankerhold, R. Ankerhold, and G. P. C. Drummen, "Advanced fluorescence microscopy techniques-FRAP, FLIP, FLAP, FRET and FLIM," *Molecules*, vol. 17, no. 4, pp. 4047–4132, 2012, doi: 10.3390/molecules17044047.

[130] K. Braeckmans, H. Deschout, J. Demeester, and D. S. S. C., "Measuring molecular dynamics by FRAP, FCS, and SPT," in *Optical Fluorescence Microscopy*, A. Diaspro, Ed. Springer-Verlag Berlin Heidelberg, 2011, pp. 153–163.

[131] D. Axelrod, D. E. Koppel, J. Schlessinger, E. Elson, and W. W. Webb, "Mobility measurement by analysis of fluorescence photobleaching recovery kinetics," *Biophys. J.*, vol. 16, no. 9, pp. 1055–1069, 1976, doi: 10.1016/S0006-3495(76)85755-4.

[132] G. I. Hauser, S. Seiffert, and W. Oppermann, "Systematic evaluation of FRAP experiments performed in a confocal laser scanning microscope - Part II: Multiple diffusion processes," *J. Microsc.*, vol. 230, no. 3, pp. 353–362, 2008, doi: 10.1111/j.1365-2818.2008.01993.x.

[133] D. Blumenthal, L. Goldstien, M. Edidin, and L. A. Gheber, "Universal approach to FRAP analysis of arbitrary bleaching patterns," *Sci. Rep.*, vol. 5, pp. 1–9, 2015, doi: 10.1038/srep11655.

[134] S. Tang, A. Habicht, S. Li, S. Seiffert, and B. D. Olsen, "Self-Diffusion of Associating Star-Shaped Polymers," *Macromolecules*, vol. 49, no. 15, pp. 5599–5608, 2016, doi: 10.1021/acs.macromol.6b00959.

[135] F. Di Lorenzo, "Nanostructural Complexity in Polymer Gels and Microgel Packings," Freie Universität Berlin, 2015.

[136] A. Einstein, "Über die von der molekularkinetischen Theorie der Wärme geforderte Bewegung

von in ruhenden Flüssigkeit suspendierten Teilchen," *Ann. d. Phys.*, vol. 322, no. 8, pp. 549–560, 1905, [Online]. Available: http://onlinelibrary.wiley.com/doi/10.1002/andp.19053220806/abstract.

[137] A. Einstein, "Zur Theorie der Brownschen Bewegung," *Ann. Phys.*, vol. 19, pp. 371–381, 1906, doi: 10.1002/masy.200550403.

[138] J. Stetefeld, S. A. McKenna, and T. R. Patel, "Dynamic light scattering: a practical guide and applications in biomedical sciences," *Biophys. Rev.*, vol. 8, no. 4, pp. 409–427, 2016, doi: 10.1007/s12551-016-0218-6.

[139] K. Saalwächter and S. Seiffert, "Dynamics-based assessment of nanoscopic polymer-network mesh structures and their defects," *Soft Matter*, vol. 14, no. 11, pp. 1976–1991, 2018, doi: 10.1039/c7sm02444d.

[140] J. Li and D. J. Mooney, "Designing hydrogels for controlled drug delivery," *Nat. Rev. Mater.*, vol. 1, no. 12, p. 16071, 2016, doi: 10.1038/natrevmats.2016.71.

[141] N. A. Peppas, K. B. Keys, M. Torres-lugo, and A. M. Lowman, "Poly (ethylene glycol) - containing hydrogels in drug delivery," vol. 62, pp. 81–87, 1999.

[142] S. Kondo, H. Sakurai, U. Il Chung, and T. Sakai, "Mechanical properties of polymer gels with bimodal distribution in strand length," *Macromolecules*, vol. 46, no. 17, pp. 7027–7033, 2013, doi: 10.1021/ma401533z.

2. Motivation and scientific goals

The aqueous composition of hydrogels makes them appealing candidates for biomedical applications such as tissue engineering, drug delivery, or wound healing pads. At the same time, they are suitable for hygiene and cosmetic everyday products like contact lenses, diapers, or cosmetic creams. In addition, they can also be used industrially for example for heavy metal removal, as separation/membrane media, and much more.

To keep up with this diverse range of applications and relative specific prerequisites, materials scientists are constantly researching and developing new materials. If we look at the different aforementioned applications, each material has its own specific requirements in terms of mechanics and functionality. In contact lenses, for example, the diffusion of oxygen molecules is crucial. In diapers however, the most important property is the absorbance capacity, whereas in cosmetic creams it is the spreadability. On the contrary, in tissue engineering it is the mechanics that plays a fundamental role and in drug delivery it is the tunable diffusion of the drugs and eventual final degradation of the carrier. Finally, for wound healing applications the injectability or sprayability of the gel would be appealing.

To engineer hydrogels that have such targeted properties, the first step for material scientists is to 'translate' these characteristics into polymer science language. Consequently, diffusion of molecules translates into having a permeable hydrogel, whereas absorbance is synonymous for high hydrophilicity. In addition, injectability and degradation are linked to supramolecular systems and tunable properties call for stimuli-responsive polymers.

After having identified the specific characteristics, the next step is the incorporation and combination of chemical interactions into polymer structures that enables these peculiarities. However, this constitutes a bottleneck, as the spectrum of targeted properties is very broad and diverse and can often not be achieved by a single polymer. To complicate the situation even further, frequently there is the requirement to have multiple features combined in one material and/or the freedom to change these properties on demand. In addition, while the knowledge about single molecules is more established in macromolecular chemistry, less is known about the combination of two or more components in the same polymer network. The prediction of the final abilities of the material is further challenged by the fact that the ultimate properties of the ensemble may differ from the simple sum of the single element's characteristics. In this context, to expand the applicability of hydrogels, the ability to predict the properties of more complex systems is an essential tool for materials scientists and therefore, a field in continuous development. To contribute to this field, the determination of structure–property relationships of multi-component systems is required. In particular, the most rational way to tackle this aspect is methodological studies on model systems.

The fundamental elements that constitute the base for engineering new materials are depicted in **Figure 21**. Having as ultimate goal the requirements of the various applications, the mechanics and functionality of the hydrogel can be accordingly tailored. In addition, to fulfill the increasing interest in sustainability, it is highly desirable to have materials that can be recycled. Finally, it is likewise crucial to be aware of the influence of possible defects on the hydrogels' properties.

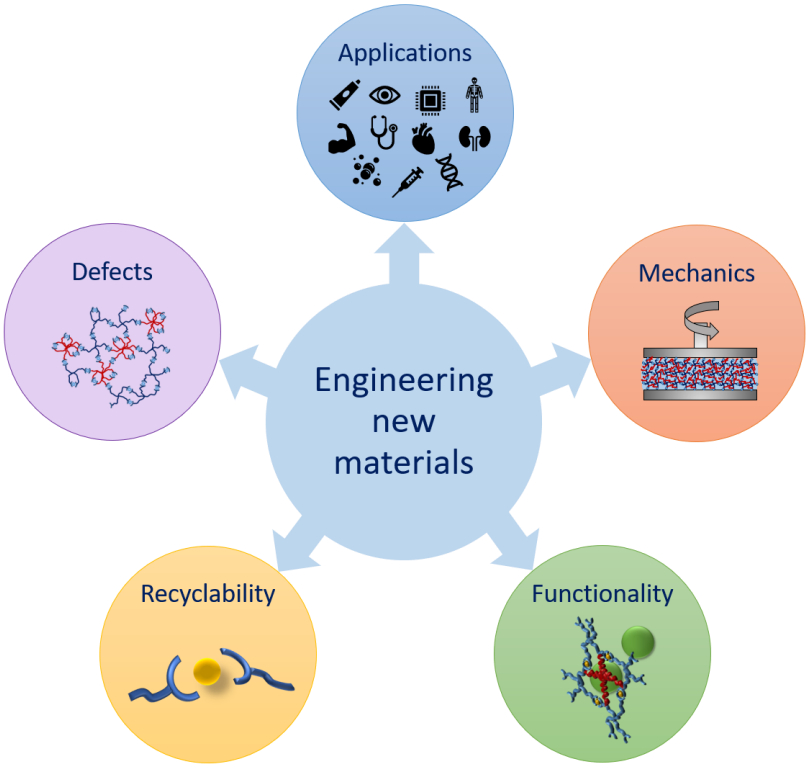

Figure 21. Fundamental elements that constitute a base for a rational engineering of new materials.

This thesis takes all these requirements into consideration and aims to contribute to the field of materials engineering on different levels. First of all, a novel multi-responsive material that is recyclable and that shows tunable mechanics and permeability, is synthesized. Afterwards, to further adjust these properties, the structure–property relationships of this multi-responsive material are studied in a systematic fashion. Finally, the influence of imperfections in the network topology on the mechanics and dynamics of model hydrogels is methodically investigated.

In the **first study**, the synthesis of a novel multi-responsive hydrogel is presented. This material has been designed to account for the high interests on hydrogels to possess multiple different properties that can be further tuned on demand. The multi-responsivity is realized via a dual dynamic network that comprises two dynamic motifs combined in a 4-arm poly(ethylene glycol) (pEG) polymer matrix. The first dynamicity is given by terpyridine, which is a well-known ligand capable of binding in a tridentate fashion to many metal ions and where the choice of different metals allows to tune the strength of the network. In addition, the reversibility of the metal-ligand coordination enables to obtain a recyclable polymer network where the crosslinking can be altered with the pH. Next to the terpyridine

ligand, the second dynamic motif is attached as a grafting chain to the pEG and it comprises the widespread thermo-responsive polymer poly(*N*-isopropylacrylamide) (pNIPAAm). This polymer phase-separates above its lower critical solution temperature undergoing coil to globule transition. If during this process, multiple pNIPAAm chains are in proximity of each other, they might collapse together, resulting in an increase of the elastic modulus as determined by oscillatory shear rheology. In addition, this collective collapse has the further consequence to hinder the diffusion of small diffusants inside the network meshes as investigated by fluorescence recovery after photobleaching. Therefore, the combination of terpyridine and pNIPAAm crosslinks in one single network, enables to exquisitely tune the fundamental network strength and dynamics of the hydrogel in an independent fashion.

To further customize the mechanics of this dual dynamic network, a toolkit for DDN is provided in the **second study**. By varying the molar mass and ratio between the pEG and pNIPAAm units within the network and by applying different metal ions for the terpyridine complexation it is possible to tailor the mechanical properties *ad hoc* by choosing the right combination of these building blocks. The mechanical properties are assessed *via* temperature-dependent oscillatory shear rheology. In addition, comparing the temperature dependence of the elastic plateau moduli in the different samples, it is further possible to draw conclusions about the micro-structure of these dual dynamic networks.

Finally, for rational materials design it is crucial to consider all factors that might have an influence on mechanics and functionality of polymer networks. This includes the presence of defects that can always naturally occur in hydrogels. However, as aforementioned, the determination of structure–property relationships is more challenging for multi-component systems. Therefore, the optimal way to tackle the effect of defects in supramolecular polymer networks is to start with a known model system and later scaling it up to further systems. Taking these considerations into account, in the **third study**, the influence of natural imperfections occurring in supramolecular polymer networks on the elasticity and permeability of a metallo-supramolecular model system is assessed. Since one of the most occurrent types of topological imperfections in polymer networks are connectivity defects, these are inserted systematically into a 4-arm pEG-terpyridine system. The connectivity mismatch is created by introducing different volume ratios of an 8-arm pEG-terpyridine precursor that forms numerous topological defects such as loops as confirmed *via* DQ-NMR. The effect of these defects on the mechanics is unraveled *via* oscillatory shear rheology, whereas the effect on the permeability is determined *via* fluorescence recovery after photobleaching.

Through the systematic study of these dynamic polymer systems, structure–property relationships are assessed on different levels. This assessment constitutes an excellent tool for material scientists for rational engineering of innovative multi-responsive materials for the targeted application.

3. Reversible hydrogels with switchable diffusive permeability

Paola Nicolella,[a] Daniel Lauxen,[a] Mostafa Ahmadi,[a] Sebastian Seiffert[a]

Published in: *Macromolecular Chemistry and Physics*, **2021**, 222: 2100076

DOI: 10.1002/macp.202100076

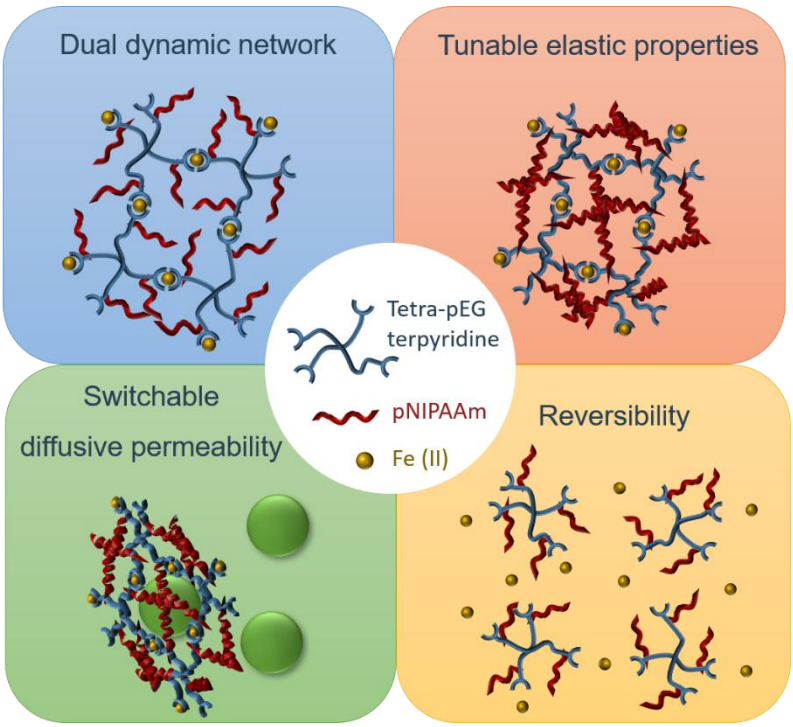

Supplementary information is available in Chapter 10.1.

Author Contributions:

Paola Nicolella: Idea and realization of the project, design of the synthesis route, supervision of Daniel Lauxen during the reproduction of the synthesis, rheological measurements, FRAP experiments, analysis and interpretation of the results, degradability experiments, manuscript preparation, and illustrations

Daniel Lauxen: Reproduction of the synthesis of the polymers under supervision of Paola Nicolella, synthesis of the dye-labelled probe, preliminary FRAP experiments and analysis

Mostafa Ahmadi: Useful discussions on rheology and degradability studies

Sebastian Seiffert: Concept and supervision of the work, correction of the manuscript

[a]*Johannes Gutenberg-Universität Mainz, Department of Chemistry,*
Duesbergweg 10-14, D-55128 Mainz, Germany

Summary

To account for the increasing demand of engineering hydrogels that possess multiple properties in the same material and therefore, expand their applicability, dual dynamic networks (DDN) offer an outstanding platform. These materials provide an unparalleled tunability of the properties of polymer networks, as they combine two dynamic motifs within a single network. These can be activated independently and thus provide the basis for multi-stimuli responsive materials.

In this work, a novel dual dynamic network is synthesized and its tunable properties are explored. The DDN is composed of tetra-arm poly(ethylene glycol), where each arm is functionalized with two dynamic motifs. The first one is terpyridine, which forms metallo-supramolecular complexes with bivalent metal ions such as iron(II). The second dynamic motif is the widespread thermo-responsive polymer poly(*N*-isopropylacrylamide) which undergoes a phase-separation in water above its lower critical solution temperature (LCST).

The presence of the terpyridine groups enables the hydrogel to be reversibly degraded and restored, upon change of the pH, laying the ground for recyclability. Moreover, upon switching the temperature above the LCST, the DDN doubles its elastic modulus as investigated by oscillatory shear rheology and the diffusion of small diffusants is hindered as investigated by fluorescence recovery after photobleaching.

These results are achieved through the collective collapse of the thermo-responsive chains above the LCST with consequent formation of new reversible crosslinks, increase in the elastic modulus, and decrease of the average mesh-size. This multi-responsive polymer system offers a material basis for potential separation or membrane applications.

Acknowledgments

This work was financially supported by funding from the H2020 Programme (MARIE SKŁODOWSKA-CURIE ACTIONS) of the European Commission's Innovative Training Networks (H2020-MSCA-ITN-2017) under DoDyNet REA Grant Agreement No. 765811. The authors thank Holger Adams for the construction of the FRAP measurement cell. Paola Nicolella thanks Marco Cirelli, Christina Pyromali, and Katharina Breul for useful discussions.

Open access funding enabled and organized by Projekt DEAL.

1. Introduction

Hydrogels are polymer network bodies filled and swollen by water. [1, 2] This constitutes "shape-stable water", that is, fluid water held in place by a polymer-network skeleton. The most characteristic and favorable properties of hydrogels are their soft mechanics and high diffusive permeability for molecular diffusants. [3, 4] The latter is made possible by slip-through of small molecular-scale diffusants through the nanometer-scale network meshes. [5, 6] This property can be used in applications like separation techniques or membrane systems. [7] However, to increase the application spectrum, it is necessary to be able to control the diffusive permeability on demand via an external stimulus; gaining such control is a developing research direction. [8]

A way to achieve such control of the diffusive permeability is to use thermoresponsive membranes, where a thermoresponsive polymer is either attached to a solid substrate or is present in form of a thin hydrogel film. [8-10] In general, diffusion through a polymer-network gel is determined by the mesh size, and this can be controlled in several ways, such as increasing the concentration of the polymer or by changing the structure of the polymer network, for example, through introduction of dangling chains. [11, 12] Here, we employ thermoresponsive dangling chains to exquisitely control the mesh size on demand upon switch of temperature. On top of that, in polymer science, as well as in every other branch of materials science, there is an increasing demand for a sustainable footprint, here meaning a gel that is reversible. [13] An advance in the field of thermoresponsive membranes would be to have a switchable material that can not only reversibly change its diffusive permeability upon application of an external trigger like a change of temperature, but that can also improve its mechanical properties upon the application of such a stimulus. To our knowledge, these three properties, namely reversibility, switchable diffusive permeability, and enhanced mechanical properties, have not been yet investigated in the same hydrogel. In this paper, we present a dual dynamic network (DDN) that provides all the above-mentioned needs in one material with the opportunity to tune them in an independent fashion, as it can be visualized in **Figure 1**.

For this purpose, we make use of two suitable chemical motifs: for the thermosensitive switchability, we use the most widespread and famous thermoswitchable polymer, which is poly(*N*-isopropylacrylamide) (pNIPAAm). [14] For the reversibility, we make use of terpyridine, which is capable of forming metallo-supramolecular bonds with metal ions. [15] The resultant noncovalent bond is stable like covalent bonds at certain conditions, [16] but degradable at others. To realize a well-defined permeable microstructure, [17] we use four-arm polyethylene glycol (pEG) that is capable of forming a model supramolecular network; [18] this will allow us to rationally understand the switching material properties on the basis of a nanostructural picture. We realized a dual network composed of tetra-arm pEG, in which each arm is functionalized with terpyridine, capable of forming metal–ligand complexes, and a thermoresponsive polymer, pNIPAAm. Reversibility is achieved by treating the gel with acid and base. The switchable diffusive permeability of the network is investigated via tracer diffusivity probed

by fluorescence recovery after photobleaching (FRAP) below and above the lower critical solution temperature (LCST) of pNIPAAm. Macroscopically, the elasticity of the network is investigated with linear rheology upon variation of temperature.

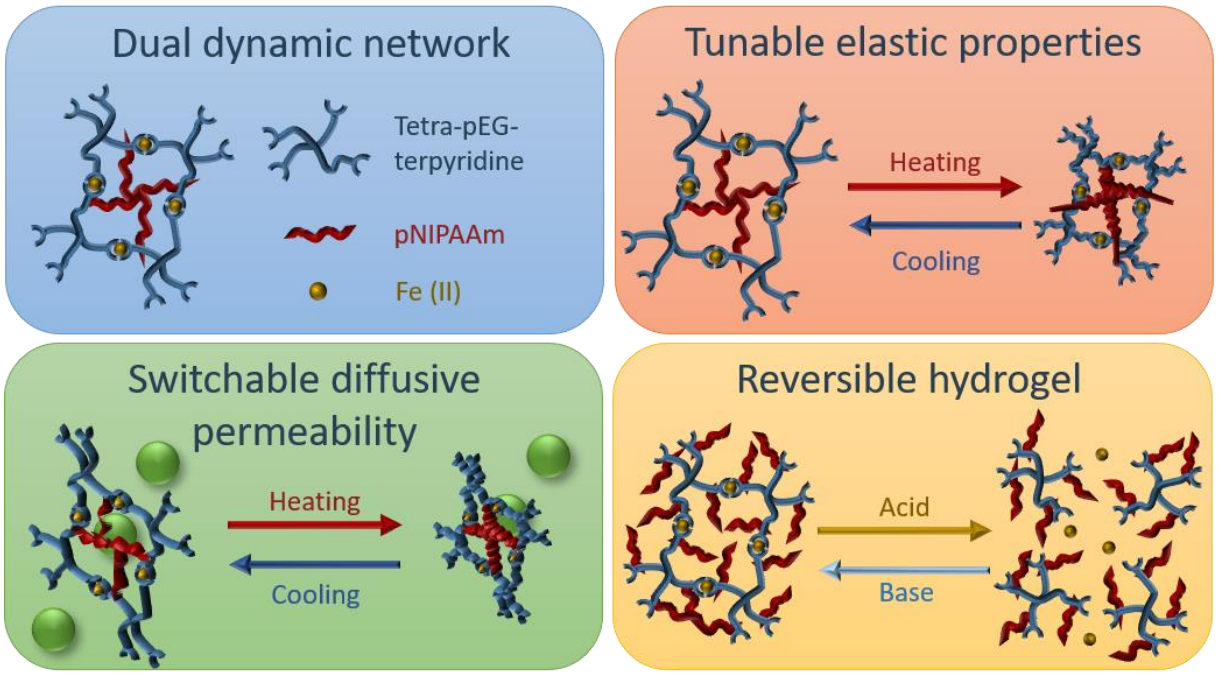

Figure 1. Concept of this work. A dually dynamic polymer network makes it possible to combine multiple properties in one material. Specifically, the diffusive permeability and the elastic modulus of the hydrogel can be tuned with temperature, and the reversibility of the gel can be triggered with pH.

2. Results and Discussion

2.1 Synthesis of the Dual Dynamic Network

The synthesis of the dual dynamic network is sketched in **Scheme 1**. The starting point of the synthesis is a four-arm pEG with terminal –OH groups. These are converted into epoxy rings through the addition of epichlorohydrin. Afterward, the epoxy ring is opened and the pEG then has two functional groups on each arm: one hydroxyl and one azide group. The azide group reacts with propargyl-terpyridine, where the terpyridine (together with the metal) provides the first dynamic moiety. The hydroxyl groups are then transformed first into *N*-hydroxysuccinimidyl (NHS) groups, and afterward these react with amine-functionalized pNIPAAm, to form the second dynamic moiety.

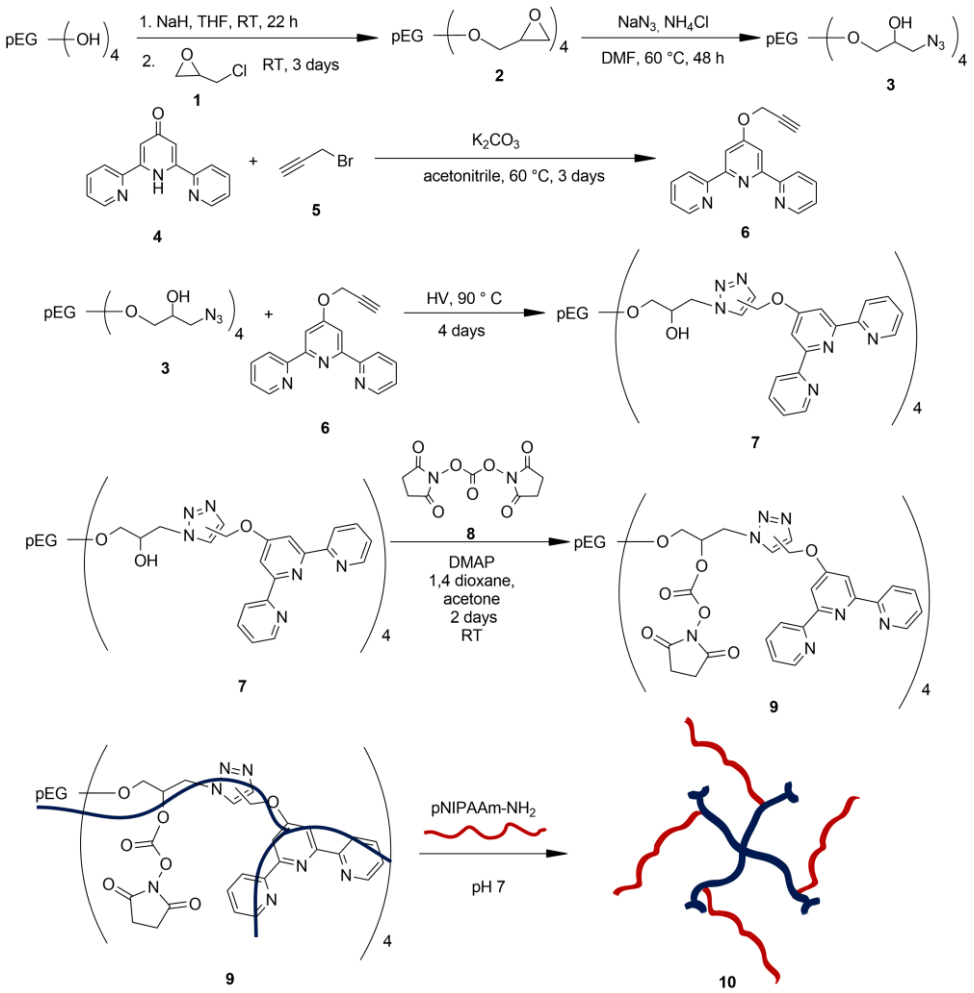

Scheme 1. Synthesis of the dual dynamic network composed of tetra-pEG-pNIPAAm-terpyridine (10).

2.2 Dual Dynamic Hydrogels

The aim of this work is to provide a polymer hydrogel that combines switchable elasticity and diffusive permeability as well as reversibility in one material, with independent tunability of these properties. We realize this goal in a dual dynamic hydrogel based on tetra-arm pEG, where each arm provides a double dynamic functionalization. The first functional motif is terpyridine, which is able to form a metal–ligand complex with metal ions. In this work, we used Fe(II) tetrafluoroborate hexahydrate for complexation in stoichiometric amount to the terpyridine, i.e., for every pair of terpyridine there is a metal ion. The second dynamic motif is pNIPAAm graft oligomers, which is a thermoresponsive polymer with an LCST around 32 °C in aqueous surrounding. [14] The cloud point of the complete tetra-pEG-pNIPAAm-terpyridine polymer is probed with UV–vis spectroscopy and taken as an indication of the LCST, denoting it to be 32.5 °C, that is, not distant from the LCST of pure pNIPAAm. We assume that the transition is complete beyond that temperature, as the sample transmittance is afterward constantly zero from there on (see **Figure S1** in the Supporting Information). We chose a tetra-pEG basis of 10 000 g mol^{-1} and a pNIPAAm of 5500 g mol^{-1}. There are four pNIPAAm chains for each star-pEG, so the total amount of pNIPAAm in weight is 68.75%. The polymer concentration for the gels is 100 g L^{-1}. So, in a

100 g L^{-1} sample, the concentration of pEG is 31.25 g L^{-1}, and the concentration of pNIPAAm is 68.75 g L^{-1}. With that platform, we form gels that can be switched by toggling the pNIPAAm branches from solvated to collapsed states, thereby toggling the gel-network mesh sizes and hence the gel elasticity, and that can be degraded by dissociation of the iron–terpyridine complexes. To assess this, we probe the gel diffusive permeability by monitoring the diffusivity of a fluorescent probe in the gel with FRAP, and we also study the change in the gel elastic modulus upon switch of temperature below and above the LCST of pNIPAAm in water with rheology. We also study the reversibility of the network upon change of pH.

2.3 Reversibility

To obtain a reversible gel, we include a motif that can be broken and rebuilt on demand; we realize this by terpyridine–metal complexes. Depending on the choice of metal ion, the strength of the complex varies. We chose a "strong" ion such Fe(II), that forms a strong complex with terpyridine that is active at 554 nm of the visible spectrum, giving to the complex a peculiar purple color. [19] This complex is stable in air: during observations over a long time scale (months), we did not observe any change in color. Moreover, Fe(II) has a preference to coordinate with nitrogen atoms rather than oxygen atoms, in contrast to its oxidated form Fe(III), that has preference to be in coordination with oxygen atoms. [20] Complexes with iron can be as strong as covalent bonds, but by change of the ion oxidation state, that strength can be drastically altered. For example, hydrogels with Fe(II) are durable and appear like covalent gels, whereas hydrogels with Fe(III) are fluidic on long timescales. If the aim is to weaken the gel, then oxidation of the metal ion is the way to go; however, since we intend to achieve a complete disassembly and not only a weakening of the network, we use a different approach and act on the bond between the terpyridine and the metal ion rather than just on the metal ion. Based on that premise, we form a hydrogel by adding 10 µL of Fe(II) solution to a 90 µL concentrated solution of pEG-pNIPAAm terpyridine, thereby achieving a total polymer concentration of 100 g L^{-1} in the gel. To the 100 µL gel, 30 µL of 37% HCl solution are added, and the flask is vortexed vigorously. Decomplexation is achieved in about 20 min, as shown in **Figure 2**.

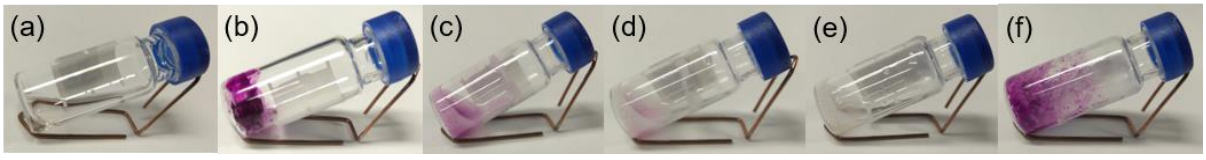

Figure 2. Reversibility of the double dynamic kind of gel treated in this work. The polymer solution (a) is mixed with Fe(II) and forms a gel (b). Upon addition of HCl, the metal complex between the iron and the terpyridine breaks (c–d), and the gel turns into a sol (e). Upon addition of NaOH, the metal complex forms again and the gel is restored (f).

As it can be seen in **Figure 2 (b–e)**, upon addition of the acid, the color of the gel changes from purple to colorless gradually. The gel linking nodes decomplex because the acid protonates the nitrogen atoms of the terpyridine that are therefore no more capable of forming the complex with the iron. This way, the complex between the terpyridine and the iron is broken and the network disassembles. However, this process is reversible. By using a base, such as NaOH, the terpyridine is deprotonated and the nitrogen atoms can form again the supramolecular bond with the iron. To reform the gel, 20 µL of 50% NaOH solution is added and the solution is vortexed. Upon that, the gel forms back within 10 min and regains its purple color, indicating that the bond between the terpyridine and the iron has reformed again.

2.4 Switchable Diffusive Permeability

The diffusive permeability of the network is assessed by monitoring the diffusivity of a macromolecular probe within the gel with FRAP. To see how the permeability changes upon switch of temperature, FRAP measurements are done below and above the LCST of pNIPAAm in water, respectively at 25 and 36 °C. The fluorescent probe is a four-arm pEG 10 000 g mol^{-1} functionalized with rhodamine B. FRAP measurements are performed in a custom-made cell that allows the temperature to be controlled with ±1 °C precision. In FRAP, a fluorescent probe that is incorporated in the sample is bleached with high intensity laser light in a spot in the sample. In that spot, the bleaching produces a dark region with Gaussian radial intensity profile of the extent of bleaching, exhibiting typical width (measured as the variance of the Gaussian) of about 2 µm right after bleaching. After the bleaching, a series of post-bleach images are recorded at fixed time intervals. During that period, bleached molecules diffuse outside the spot whereas not-bleached molecules diffuse inside of it. This exchange of bleached and unbleached molecules leads to diffusive smearing of the Gaussian, which can be quantified and analyzed by comparison to analytical functions that solve the diffusion equation for that kind of initial and boundary conditions. As a result, we obtain the translational diffusion coefficient. [21] If the data fitting is done with a superposition of multiple Gaussians, we obtain a distribution of diffusion coefficients, thereby appropriately treating polydisperse diffusion scenarios. [22] In our work, we compare how the diffusion of tetra-pEG-rhodamine is influenced by the temperature in the tetra-pEG-pNIPAAm-terpyridine hydrogel respectively below and above the LCST of pNIPAAm in water.

In **Figure 3**, the FRAP series of images are shown for 25 °C i) and 36 °C ii). The first images (a) display the pre-bleach situation and are the result of an averaging of four pictures. Image (b) shows the sample immediately after the bleaching. Images (c–f) represent the evolution upon diffusion respectively after 1, 2, 5, and 10 s after the bleach. As it can be seen in **Figure 3i**, in the case of the sample at 25 °C, the bleached spot disappears within the first 5 s, whereas, as it can be seen from **Figure 3ii**, in the case of 36 °C, the bleached spot remains constant in the considered timeframe.

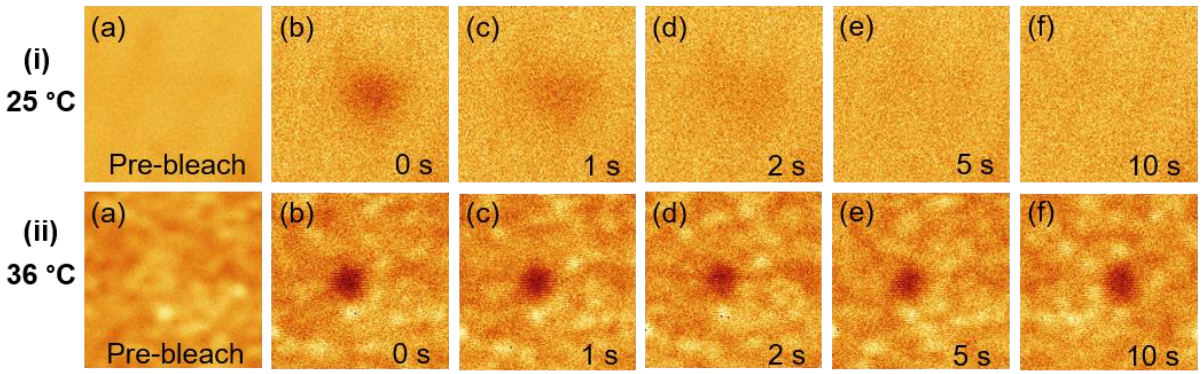

Figure 3. FRAP measurements of the dual dynamic hydrogel performed below i) and above ii) the LCST of pNIPAAm in water, where the diffusive probe is a tetra-pEG functionalized with rhodamine B. The first image of each series (a) is before the bleaching, the second image (b) is at the bleaching, while the others (c–f) are taken respectively after 1, 2, 5, and 10 s. Below the LCST, the bleached spot disappears within the first 5 s, whereas above the LCST, the bleached spot remains. Each image is about 50 × 50 μm^2.

Diffusion coefficients are calculated by averaging six measurements for each temperature and calculating the standard error. The Gaussian curves relative to the two temperatures can be found in **Figure S2** (Supporting Information) where it can be noticed that the number of curves at room temperature is low compared to the ones at higher temperature, due to the fact that the bleaching spot disappears fast at room temperature. At 25 °C, the average diffusion coefficient is (9.46 ± 1.53) $\mu m^2\ s^{-1}$, while at 36 °C, the average diffusion coefficient is (0.10 ± 0.07) $\mu m^2\ s^{-1}$. Hence, above the LCST of pNIPAAm, the diffusion coefficient is almost two orders of magnitude smaller than at room temperature. This means that the diffusion of the fluorescent probe is drastically hindered above the LCST of pNIPAAm. This can be ascribed to the pNIPAAm chains that collapse and aggregate with each other in the gel network at those conditions, thereby blocking the passage of the dye-labeled probe by forming an obstacle for the diffusion of the probe between the meshes. To further investigate the system, the same FRAP experiments were performed by probing the diffusion of only the dye. For this purpose, the tetra-pEG-pNIPAAm-terpyridine was mixed with a solution of rhodamine B isocyanate having the same concentration of the dye on the pEG-rhodamine probe. By performing the experiment above the LCST, it could be noted that also in the case of only dye, the bleaching spot stayed. Therefore, the decrease in the diffusion coefficient of the fluorescent dyes results from the combination of two effects. On one side there is the decrease of the mesh sizes due to the aggregation of multiple collapsing pNIPAAm chains, as manifesting itself also in rheology, and on the other side there is the contribution of the interaction and partial entrapment of the dye molecules with pNIPAAm. Moreover, it is observed that the total volume of the hydrogel remains constant with temperature (see **Figures S3** and **S4** in the Supporting Information). Therefore, the volume shrinks locally due to the collapsing of the pNIPAAm chains, and there will then be highly concentrated zones where the diffusion of the probe is completely blocked and less concentrated zones where the probe can still diffuse. Therefore, there is still some diminished but not completely vanished mobility of the traces. This interpretation is supported visually in **Figure 3**,

where the sample above the LCST shows brighter and darker spots. Prospectively, super-resolution microscopy techniques could be employed to characterize that type of sample heterogeneity. These heterogeneities derive from the microphase-separation and the aggregation of pNIPAAm in bigger clusters. Below LCST, by contrast, the probe species can diffuse quite freely within the gel. This pronounced difference in molecular mobility provides a useful means for the development of thermo-responsive membranes with switchable diffusive permeability.

2.5 Tunable Elastic Properties

To test the change of the elastic properties of the gel, rheological measurements are performed. For this purpose, frequency sweeps are recorded at 25 and 35 °C, respectively below and above the LCST of the pNIPAAm chains in the samples. In addition, temperature cycles are performed to study the elastic response on a larger scale of temperatures.

2.5.1 Frequency Sweeps

To test the temperature dependence of the elastic modulus of the polymer below and above the LCST of the pNIPAAm chains in the samples, frequency sweeps are recorded from 20 to 0.01 rad s^{-1}, respectively at 25 and at 35 °C with a shear amplitude of $\gamma = 1\%$. To avoid rupture of the gel with the transfer to the rheometer, the gel is formed directly on the instrument with a polymer concentration of 100 g L^{-1}.

The storage (full symbols) and loss (empty symbols) moduli are shown as a function of the frequency at 25 °C (blue) and 35 °C (red), respectively, below and above the LCST of pNIPAAm, as shown in **Figure 4**. The rheological spectra display that G' and G'' are constant in the considered frequency range. This covalent-gel like signature is caused by the strong complexes that iron forms with the terpyridine. Upon increase of the temperature from 25 to 35 °C, the elastic modulus doubles from 1000 Pa to 2000 Pa. Qualitatively, this finding is explainable by the microphase-separation of the pNIPAAm chains above their LCST in our hydrogels, which creates domains that act as additional crosslinks, thereby enforcing the gel. Quantitatively, though, these values are still lower than their estimates calculated with the phantom-network model, that are 7740 and 8002 Pa, respectively, for 25 and 35 °C. There are several factors that can contribute to lowering the modulus, and the main factor is probably network defects and inhomogeneities. [23] The theoretical value of the modulus is calculated taking into account a perfectly homogeneous network where each arm is an elastically active chain. However, in real networks there are defects and inhomogeneities such as dangling chains, loops, and spatial variation of the crosslinking density. [23] These could be also partially due to the steric hindrance of the pNIPAAm chains in proximity of the terpyridine group. From the elastic modulus, we can also estimate the average mesh-size of the hydrogel network as $\xi = (RT/G'N_A)^{1/3}$, where R is the gas constant (8.13 J mol^{-1} K^{-1}), T is the temperature (respectively 298.15 K and 308.15 K), G' is the elastic modulus and N_A is the Avogadro constant. [24] With that simple estimate, the average mesh size at 25 °C is found to be 16 nm, whereas

the one at 35 °C is 13 nm. This mesh-size is reasonable, as the average distance between pNIPAAm dangling chains calculated through its molar concentration is 8 nm. [25]

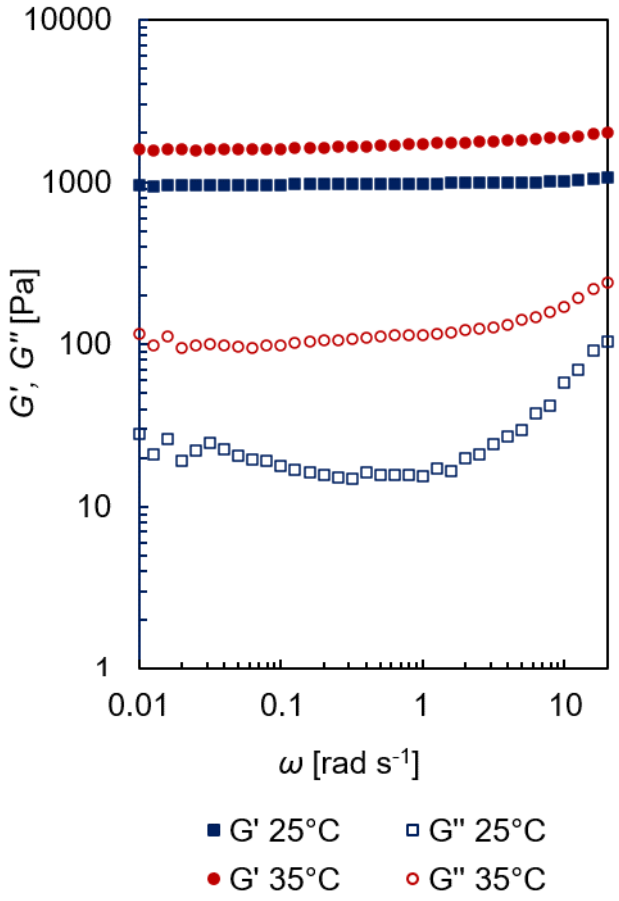

Figure 4. Frequency dependence of the storage modulus (full symbols) and loss modulus (empty symbols) at 25 °C (blue squares) and 35 °C (red circles) of the dual dynamic hydrogel, for a polymer concentration of 100 g L^{-1} and measured with a shear amplitude of $\gamma = 1\%$.

2.5.2 Temperature Cycles

To further study the temperature-dependence of the storage and loss moduli in an even extended temperature range, temperature cycles are recorded between 10 and 40 °C with $\gamma = 1\%$ and $\omega = 1$ rad s^{-1} for a polymer concentration of 100 g L^{-1}. First, the sample is allowed to equilibrate at 10 °C, and then a heating ramp is performed up to 40 °C. After equilibrating the sample at 40 °C, a cooling ramp is performed back down to 10 °C with the same rate as the heating ramp. A complete heating–cooling cycle is shown in **Figure 5**.

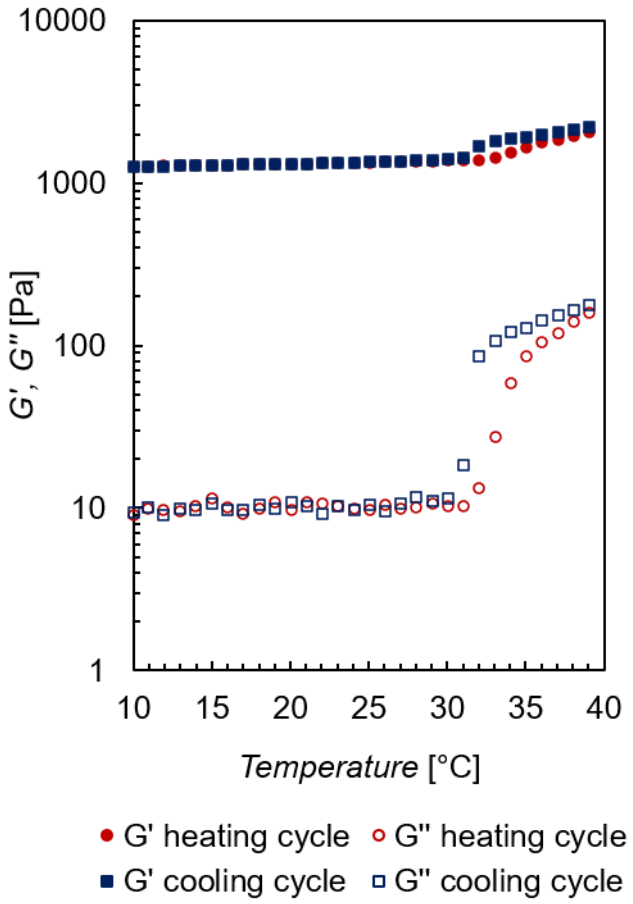

Figure 5. Temperature dependence of the storage modulus (full symbols) and loss modulus (empty symbols) recorded at $\gamma = 1\%$ and $\omega = 1$ rad s^{-1} for a polymer concentration of 100 g L^{-1}. The red dataset (circles) denotes the heating cycle and the blue dataset (squares) denotes the cooling cycle. Around the LCST, a hysteresis in the cooling cycle is observed.

The storage and loss moduli are linear from 10 to 32 °C. From 32 °C, the pNIPAAm starts to phase-separate. This can be seen in the heating cycle with an increase of both the storage and loss moduli. While the elastic modulus increases smoothly, the loss modulus increases more steeply, with an inflection point around the LCST of pNIPAAm. At 40 °C, the elastic modulus has doubled and the loss modulus has increased of one order of magnitude, compared to their respective values at 10 °C. The cooling cycle shows hysteresis around the LCST for both moduli. This can be explained by considering that when the pNIPAAm chains collapse due to phase separation, they form clusters, and the time and/or energy needed for breakage of these clusters causes a hysteresis in our kind of experimental assessment. From 30 °C, the cooling cycle overlaps with the heating cycle again. This means that the material recovers completely and that its elastic properties are reversible.

3. Conclusion

The multifunctional dual dynamic polymer network introduced in this work proved a material platform that has switchable diffusive permeability and is reversible with the possibility to tune these properties independently from each other. Reversibility can be achieved by acidification, whereby the gel can be recovered with a base. In addition, switchable diffusive permeability can be achieved by varying the temperature. Along with that, the gel doubles its elastic modulus upon heating. Combining all these properties in one material is appealing for separation or membrane applications. Further studies may include different lengths of the thermo-responsive graft polymer and use of different metal ions for the metallo-supramolecular junctions, thereby exploring the range of switchability and reversibility.

4. Experimental Section

Synthesis–Materials: Tetra-hydroxyl polyethylene glycol (pEG) (10 000 g mol^{-1}) was purchased from JenKem Technology (Plano, Texas, USA). Tetra-pEG-amine (10 000 g mol^{-1}) was purchased from Biochempeg Scientific. Amine-functionalized pNIPAAm (5500 g mol^{-1}) was purchased from Sigma Aldrich. Sodium hydride 57–63 wt% oil dispersion and 4-(dimethylamino)-pyridine 99% were purchased from Alfa Aesar (Thermo Fisher). Tetrahydrofuran 99.8% (THF), dichloromethane 99.8% (DCM), diethyl ether 99.5%, dimethylformamide 99.5% (DMF), methanol 99.8%, sodium chloride, and potassium carbonate (anhydrous) were purchased from Fisher Scientific. Sodium azide 99% and sodium carbonate (anhydrous) 99.5% were purchased from Fluka. Epichlorohydrin 99%, magnesium sulphate 97% (pure anhydrous), ammonium chloride, dry 1,4 dioxane 99.5%, acetonitrile 99.99%, and propargyl bromide 80 wt% in toluene were purchased from Acros Organics. Potassium dihydrogen phosphate 99% was purchased from ROTH. Activated carbon Norit A was purchased from Aldrich Chemical Company Inc. 2,6-bis (2-Pyridyl)-4(1H)-pyridone 98% was purchased from TCI. Chloroform Uvasol and sodium hydroxide solution 50% were purchased from Merck. Hydrochloric acid 37%, n-heptane, and di-sodium hydrogen phosphate anhydrous were purchased from VWR Chemicals. Dimethylsulfoxide-d_6 99.8% (DMSO) was purchased from Deutero. Iron(II) tetrafluoroborate hexahydrate 97%, rhodamine B isocyanate, and *N*,*N*′-disuccinimidyl carbonate 95%, were purchased from Aldrich.

Tetra-pEG-Epoxide (2): Tetra-pEG-hydroxyl 10 000 g mol^{-1} (13.06 g, 1.306 mmol, 1 eq.) is melted at 80 °C in high vacuum. The temperature is decreased to 40 °C and dry THF (320 mL) is added for dissolution. Sodium hydride 60 wt% in mineral oil (1.67 g, 41.79 mmol, 32 eq.) is added at room temperature and the mixture is stirred for 22 h. Afterward, epichlorohydrin (**1**) (8.2 mL, 104.48 mmol, 80 eq.) is added and the solution is stirred for 3 days. Few drops of distilled water are added and the product is extracted five times with DCM (300 mL) and brine (50 mL). Afterward, it is dried with magnesium sulphate and filtered. The concentrated solution is precipitated in cold diethyl ether (1 L), stirred for 30 min, filtered, and dried overnight in high vacuum (yield 80.5%). ^{1}H-NMR (DMSO-d_6, 400 MHz, δ = ppm): 3.70 (m, 3H), 3.51 (m, 909H, pEG backbone), 3.25 (m, 3H), 3.09 (m, 3H), 2.72 (m, 3H), 2.52 (s, 1H), 3.87 (s, 4H).

Tetra-pEG-Hydroxy-Azide (3): Tetra-pEG-epoxide (**2**) (10.63 g, 1.04 mmol, 1 eq.) is dissolved in DMF (110 mL), then sodium azide (2.77 g, 42.65 mmol, 41 eq.) and ammonium chloride (4.54 g, 84.88 mmol, 82 eq.) are added and the solution is stirred for 48 h at 60 °C. The product is extracted three times with brine (50 mL) and DCM (400 mL). Afterward, it is dried with magnesium sulphate, filtered, distilled, and precipitated in cold diethyl ether (1 L). After stirring for 30 min, it is filtered and dried overnight in high vacuum (yield 67%). ^{1}H-NMR (DMSO-d_6, 400 MHz, δ = ppm): 5.25 (d, 3H), 3.77 (m, 3H), 3.68 (m, 5H), 3.51 (m, 909H, pEG backbone), 3.37 (m, 5H), 3.25 (d, 10H), 3.19 (m, 3H).

Propargyl-Terpyridine (6): To obtain the propargyl-terpyridine (**6**), potassium carbonate (10.08 g, 72.938 mmol, 6.1 eq.) is dried in high vacuum for 90 min, and then 2,6-bis(2-pyridyl)-4(1H)-pyridone (**4**) (3 g, 12.035 mmol, 1 eq.) is added. The reagents are suspended in dry acetonitrile (120 mL) for 2 h, and afterward propargyl bromide (5) (9.2 m in toluene, 1.6 mL, 14.72 mmol, 1.2 eq.) is added dropwise. The mixture is stirred for 3 days at 60 °C and then precipitated in cold water (500 mL), filtered and dried overnight in high vacuum. In order to have a colorless product, the resulting propargyl-terpyridine is dissolved in n-heptane (500 mL) at 98 °C and two spoons of active carbon are added. Then, the suspension is filtered over a hot funnel with an ice bath around the flask for recrystallization. Afterward, the product is filtered and dried overnight in high vacuum (yield 52%). ^{1}H-NMR (DMSO-d_6, 400 MHz, δ = ppm): 8.74 (ddd, 2H), 8.62 (dt, 2H), 8.05 (s, 2H), 8.01 (td, 2H), 7.51 (ddd, 2H), 5.11 (d, 2H), 3.72 (t, 1H).

Tetra-pEG-Hydroxy-Terpyridine (7): Tetra-pEG-hydroxy-azide (**3**) (7.15 g, 0.688 mmol, 1 eq.) is dried in high vacuum for 30 min. Afterward, propargyl-terpyridine (**6**) (1.64 g, 5.708 mmol, 8.3 eq.) is added, and the mixture is heated to 90 °C. It is stirred under high vacuum at 90 °C for 4 days. After cooling the temperature down to 40 °C, DCM (50 mL) is added. The solution is precipitated in cold diethyl ether (1 L) and stirred for 30 min. Afterward, it is filtered and dried overnight in high vacuum (yield 78%). The degree of functionalization is assessed by UV–vis spectroscopy in chloroform Uvasol to be 90% and with H-NMR to be 75–87.5%. This difference in functionality might be due to phase/baseline correction in the NMR spectra. However, this 10% difference should not impact the properties of the hydrogel, as a lower functionalization falls together with the effect of defects, such as for example dangling chains, as discussed before. Moreover, in case there would be an additional effect, it would be the same for both temperatures and therefore the relative behavior that is investigated would not change. ^{1}H-NMR (DMSO-d_6, 400 MHz, δ = ppm): 8.73 (m, 6H), 8.63 (m, 6H), 8.21 (s, 1H), 8.10 (d, 6H), 8.02 (m, 6H), 7.88 (s, 1H), 7.51 (m, 6H), 5.61 (s, 2H), 5.45 (s, 4H), 5.37 (d, 1H), 5.32 (d, 2H), 4.45 (m, 7H), 4.00 (m, 4H), 3.68 (t, 5H), 3.47 (m, 909H, pEG backbone), 1.24 (s, 1H).

Tetra-pEG-N-Hydroxysuccinimide-Terpyridine (9): Tetra-pEG-hydroxy-terpyridine (**7**) (6.2 g, 0.537 mmol, 1 eq.) is dried for one hour in high vacuum. Afterward, dry 1,4-dioxane (30 mL) is added, and the tetra-pEG-hydroxy-terpyridine is dissolved at 40 °C. At the same time, *N*,*N*′-disuccinimidyl carbonate (**8**) (1.10 g, 4.298 mmol, 8 eq.) is dissolved in dry acetone (10 mL) and 4-

dimethylaminopyridine (DMAP) (0.53 g, 4.338 mmol, 8.1 eq.) is dissolved in dry acetone (10 mL). To the *N*,*N*′-disuccinimidyl carbonate suspension, first the tetra-pEG-hydroxy-terpyridine and then the DMAP are added dropwise. The solution is stirred for 2 days and then precipitated in cold diethyl ether (500 mL). After filtering, the product is dried overnight in high vacuum (yield 78%). ^{1}H-NMR (DMSO-d_6, 400 MHz, δ = ppm): 8.73 (d, 6H), 8.63 (m, 6H), 8.28 (s, 2H), 8.10 (m,6H), 8.02 (m, 6H), 7.52 (m, 6H), 5.47 (m, 10H), 4.77 (m, 7H), 3.47 (m, 909H, pEG backbone), 2.78 (m, 13H).

Tetra-pEG-pNIPAAm-Terpyridine (10): Amine-functionalized pNIPAAm is attached to the tetra-pEG-*N*-hydroxysuccinimide-terpyridine (**9**) via a click reaction. For this purpose, a buffer solution (500 mL) with a pH value of 7 is prepared with potassium dihydrogen phosphate (3.52 g, 25.871 mmol) and disodium hydrogen phosphate (5.79 g, 40.798 mmol). A neutral pH is achieved with addition of 50% sodium hydroxide solution. Tetra-pEG-*N*-hydroxysuccinimide-terpyridine (**9**) (1.01 g, 0.083 mmol, 1.0 eq.) and 5500 g mol^{-1} amine-terminated pNIPAAm (3.93 g, 0.714 mmol, 8.6 eq.) are dissolved in the buffer solution (100 mL) and stirred overnight. Afterward, the solution is freeze dried, and the unreacted pNIPAAm is separated by dialysis over two weeks, with membranes having a MWCO value of 6–8 kDa (yield 106%). The success of the chain-end functionalization is determined with DOSY-NMR (see **Figures S14–S16** in the Supporting Information), as in the spectra of the copolymer, the pEG and the pNIPAAm show the same diffusion coefficient being 20.9 μm^2 s^{-1} for the pNIPAAm and 19.6 μm^2 s^{-1} for the pEG, thereby denoting them to be one united species, whereas the free pNIPAAm shows a faster diffusion coefficient of 30.1 μm^2 s^{-1}.

The degree of functionalization can be determined with NMR by comparison of the integrated peaks of the pEG backbone and of the pNIPAAm. The integrals of the pNIPAAm chains show an additional 30% in respect to the theoretical values, and the total reaction yield is 106%. Even though the pNIPAAm content has halved during dialysis, as it can be observed by comparing the integrated pNIPAAm peaks in the NMR spectra before and after dialysis (see **Figures S12** and **S13** in the Supporting Information), there is an additional percentage of loose pNIPAAm chains that are still in the network and that were not possible to dialyze out. These pNIPAAm chains will certainly collapse above the LCST, and in case they are in proximity of the graft chains in the network, they might take part in the clusters. However, it is not expected that these loose chains have a marked influence on the network properties as they are not connected to the network. The cloud point of the tetra-pEG-pNIPAAm-terpyridine, is assessed via UV–vis spectroscopy to be 32.5 °C by measuring the transmittance at different temperatures and extrapolating the inflection point of the curve and taking it as an indication of the LCST.

^{1}H-NMR before dialysis (DMSO-d_6, 400 MHz, δ = ppm): 8.72 (m, 7H), 8.62 (m, 8H), 8.21 (s, 2H), 8.04 (m, 17H), 7.54 (m, 17H), 7.18 (m, 479H), 6.15 (m, 6H), 5.67–5.49 (m, 11H), 4.62 (s, 6H), 3.84 (s, 556H, pNIPAAm), 3.50 (s, 909H, pEG), 1.96 (s, 522H, pNIPAAm), 1.45 (m, 1225H, pNIPAAm), 1.04 (s, 2697H, pNIPAAm). ^{1}H-NMR after dialysis (DMSO-d_6, 400 MHz, δ = ppm): 8.73 (m, 7H), 8.63 (m, 6H), 8.22 (d, 2H), 8.10 (m,7H), 8.01 (m, 6H), 7.52 (m, 6H), 7.16 (m, 252H pNIPAAm), 5.61 (s, 3H), 5.45 (s, 4H), 5.08 (m, 2H), 4.67 (m, 1H), 3.85 (m, 286H, pNIPAAm), 3.49 (m, 909H, pEG backbone),

1.98 (s, 335H, pNIPAAm), 1.46 (m, 623H, pNIPAAm), 1.12 (m, 1898H, pNIPAAm). All NMR spectra can be found in the Supplementary Information.

Tetra-pEG-Rhodamine B: For FRAP experiments, a fluorescent probe is synthesized, composed of four-arm 10 000 g mol^{-1} pEG, functionalized with rhodamine B. For this purpose, a saturated solution (200 mL) of sodium carbonate in methanol is prepared, and tetra-pEG-amine 10 000 g mol^{-1} (0.51 g, 0.051 mmol, 1 eq.) is added to it. In a flask covered with aluminum foil, rhodamine B isothiocyanate (0.333 g, 0.621 mmol, 12 eq.) is dissolved in dry methanol (40 mL). After dissolution, it is added to the sodium carbonate solution dropwise. The mixture is stirred under argon for 4 days in the dark. Then, ammonium chloride (0.722 g, 13.498 mmol, 265 eq.) and methanol (30 mL) are added and the mixture is stirred overnight. The product is precipitated twice in ice-cold diethyl ether (1 L), filtrated, and dried overnight in high vacuum. Afterward, it is dissolved in methanol (30 mL) and passed through a Sephadex LH-20 column. The fractions of the product are collected and the solvent is removed via rotary evaporation. Then, the product is dissolved in DCM (5 mL), precipitated in diethyl ether (600 mL), and dried overnight in high vacuum (yield 36%). The degree of functionalization is determined with UV–vis spectroscopy to be 34%. Despite the 12 equivalents of rhodamine, it was not possible to achieve a 100% functionalization, since the intended degree of functionalization was already high. The degree of labeling, which is 2% of the monomer units, is already higher than the usual degree of functionalization used. A 34% functionalization means that every star carries on average at least one fluorophore and this is sufficient for FRAP characterization. ^{1}H-NMR (DMSO-d_6, 400 MHz, δ = ppm): 8.72 (m, 8H), 3.51 (m, pEG backbone, 909 H), 1.09 (m, 12H), 6.56 (m, 4H), 7.05 (m, 5H).

Methods–Reversibility: Gels are prepared in milli-Q water with 100 g L^{-1} concentration of polymer and a stoichiometric amount of Fe(II) tetrafluoroborate hexahydrate in respect to the terpyridine (one metal ion for two terpyridines). To a 90 µL polymer solution, 10 µL of metal solution is added and immediately vortexed. The complexation between the terpyridine and the iron gives the gel a characteristic purple color. [19] To a 100 µL of 100 g L^{-1} gel, 30 µL of 37% solution of HCl is added and everything is vortexed. Decomplexation occurs within 20 min with repeated vortexing. During decomplexation the gel loses the characteristic purple color of the iron–terpyridine complex and becomes colorless again. The original gel is recovered by adding 20 µL of a 50% solution of NaOH, whereupon the gel recovers in about 10 min.

FRAP: FRAP measurements are performed on a Leica TCS SP2 microscope with 10x dry objective of NA 0.3 at 30× zoom. The excitation wavelength is 543 nm (He-Ne Laser) at 18–19% of its full intensity for 25 °C and at 12–18% for 36 °C. Bleaching is achieved with 100% intensity of the 458 nm (Ar Laser), 488 nm (Ar Laser), 514 nm (Ar Laser), and 543 nm (He-Ne Laser) lines. The detection wavelength is 550–600 nm. The image resolution is 128 × 128 pixels, resulting in 50.7 × 50.7 μm^2 recorded images at the utilized zoom level. Scans are performed bidirectional with a line scanning speed of 400 Hz. Before bleaching, four images are recorded and averaged. The bleaching time is set to 1 s, and after the

bleaching, a series of images is recorded with a time between the images of 354 ms. For all that, the sample is placed in a custom-made measuring cell that is connected to a power supply for temperature control. Measurements below the LCST of pNIPAAm are performed at about 25 °C, whereas measurements above the LCST are performed at around 36 °C. Below the LCST, 50 pictures are recorded, while above the LCST 300 pictures are recorded after the bleaching. Analysis of the data is done with a multicomponent diffusion model. [22] As fluorescent diffusive probe, four-arm pEG of the same molar mass as the tetra-pEG in the network (10 000 g mol^{-1}) is functionalized with rhodamine B. To 10 mg of tetra-pEG-pNIPAAm-terpyridine, 1.1 mg of the fluorescent probe is added and they are dissolved together in 90 µL of milli-Q water. Then, 10 µL of a solution of Fe(II) tetrafluoroborate hexahydrate in stoichiometric ratio to the terpyridine is added. The gel is prepared the day before, allowed to equilibrate overnight, and then transferred into the measuring chamber.

Rheology: Rheological studies are performed on a stress-controlled Anton Paar Physica MCR 302 rheometer equipped with a parallel plate geometry with 8 mm diameter. To account for the thermal expansion of the geometry with temperature, the geometry is positioned on the bottom plate of the rheometer at 25 °C for 20 min. Experiments are performed with a polymer concentration of 100 g L^{-1}, and the gel is formed directly on the rheometer. 70 µL of tetra-pEG-pNIPAAm-terpyridine solution is poured with a pipette on the bottom plate of the rheometer. The upper geometry is lowered, so that the upper plate would come in contact with the polymer solution, and then lifted up again. 7.77 µL of Fe(II) tetrafluoroborate hexahydrate solution with stoichiometric amount of metal ions to terpyridine is pipetted to the center of the polymer solution. Since the gelation starts instantaneously, the upper geometry is immediately lowered again. To ensure better mixing, and consequently gelation, of the polymer solution and the metal ions, the upper geometry is lifted up and lowered again a couple of times. Afterward, a dynamic time sweep is performed at 25 °C with a constant frequency of 1 rad s^{-1} and shear amplitude of 1%, until the sample is fully equilibrated, manifesting itself such that the storage and loss modulus are constant with time. Amplitude sweeps are performed at each temperature to ensure measurements in the linear regime. At 25 °C, with a frequency of 20 rad s^{-1}, the sample shows linear regime in the range of γ = 0.1–40%. A frequency sweep from 20 to 0.01 rad s−1 is performed with an amplitude of γ = 1%. Afterward, the sample is heated to 35 °C and allowed to equilibrate again at this temperature with a dynamic time sweep with constant frequency of 1 rad s^{-1} and shear of 1%. Afterward, an amplitude sweep is carried out at 35 °C. With a frequency of 20 rad s^{-1}, the sample shows a linear regime in the range γ = 0.1–10%. Next, a frequency sweep at 35 °C is performed from 20 rad s^{-1} to 0.01 rad s^{-1} with γ = 1%. Then, the sample is brought to 10 °C and let equilibrate again with a dynamic time sweep. A temperature sweep is performed by increasing the temperature of 1 °C every 45 s, from 10 to 40 °C, with frequency of 1 rad s^{-1} and shear of 1%. After equilibrating the sample at 40 °C, it is cooled down at the same rate of the heating cycle, from 40 °C to 10 °C, with frequency of 1 rad s^{-1} and shear of 1%.

References

[1] S. Seiffert, *Polym. Chem.* **2017**, *8*, 4472.

[2] F. Di Lorenzo, S. Seiffert, *Polym. Chem.* **2015**, *6*, 5515.

[3] J. P. Gong, *Soft Matter* **2010,** *6*, 2583.

[4] T. Rossow, A. Habicht, S. Seiffert, *Macromolecules* **2014,** *47*, 6473.

[5] A. S. Hoffman, *Adv. Drug Deliv. Rev.* **2012**, *64*, 18.

[6] T. Fujiyabu, X. Li, U.-il Chung, T. Sakai, *Macromolecules* **2019,** *52*, 1923.

[7] M. K. Yazdi, V. Vatanpour, A. Taghizadeh, M. Taghizadeh, M. R. Ganjali, M. T. Munir, S. Habibzadeh, M. R. Saeb, M. Ghaedi, *Mater. Sci. Eng.: C* **2020,** *114*, 111023.

[8] R. Ghosh, in *Functional Biopolymers*, Springer Nature Switzerland AG 2019, Ch.15.

[9] L. Chu, R. Xie, X. Ju, *Chinese J. Chem. Eng.* **2011,** 19, 891.

[10] I. Tokarev, S. Minko, *Adv. Mater.* **2010**, 22, 3446.

[11] J. Li, D. J. Mooney, *Nat. Rev. Mater.* **2016**, 1, 16071.

[12] P. Dong, B. J. Schott, A. K. Means, M. A. Grunlan, *ACS Appl. Polym. Mater.* **2020**, 2, 5269.

[13] C. Creton, *Macromolecules* **2017** *50*, 8297.

[14] M. Najafi, E. Hebels, W. E. Hennink, T. Vermonden, in *Temperature-Responsive Polymers: Chemistry, Properties and Applications*, (Eds: V. V. Khutoryanskiy, T. K. Georgiou), Wiley **2018**, Ch. 1.

[15] U. S. Schubert, H. Hofmeier, G. R. Newkome, *Modern Terpyridine Chemistry*, Wiley-VCH, Weinheim, Germany **2006**.

[16] G. R. Whittell, M. D. Hager, U. S. Schubert, I. Manners, *Nat. Mater.* **2011** *10*, 176.

[17] M. Shibayama, X. Li, T. Sakai, *Colloid Polym. Sci.* **2019,** *297*, 1.

[18] T. Rossow, S. Seiffert, *Polym. Chem.* **2014,** *5*, 3018.

[19] S. Bode, L. Zedler, F. H. Schacher, B. Dietzek, M. Schmitt, J. Popp, M. D. Hager, U. S. Schubert, *Adv. Mater.* **2013**, 25, 1634.

[20] M. Sánchez, L. Sabio, N. Gálvez, M. Capdevila, J. M. Dominguez-Vera, *IUBMB Life* **2017**, 69, 382.

[21] S. Seiffert, W. Oppermann, *J. Microsc.* **2005,** *220*, 20.

[22] G. I. Hauser, S. Seiffert, W. Oppermann, *J. Microsc.* **2008,** *230*, 353.

[23] M. Ahmadi, S. Seiffert, *Soft Matter* **2020**, 16, 2332.

[24] J. Karvinen, T. O. Ihalainen, M. T. Calejo, I. Jönkkäri, M. Kellomäki, *Mater. Sci. Eng.: C* **2019**, 94, 1056.

[25] S. Hackelbusch, T. Rossow, D. Steinhilber, D. A. Weitz, S. Seiffert, *Adv. Healthc. Mater.* **2015**, 4, 1841.

4. Mechanical switching of a comb-like dual dynamic polymer network

Paola Nicolella[a] and Sebastian Seiffert[a]

Accepted in: *Journal of Rheology*, **2022**

DOI: 10.1122/8.0000388

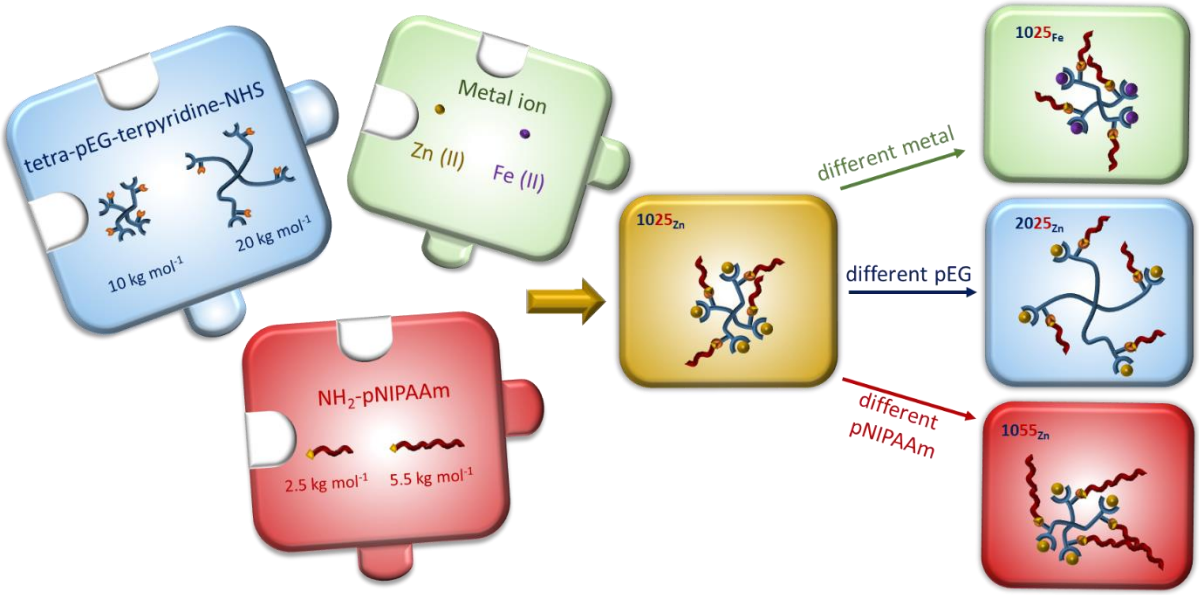

This manuscript has been accepted by the Journal of Rheology and will be published in the *Special Issue for Double Dynamics Polymeric Networks*. Reprinted with permission of the Editor.

Supplementary information is available in Chapter 10.2.

Author Contributions:

Paola Nicolella: Idea and concept of the work, rheological characterization, analysis and interpretation of the results, preparation of the manuscript, design and realization of figures

Sebastian Seiffert: Supervision of the work, correction of the manuscript

[a]*Johannes Gutenberg-Universität Mainz, Department of Chemistry, Duesbergweg 10-14, D-55128 Mainz, Germany*

Summary

The determination of structure–property relationships in multi-responsive materials is an essential tool for the rational engineering of new materials. However, this constitutes still a challenge as the properties of multi-component materials is often not straightforward. To make the interpretation of the results more accessible, a known polymer basis is needed in addition to a methodological approach.

In the previous chapter a novel dual dynamic network (DDN) was introduced which is comprised by a tetra-arm poly(ethylene) glycol (pEG) precursor bearing terpyridine ligands and poly(*N*-isopropylacrylamide) (pNIPAAm) linear chains on each arm. However, to expand the utility and tunability of this material basis, in this chapter structure–property relationships on this DDN are investigated in a systematic fashion.

Starting from the two polymer precursors, respectively the tetra-arm pEG functionalized with a *N*-hydroxysuccinimidyl (NHS) and a terpyridine group, and an amine-functionalized pNIPAAm chain, it is possible to create a toolkit for DDNs by changing the molar mass of both precursors, as well as the metal ion. Upon increasing the temperature above the lower critical solution temperature (LCST), the plateau modulus increases due to the collaborative collapse of the pNIPAAm chains. However, the elastic properties depend strongly on the pEG/pNIPAAm ratio and the metal ion. In particular, the hydrogels with a higher amount of pNIPAAm and longer pNIPAAm chains showed a more pronounced increase in the plateau moduli compared to the samples with shorter pNIPAAm chains and a higher amount of pEG. In addition to the metal-ion related plateau modulus at high frequencies, the samples showed an additional plateau in their elastic modulus at lower frequencies, upon increase of temperature above the LCST. This feature can be ascribed to the pNIPAAm chains as its extent is higher with increasing pNIPAAm content.

The different elastic properties of the samples depend strongly on the length of the grafted pNIPAAm chains. While longer chains reach each other and thereby collapse cooperatively creating new connections that reinforce the hydrogel, shorter chains collapse mainly on themselves which results in a less pronounced increase of the mechanical properties. The wide range of the achievable properties and easy tunability of the system, show the convenience and versatility of toolkits for DDN.

Acknowledgments

This work was financially supported by funding from the H2020 Programme (MARIE SKŁODOWSKA-CURIE ACTIONS) of the European Commission's Innovative Training Networks (H2020-MSCA-ITN-2017) under DoDyNet REA Grant Agreement N°.765811. Paola Nicolella thanks Evelyne Van Ruymbeke and Mostafa Ahmadi for useful discussions, Daniel Lauxen for support with the synthesis, and Martha Franziska Koziol for review of the manuscript before submission. The authors would like to thank the reviewers for insightful suggestions of the improvement of the manuscript.

1. Introduction

Hydrogels are polymer networks swollen in water; they have raised significant attention due to their capability to mimic natural tissues. [1], [2] This ability, though, comes along with a challenge, as such an application requires their mechanics and functionality to resemble those of the natural tissues. [3]

For example, for drug delivery applications, it is crucial to control the diffusion of the drug inside the hydrogel, which strictly depends on the polymer network mesh-size ξ. [4] If that mesh-size is smaller than the size of the drug, then its diffusion will be slow or even impossible, and vice versa. In view of that, Grunlan *et al*. controlled the mesh-size, and consequently the diffusion, by adding dangling thermo-responsive charged chains to the main polymer network. They showed that smaller meshes can be achieved with negatively charged chains. [5] In a similar own previous work, we introduced poly(*N*-isopropylacrylamide) (pNIPAAm) dangling chains to a supramolecular tetra-poly(ethylene) glycol (pEG)-terpyridine network, showing that the diffusion of small diffusants is possible at room temperature but hindered above the lower critical solution temperature (LCST) of pNIPAAm, and that this is also followed by an increase of the gel elastic modulus. [6]

In view of biomedical applications, also the mechanical properties of hydrogels play a crucial role, and material scientists are continuously working on the improvement of such properties. In 2003, Gong and her group obtained a hydrogel with outstanding mechanical properties, composed of two covalent polymer networks, one highly and one loosely crosslinked, interpenetrated into each other and there-by forming a double network (DN). Their first DN composed of poly(2-acrylamide-2-methylpropane sulfonic acid) (PAMPS) and polyacrylamide (PAM), showed a fracture stress of 17.2 MPa (20 times higher than the one of the two polymers separately). [7] Upon application of stress, the first network breaks, thereby dissipating energy. [7] With this mechanism, it is possible to obtain simultaneously tough and elastic hydrogels. These covalently crosslinked networks, though, have the disadvantage that the breakage of their sacrificial part occurs irreversibly, and the material does not recover afterwards. That shortcoming can be overcome by incorporation of transient supramolecular crosslinks into the double network. In first attempts, only one covalent network was substituted by a supramolecular network, thereby forming hybrid double networks. For example, Hébraud and co-workers have shown that hybrid double networks formed by covalently crosslinked poly(vinyl alcohol) (PVA) and transiently bound PVA with borate ions have superior mechanical properties than the two single networks. [8] Later on, both covalent networks were substituted by supramolecular networks, forming double supramolecular networks (DSN). Besides rendering the breakage reversible, in such supramolecular double networks, both networks actually contribute to the dissipation of energy. [9] For example, Zheng *et al*. synthesized such a network based on agar and poly (acrylic acid)-Fe^{3+}. This network showed good mechanical properties along with self-healing. [10] However, even though they realized these networks through a ‘one pot method’, there is no existing systematic study on how changes in structural parameters influence the final properties of these DSN. In addition, these works focus mainly on non-

linear rheology. We intend to fill this gap and present here a complete linear rheological characterization study. We do this with a systematic approach based on a toolkit where two dynamic building blocks are attached to a common network, thereby forming a dual dynamic network (DDN). These building blocks can be chosen on demand, thereby conferring targeted properties to the hydrogel.

The main common network is composed of tetra-pEG building blocks where each arm is end-capped by ligands capable of forming metal ion complexes and additionally grafted with thermo-responsive oligomers capable to undergo nano-phase-separation in a comb-like configuration. As ligand, we chose terpyridine that is able to form complexes upon addition of different divalent metal ions (for example Zn^{2+}, Fe^{2+}, Ni^{2+}) and consequently transfers different binding strengths to the final hydrogel. In addition to that ability, tetra-pEG-terpyridine networks are capable to form supramolecular model networks, [11] and this offers a well-known platform for the introduction and rational investigation of the impact of a second dynamicity. In our work, this second dynamicity is given by the most widespread thermo-responsive polymer pNIPAAm (the second building block) that changes its conformation from coil to globule above its LCST, which is around 32 °C in water, making it appealing for biomedical applications. [12]

In an own aforementioned previous work, we have shown that this dual dynamic network is able to double its elastic modulus upon raise of temperature above the LCST of pNIPAAm, as unravelled by oscillatory shear rheology, due to multiple pNIPAAm chains collapsing together and therefore creating new connections in the network. [6] Moreover, this temperature-tuneable collapse has the additional result that the diffusion of small molecules inside the hydrogel can be controlled, as quantified by fluorescence recovery after photobleaching (FRAP), making the hydrogel suitable for membranes or separation techniques. [6] Finally, we demonstrated the utility of the supramolecular moieties, by showing that our hydrogel can be degraded and restored. [6]

In this paper, we go a step further and investigate the linear viscoelastic response of the DDN systematically by variation of the molar mass of the thermo-responsive polymer and of the tetra-pEG-terpyridine precursors, as well as the type of the metal ions. Amine-functionalized pNIPAAm chains are clicked onto each arm of a tetra-pEG-terpyridine that has an additional *N*-hydroxysuccinimidyl (NHS) group. This strategy offers the possibility to easily form different combinations of hydrogels by systematically varying the molar mass of tetra-pEG and of the attached pNIPAAm chains, or the metal ions, as shown in **Figure 1**. With that approach, we systematically change the molar mass of the tetra-pEG precursors, using 10 kg mol^{-1} or 20 kg mol^{-1}, and using 2.5 kg mol^{-1} or 5.5 kg mol^{-1} amine-functionalized pNIPAAm chains. To study the elastic properties of the different systems obtained with that modular approach, we use oscillatory shear rheology in the linear regime and probe the samples at different temperatures below and above the LCST of the system. Our findings show that above the LCST of pNIPAAm, the samples bearing longer pNIPAAm chains increase their plateau modulus more than the samples with lower amount of pNIPAAm. Moreover, a second plateau is found for these samples

above the LCST at low frequencies that could be an indication of the second dynamicity given by pNIPAAm.

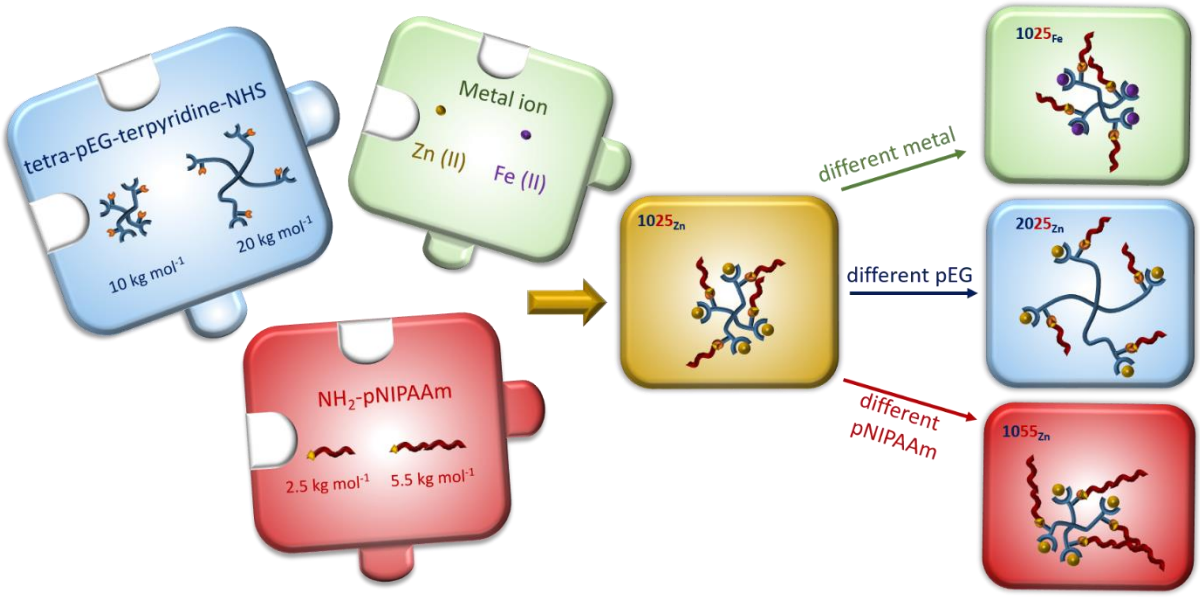

Figure 1. Concept of this work. A toolkit for dual dynamic networks is realized with a tetra-pEG-terpyridine precursor further functionalized with thermo-responsive pNIPAAm and by systematically changing the pEG/pNIPAAm ratio, as well as the metal ion in the system.

2. Experimental part

The material basis of our work are tetra-pEG macromolecules where each arm is functionalized with two independent dynamic motifs. The first motif is terpyridine which forms complexes with different bivalent metal ions, whereas the second dynamic motif is pNIPAAm which undergoes phase-separation above its LCST.

To study the elastic properties in a systematic fashion and to construct a toolkit for dual dynamic networks, we vary the molar mass of the pEG and pNIPAAm precursors, as well as the metal ion used for complexation.

Our networks are denoted as follows: the first two digits of our 1025-Zn_{120} notation describe the molar mass of the tetra-pEG-terpyridine macromolecule (with 10 being 10 kg mol^{-1} and 20 being 20 kg mol^{-1}) and the subsequent two digits refer to the molar mass of the attached pNIPAAm unit (with 2.5 kg mol^{-1} being 25 and 5.5 kg mol^{-1} being 55). The final gel concentration is denoted as subscript number. Starting from a dual polymer network composed of 10 kg mol^{-1} tetra-pEG-terpyridine (10K) and 2.5 kg mol^{-1} pNIPAAm (1025), we first increase the amount of thermo-responsive polymer by using a 5.5 kg mol^{-1} pNIPAAm on the 10K tetra-pEG-terpyridine matrix (1055), and then increase the amount of pEG by using a 20 kg mol^{-1} tetra-pEG matrix (2025), as depicted in **Figure 1**. Finally, we investigate the influence of the metal ion and compare the elastic response of the 1025 dual network with zinc and with iron.

2.1 Materials

Tetra-hydroxyl poly (ethylene) glycol (pEG) 10 kg mol^{-1} and 20 kg mol^{-1} are purchased from JenKem Technology (Plano, Texas, USA) and further functionalized as previously described. [6] Amine-functionalized poly(*N*-isopropylacrylamide) (pNIPAAm) 2.5 kg mol^{-1} and 5.5 kg mol^{-1}, and iron (II) tetrafluoroborate hexahydrate 97% are purchased from Sigma Aldrich. Zinc nitrate hexahydrate 98% is purchased from Alfa Aesar.

2.2 Synthesis

The synthesis of our system has been described elsewhere [6] and further information can be found in the Supplementary Material. In short, tetra-pEG-OH reacts with epichlorohydrin to result in epoxy-functionalized tetra-pEG, and subsequently, the epoxy ring is opened via azide, leaving the pEG with two functional groups on each arm: one hydroxyl and one azide group. In parallel, propargyl terpyridine is synthesized and attached to the azide group. The hydroxyl group is transformed into an NHS group and amine-functionalized pNIPAAm chains are attached to it via a click reaction, as shown in **Scheme 1**. The excess of pNIPAAm is then dialyzed out.

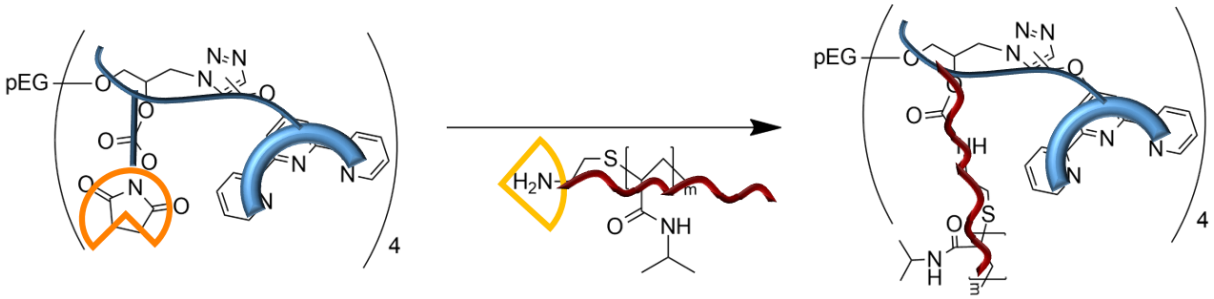

Scheme 1. Formation of a tetra-pEG-terpyridine-pNIPAAm dual network through click-reaction between tetra-pEG-terpyridine-NHS and amine-functionalized pNIPAAm building blocks. This reaction mechanism allows for an easy interchange of the building blocks for the realization of different polymer networks.

The degree of functionalization of terpyridine for the 10K and 20K tetra-pEG-terpyridine samples are determined by NMR to be respectively 80% and 95%. This difference in functionality will not affect the rheological results, as the chosen concentration of the polymer as well as the concentration of the metal ion take into account the different functionalization grades of the terpyridine such that and in all compared samples, the same concentration of metallo-supramolecular complexes is assured. The functionalization with NHS groups is determined by NMR to be 75% and 90%, respectively for the 10K and 20K tetra-pEG-terpyridine-NHS. This same functionalization can be attributed to the attached pNIPAAm chains, as from the NMR, no residual NHS groups can be detected. Through NMR it is also possible to determine the presence of extra pNIPAAm chains that was not possible to dialyze out. This percentage is 30%wt for the 1025, 50%wt for the 1055, and 10%wt for the 2025 dual networks (**Table I**). This amount has to be added on top of those that are not attached due to the NHS functionalization. The LCST of the dual dynamic networks are analyzed via turbidity measurements with an UV-VIS

instrument determining the cloud point of the solution. These are measured to be 31 °C for the 1025 and 32.5 °C for the 1055 and the 2025 dual networks.

Table I. Details of the samples.

Sample	***Metal***	***pEG*** [kg mol^{-1}]	***pNIPAAm*** [kg mol^{-1}]	$C_{Polymer}$ [g L^{-1}]	$f_{Terpyridine}$	$f_{pNIPAAm\ attached}$	$\%_{pNIPAAm\ extra}$
10K-Zn$_{60}$	Zn	10	-	**60**	80%	-	-
1025-Zn$_{120}$	Zn	10	2.5	**120**	80%	75%	30%$_{wt}$
1025-Fe$_{120}$	Fe	10	2.5	**120**	80%	75%	30%$_{wt}$
1025-Zn$_{85}$	Zn	10	2.5	**85**	80%	75%	30%$_{wt}$
1055-Zn$_{192}$	Zn	10	5.5	**192**	80%	75%	50%$_{wt}$
2025-Zn$_{70}$	Zn	20	2.5	**70**	95%	90%	10%$_{wt}$

2.3 Formation of the gels

The polymer precursor molecules are dissolved in milli-Q water with a concentration $C_{polymer}$ as shown in **Table I**. The concentrations are chosen to obtain equimolar terpyridine concentrations when comparing the different polymers and to ensure that the 10K tetra-pEG containing polymers are above the overlap concentration of the 10K tetra-pEG-terpyridine (56 g L^{-1}). [13] To form the gels, the addition of a metal ion is needed, since the dual network alone does not form a gel (even above the LCST of pNIPAAm). To achieve that, aqueous stock solutions of the metal ion are prepared by dissolving the corresponding amount of zinc nitrate hexahydrate or iron (II) tetrafluoroborate hexahydrate thereby assuring a stoichiometric ratio of terpyridine : metal = 2 : 1. We suppose that the influence of the difference in counter ion associated with the metal is negligible compared to the difference in metal ion. To form the gels with zinc, the metal ion solution is quickly added to the polymer solution in a glass vial and the mixture is immediately vortexed. The hydrogel is then allowed to equilibrate overnight on a shaking plate. To form the gel with iron, the polymer solution is poured onto a custom-made 25 mm round mold and the iron solution is added on top of it. The mold is then sealed, and the gel is allowed to equilibrate for 24 h. This procedure assures that the iron gel stays intact when transferred on the rheometer for rheological measurements.

2.4 Oscillatory shear rheology

To probe the elastic properties of the dual dynamic hydrogels, oscillatory shear rheology experiments are performed on an Anton Paar Physica MCR 302 rheometer equipped with a parallel plate geometry with a diameter of 25 mm and a solvent trap. The samples are loaded at room temperature (20 °C) and the gap adjusted to 0.5 mm. To equilibrate the sample, a temperature cycle is performed from 20 °C to 40 °C and then down to 10 °C, with a heating/cooling rate of 1 °C / min. Afterwards, to assure the stability of the sample, two additional cycles between 10 °C and 40 °C are recorded at the same heating/cooling rate. Finally, the sample is allowed to equilibrate at 20 °C for the 10K-Zn_{60}, 1025-Zn_{120}, and 1025-Fe_{120} and at 10 °C for the 1025-Zn_{85}, 1055-Zn_{192}, and 2025-Zn_{70} samples, with ω = 10 rad s^{-1}

and γ = 1%. Amplitude sweeps are performed in the range of γ = 0.01 – 30% with a shear frequency of ω = 100 rad s^{-1} to assure that viscoelastic conditions are satisfied. The amplitude sweep is then followed by another period of equilibration, this time with ω = 100 rad s^{-1} and γ = 1%. Finally, frequency sweeps are performed in the range ω = 100 – 0.01 rad s^{-1} with γ = 1%. The sample is then heated to the next temperature, allowed to equilibrate, and then amplitude and frequency sweeps are recorded as previously described. This procedure is then repeated up to 45 °C with measurements every 5 °C. In the experiments, the viscosity change of water with temperature is not taken into account, as it changes from 1 mPa s at 20 °C to 0.59 mPa s at 45 °C, [14] and this difference is low compared to the viscosity of the polymer.

3. Results & Discussion

3.1 Temperature-dependence of elastic properties

To investigate the temperature-dependence of the macroscopic elastic properties of our dual network hydrogels, we perform linear oscillatory shear rheology experiments at a broad temperature range, both below and above the LCST of the respective compound. For this purpose, frequency sweeps are performed in the range of 20-45 °C, with a temperature step of 5 °C and a constant shear amplitude of γ = 1% in the frequency range of ω = 0.01-100 rad s^{-1}. Exemplary rheological spectra of the dual network composed by 10K tetra-pEG-terpyridine precursor, further functionalized with 2.5 kg mol^{-1} pNIPAAm chains and complexed through zinc metal ions are shown in **Figure 2 a)** and compared with the rheological spectra of the single 10K tetra-PEG-terpyridine complexed with Zn (**Figure 2 b)**).

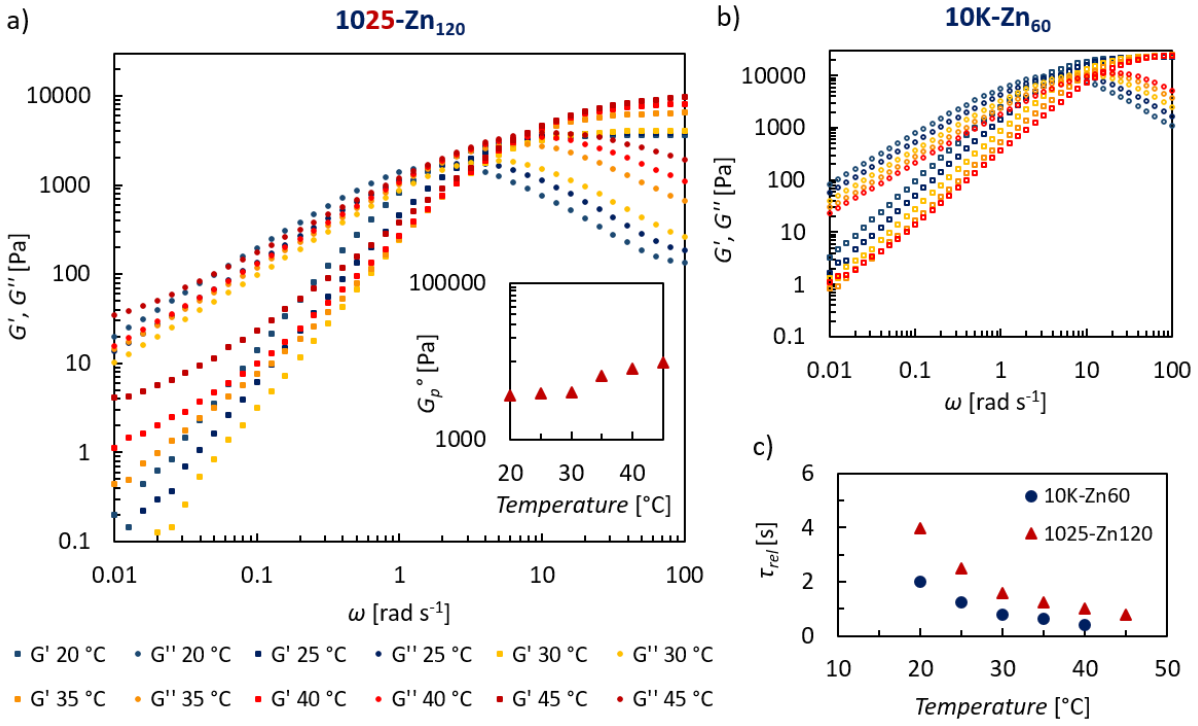

Figure 2. a) Frequency-dependence of the elastic (squares) and loss (circles) moduli at different temperatures of the 1025-Zn_{120} dual network (inset: temperature-dependence of the plateau moduli), and for comparison: b) single

network composed of 10K tetra-pEG-terpyridine with Zn (without pNIPAAm chains). c) Temperature-dependence of the terminal relaxation time of the metallo-supramolecular complexes for both networks. To ensure the same number of terpyridine complexes and that the concentration of the 10K tetra-pEG-terpyridine is above its overlap concentration (56 g L^{-1}), [13] the overall polymer concentration of the dual network is 120 g L^{-1}, whereas the overall polymer concentration for the single network is 60 g L^{-1}.

The frequency-dependent elastic moduli of the 1025-Zn_{120} dual network and the single 10K-Zn_{60} network monotonically increase with increasing frequencies, ending in a plateau at high frequencies (**Figure 2 a)** and **b)**). All curves exhibit a crossover between G' and G'' that indicates the lifetime of the terpyridine-metal complex and that can be determined with the inverse of the relaxation time ($1/\tau_{rel}$) since in that point $G' = G''$ and from the Maxwell model $G'/G'' = \omega\tau$. [15], [16] At the same time $G''/G' = tan\,\delta$, [17] therefore, this crossover frequency can be obtained by taking the frequency at which $tan\,\delta = G''/G' = 1$, then dividing it by 2π (to take into account the radiant), and finally taking the inverse to determine the relaxation times. This characteristic crossover point shifts to higher frequencies upon increase of temperature. These terminal relaxation times of the 1025-Zn_{120} dual network show a similar trend to the relaxation times of the single zinc 10K tetra-pEG-terpyridine network. Their values shift with higher temperatures due to the faster complex dissociation and therefore faster sticker exchange (**Figure 2 c)**). However, the dual network shows double relaxation times compared to the single network over the whole range of temperatures, since the relaxation time increases with increasing polymer concentration [18] and the 1025-Zn_{120} has a double overall polymer concentration when compared to the single 10K-Zn_{60} network. When comparing both networks, there are some differences evoked by the presence of the pNIPAAm dangling chains. While the frequency-independent plateau modulus of the single 10K-Zn_{60} network stays constant at every temperature, the plateau modulus of the dual 1025-Zn_{120} network stays constant until it reaches the LCST and then increases, as shown in the inset of **Figure 2 a)**. In particular, upon switching above the LCST, the plateau modulus value becomes 1.5 times higher and further increases in a linear fashion. The increase of plateau modulus with temperature above the LCST is provoked by the phase-separation of pNIPAAm chains that collapse above the LCST and thereby finding other pNIPAAm chains in proximity to form cluster. These clusters act as additional physical crosslinks and adds on top of the metallo-supramolecular complexes of the main pEG network resulting in an overall increase of the plateau modulus, which is an indication of the number of connections in the sample. [6] In addition, at temperatures above its LCST and at low frequencies, the dual network shows the onset of a second plateau which is absent in the single supramolecular network. This second plateau manifests itself due to the associations of the pNIPAAm chains and comes together with a shifting of the elastic moduli curve. From **Figure 2 b)** it can be noticed that the slope of the elastic modulus curves of the single network translates to higher frequencies with temperature. This behavior is observed for the dual networks up to the temperature of 30 °C, as it can be seen from **Figures 2 a)**. From 35 °C, therefore above the LCST, the curves of the elastic moduli do not translate anymore to higher frequencies, on the contrary they shift to lower

frequencies and the appearance of the second plateau at low frequencies occurs. Therefore, the presence of the pNIPAAm dangling chains and their collective clustering above the LCST affects both the plateau modulus at high frequencies, resulting in an increase with increasing temperatures, and the appearance of a second plateau at low frequencies.

3.2 Variation of the metal ion

To investigate the different rheological responses of the dual networks depending on different metal ions, oscillatory shear rheology experiments are performed on the 1025 dual network. For this purpose, iron (II) is chosen. To have comparability with the 1025-Zn_{120} network, the same global polymer concentration is used (c = 120 g L^{-1}).

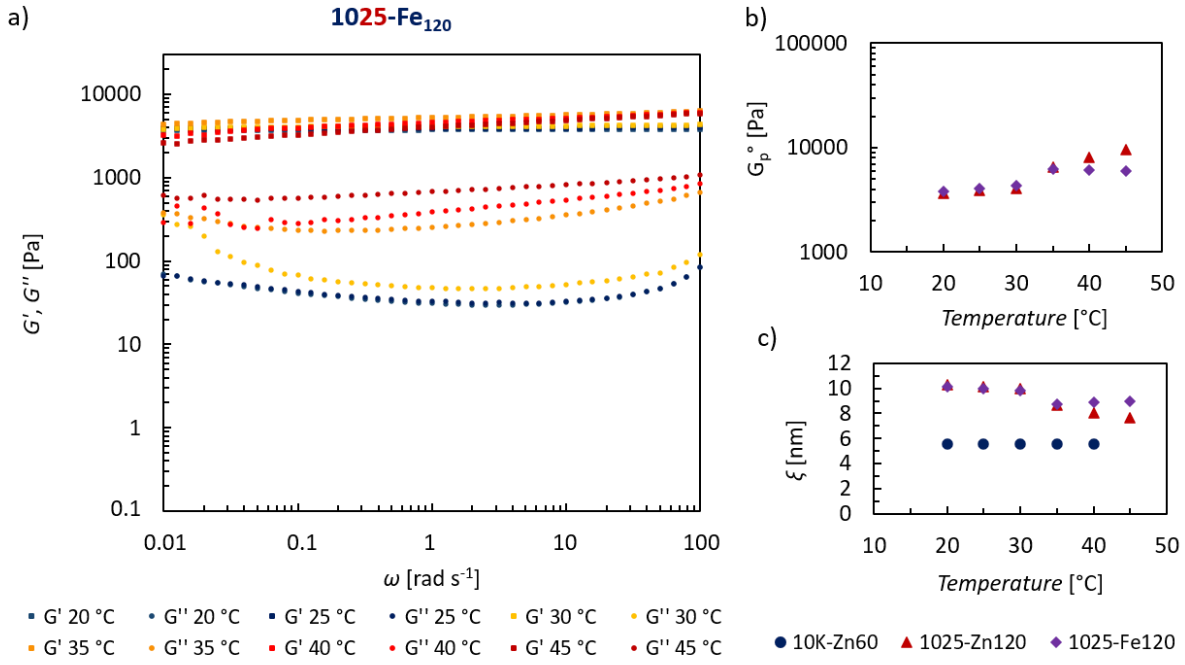

Figure 3. a) Temperature-dependence of the elastic (squares) and loss (circles) moduli of the 1025-Fe_{120} dual network. b) Comparison of the plateau moduli of the 1025-Zn_{120} and 1025-Fe_{120} dual networks. c) Comparison of network mesh-sizes between the single 10K-Zn_{60} network and the 1025-Zn_{120}, and 1025-Fe_{120} dual networks, as calculated from the plateau moduli (Equation 1).

The elastic modulus of the 1025-Fe_{120} dual network shows a different elastic behavior than the 1025-Zn_{120} network (comparing **Figure 3 a)** and **Figure 2 a)**): the 1025-Fe_{120} dual network shows a covalent gel-like behavior, with no frequency-dependence and therefore no relaxation at the accessible frequencies. Below the LCST, the elastic moduli stay constant over the whole range of frequencies, whereas above the LCST, the elastic moduli increase steadily with increasing frequencies (**Figure 3 b)**). By taking the elastic modulus at ω = 100 rad s^{-1} as a reference for the plateau modulus $G_p^{\circ}{}_{1025\text{-}Fe120}$, this value stays constant until the LCST is reached, then it doubles, and afterwards it stays constant again, as it can be seen in **Figure 3 b)**. Differently, the plateau modulus of the 1025-Zn_{120} dual network $G_p^{\circ}{}_{1025\text{-}}$

$_{Zn120}$, continues to increase linearly above the LCST. However, a comparison between the trend of the elastic plateau moduli has to be done carefully taking into consideration how these points are determined. While the 1025-Zn_{120} has a proper plateau modulus, the 1025-Fe_{120} does not and the value of the elastic modulus at the highest frequency is taken as the value of the plateau modulus and how it can be seen from the **Figure 3 a)**, all the curves above LCST convey in the same point at the highest frequency. In both samples above LCST the pNIPAAm chains meet and collapse together, however our supposition is that in the iron sample their spatial arrangement cannot vary as this hydrogel has a covalent-like behavior, whereas the sample with zinc could further internally adjust since this network is more viscous, and the number of connections can continue to increase with temperature, even above the LCST. A reason for that could be the transformation of few bigger clusters in a higher number of smaller clusters, thereby determining a higher number of connections and consequently a further increase of the plateau moduli. [19] This picture can be supported also by the temperature-increasing plateau at low frequencies that appears in the 1025-Zn_{120} sample that is connected with clusters and that increases with temperature.

In addition, from the plateau moduli the mesh-size values of the polymer network can be estimated through:

$$\xi = \left(\frac{RT}{G_P^{\circ} N_A}\right)^{1/3} \quad (1)$$

where R denotes the universal gas constant, T is the temperature, G_P° is the measured plateau modulus, and N_A is the Avogadro constant. [17] The trend of the mesh-size is the same of the respective plateau moduli. The mesh-size of the dual network with iron decreases upon switching above the LCST, but then it remains constant, whereas the mesh-size of the dual network with zinc continues to decrease with increasing temperatures (**Figure 3 c)**). In comparison, the mesh-size of the single network stays constant over the whole temperature range, denoting that in this case the structure does not change with temperature.

3.3 Toolkit with different pEG/pNIPAAm ratios

To investigate universal structure-property relationships of this dual network kit, the ratio of tetra-pEG-terpyridine to pNIPAAm is varied. In particular, starting from the 1025-Zn_{85} dual network, we first change the molar mass of the attached pNIPAAm, obtaining the 1055-Zn_{192} dual network bearing pNIPAAm dangling chains with a molar mass of 5.5 kg mol^{-1}. Another set of polymers is obtained by changing the molar mass of tetra-pEG-terpyridine to be 20 kg mol^{-1} with 2.5 kg mol^{-1} attached pNIPAAm chains, resulting in the 2025-Zn_{70} dual network. To assure comparability, we keep the concentration of terpyridine–zinc complexes equal in all samples. The final concentrations are 85, 192, and 70 g L^{-1} respectively for the 1025-Zn_{85}, 1055-Zn_{192}, and 2025-Zn_{70} samples.

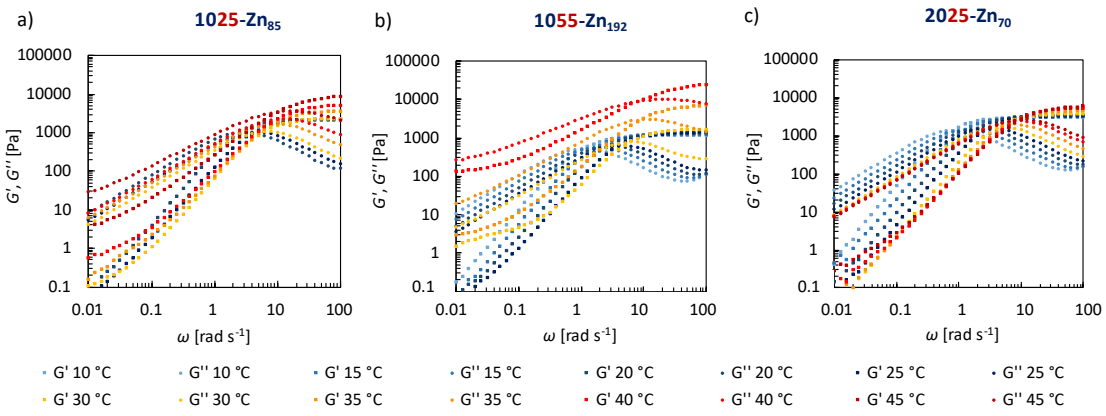

Figure 4. Frequency-dependent storage and loss moduli of dual hydrogels formed with zinc and different pEG / pNIPAAm precursors. The concentration is 85, 192 and 70 g L^{-1} for the 1025-Zn_{85}, 1055-Zn_{192} and 2025-Zn_{70} samples respectively, to assure the same zinc-terpyridine complex concentration.

All three dual networks show an increasing elastic modulus with increasing frequencies, exhibiting a plateau at the maximum frequency and a crossover between the elastic and loss modulus (**Figure 4**). Moreover, at temperatures above the LCST, all samples show a higher plateau modulus and the onset of a second plateau at low frequencies. This second plateau can be ascribed to the presence of pNIPAAm, as samples with longer pNIPAAm chains show a more defined second plateau. However, this low-frequency plateau could also be an indication of the dynamicity of the system that is not completely equilibrated at such frequencies.

The inverse of the crossover frequency between the elastic and loss modulus gives the relaxation time. This shows similar absolute values for all three samples, as depicted in **Figure 5 a)**, denoting the same temperature-dependent behavior of the pure metallo-supramolecular complexes, with slightly higher relaxation times at low temperature for the sample with 20K tetra-pEG-terpyridine precursors. Even if this is the sample with lower concentration, and as we have seen before the relaxation time should increase with concentration, the 20K tetra-pEG precursor has longer arms compared to the 10K tetra-pEG precursors, and therefore a higher chain-end dilution that results with longer relaxation times.

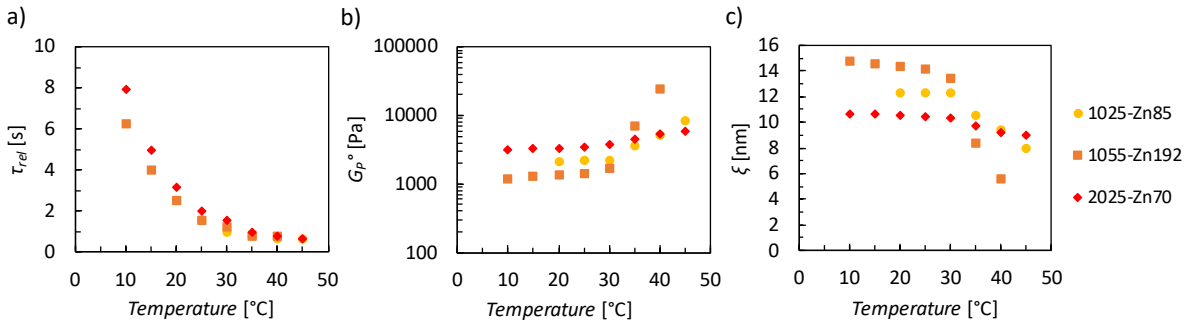

Figure 5. Temperature-dependence of the terminal relaxation time, plateau modulus, and mesh-size of the 1025-Zn_{85}, 1055-Zn_{192}, and 2025-Zn_{70} dual networks.

For all samples, the plateau modulus at the maximum frequency G_P° stays nearly constant up to the LCST and then it increases with temperature (**Figure 5 b)**). However, the extent of the increase depends on the amount of pNIPAAm in the sample and on the pEG/pNIPAAm ratio. The low-temperature plateau moduli of the samples with 10K pEG precursors exhibit similar values, with the 1055-Zn_{192} sample showing lower plateau modulus probably due to a screening effect of the longer dangling pNIPAAm chains for the terpyridine-metal complex or the higher presence of the non-attached pNIPAAm chains that might create defects in the network, thereby determining a loss in the plateau modulus. [20] However, the plateau modulus becomes 1.5 times higher for the 1025-Zn_{85} sample, whereas it becomes 7 times higher for the 1055-Zn_{192} sample upon switching the temperature around the LCST, meaning transitioning from 30 °C to 35 °C. Therefore, the increase in the plateau modulus is more significant with longer pNIPAAm chains. This can be rationalized by the fact that the 1055-Zn_{192} dual network bears pNIPAAm chains of a double molar mass than the 1025-Zn_{85} sample. Higher molar mass translates into longer dangling chains, and therefore a higher probability for the 5.5 kg mol^{-1} chains to meet and collapse than for the 2.5 kg mol^{-1} chains. The plateau moduli below the LCST of the samples with 20K tetra-pEG precursors are almost double of the ones containing the 10K tetra-pEG precursors. Even though they all have the same number of terpyridine stickers, the 20K tetra-pEG precursor has a higher terpyridine-functionalization (**Table I**), therefore a higher probability that a higher number of stars bears all four foreseen terpyridine stickers, thereby creating a fully percolated network, whereas in the 10K tetra-pEG precursor the majority of stars will bear three terpyridine stickers. In addition, the samples containing 20K precursors are far above the overlap concentration of 20K tetra-pEG, whereas the samples containing the 10K precursors are probed very near to the overlap concentration of 10K tetra-pEG, therefore, it is more sensible to small perturbations in the system. However, these factors impact mainly the plateau moduli below LCST, as above LCST the gain in plateau moduli is dictated by the length of the pNIPAAm chains and the pEG/pNIPAAm ratio. For example, keeping the amount of pNIPAAm constant but increasing the amount of pEG, such as going from the 1025-Zn_{85} to the 2025-Zn_{70} sample, we observe that the 2025-Zn_{70}, behaves more like a simple tetra-pEG-terpyridine than a dual network, as the plateau modulus at 35°C is just 1.3 times higher than the one below the LCST and it does not continue to increase with temperature as much as the plateau moduli of the 1025-Zn_{85} or 1055-Zn_{192}. In addition, another factor that has to be considered is that these three samples contain a different percentage of free pNIPAAm chains that was not possible to dialyze out (see **Table I**). These extra pNIPAAm chains will certainly collapse above their LCST in aqueous surrounding, and in case they are in proximity of other chains they will take part to the clusters that form the same way, but if they are not attached to the network, they do not represent active chains and thereby they do not contribute to the plateau modulus. [6] Nevertheless, by comparing the different percentages in **Table I** and the increase in the plateau moduli in **Figure 5 b)**, to higher percentages of non-attached thermo-responsive chains, correspond a greater increase in plateau modulus. However, the increase in plateau modulus is connected also to a higher concentration of attached pNIPAAm to the tetra-pEG precursors.

Therefore, it is more likely that the different behavior of these three different dual polymer networks derives from their different pEG/pNIPAAm ratio than from the free pNIPAAm chains.

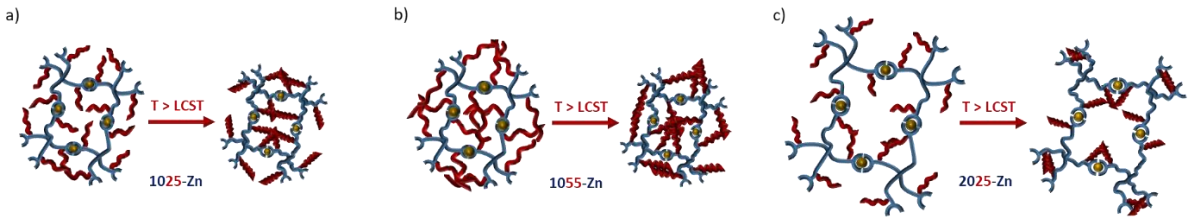

Figure 6. Comparison of the a) 1025-Zn_{85}, b) 1055-Zn_{192} and c) 2025-Zn_{70} dual networks. Longer pNIPAAm chains will do more likely meet and collapse together above the LCST, while shorter chains might collapse without further interactions.

The different pEG/pNIPAAm ratios in the samples have an influence on the mesh-size as well (**Figure 5 c)**), as above the LCST the mesh-size decreases with increasing amplitudes for the 2025-Zn_{70}, 1025-Zn_{85}, and 1055-Zn_{192} respectively. This can be translated into different ways of network configuration provoked from the collapsing of the pNIPAAm chains in the three samples, as visually depicted in **Figure 6**. In the 1025-Zn_{85} sample, the length of pEG and pNIPAAm is comparable and therefore the majority of the thermo-responsive chains from different pEG-stars will meet and collapse together (**Figure 6 a)**), thereby increasing the plateau modulus and resulting in smaller mesh-sizes above the LCST (**Figure 5 c)**). The 1055-Zn_{192} sample shows the largest mesh-size at low temperature and the smallest mesh-size above LCST. This sample contains the highest amount of pNIPAAm (attached and not attached) and the highest polymer concentration. In addition, this is the sample with the longest pNIPAAm chains compared to the pEG. Therefore, in this sample we can consider that all the pNIPAAm chains collapse together (**Figure 6 b)**) resulting in the highest improvement in the plateau modulus (**Figure 4 b)**), and smallest mesh-size (**Figure 5 c)**). While the decrease in mesh-size above the LCST occurs due to the collapse of the attached pNIPAAm chains that result in an effective reduction of the meshes, the marked continue decrease in mesh-size with temperature in the 1025-Zn_{85} and 1055-Zn_{192} samples could be a sign that with increasing temperature few bigger clusters re-arrange in a higher number of smaller clusters with reduced average mesh-size, as also deduced from the elastic plateau modulus. On the contrary, the mesh-sizes of the 2025-Zn_{70} do not show a remarkable temperature-dependence as in the other two samples as the pNIPAAm chains in the 2025-Zn_{70} network are shorter than the pEG-arms and therefore pNIPAAm chains attached to different stars might be too far apart for meeting while collapsing. This could mean that the majority of the pNIPAAm chains collapse on themselves and that only few pNIPAAm chains collapse together and form aggregates, as visually depicted in **Figure 6 c)**. The non-reachability of other pNIPAAm chains might explain the least remarked increment of the plateau moduli among change in temperature.

The different viscoelastic behavior of the 1025-Zn_{85}, 1055-Zn_{192}, and 2025-Zn_{70} shows how it is possible to tune the elastic properties of dual dynamic networks by changing the network building blocks thereby constituting a toolkit for future mechanical studies.

4. Conclusions

Hydrogels are polymer network swollen in water and this makes them appealing for biomedical applications, such as in drug delivery and tissue engineering. However, to be used in such applications, hydrogels have to mimic the functionality and the mechanics of natural tissues. For the improvement of the mechanical properties double networks can be used. In literature several examples can be found where the mechanical properties are studied by the means of non-linear rheology. We want to contribute to the field and presented here a systematic linear rheological study. Our base is a dual dynamic network (DDN) where to a common polymer network two dynamicities are attached. Our DDN hydrogel is based on tetra-pEG where each arm is end-capped with terpyridine and with pNIPAAm in a comb-like fashion. The elastic properties of these networks are investigated with linear oscillatory shear rheology under variation of the molar mass of pEG, of pNIPAAm, and the metal ion. This way we construct a toolkit for dual dynamic networks. Our results show that by increasing the chain length of pNIPAAm, the plateau modulus of the system increases accordingly. This is due to the collective agglomeration of the pNIPAAm chains above the LCST. In addition, our results suggest that longer chains are more likely to collapse together, therefore enforcing more the network, as shorter chains that are more likely to collapse on themselves. These results open a pathway for the systematic investigation of structure–property relationships in dual dynamic networks.

References

[1] Sood, N., Bhardwaj, A., Mehta, S., and Mehta, A., "Stimuli-responsive hydrogels in drug delivery and tissue engineering," Drug Deliv., 23, 748–770 (2016).

[2] Mantha, S., Pillai, S., Khayambashi, P., Upadhyay, A., Zhang, Y., Tao, O., Pham, H. M., and Tran, S. D., "Smart Hydrogels in Tissue Engineering and Regenerative Medicine," Materials 12, 3323 (2019).

[3] Guimarães, C. F., Gasperini, L., Marques, A. P., and Reis, R. L., "The stiffness of living tissues and its implications for tissue engineering," Nat. Rev. Mater., 5, 351–370 (2020).

[4] Li J. and Mooney D. J., "Designing hydrogels for controlled drug delivery," Nat. Rev. Mater., 1, 16071, (2016).

[5] Dong P., Schott B. J., Means A. K., and Grunlan M. A., "Comb Architecture to Control the Selective Diffusivity of a Double Network Hydrogel," ACS Appl. Polym. Mater., 2, 5269, (2020).

[6] Nicolella, P., Lauxen, D., Ahmadi, M., and Seiffert, S., "Reversible Hydrogels with Switchable Diffusive Permeability," Macromol. Chem. Phys., 222, 2100076 (2021).

[7] Gong, J. P., Katsuyama, Y., Kurokawa, T., and Osada, Y., "Double-network hydrogels with extremely high mechanical strength," Adv. Mater., 15, 1155–1158 (2003).

[8] Narita, T., Mayumi, K., Ducouret, G., and Hébraud, P., "Viscoelastic properties of poly(vinyl alcohol) hydrogels having permanent and transient cross-links studied by microrheology, classical rheometry, and dynamic light scattering," Macromolecules, 46, 4174–4183 (2013).

[9] Chen Q., Chen H., Zhu L., and Zheng J., “Engineering of Tough Double Network Hydrogels,” Macromol. Chem. Phys., 217, 1022, (2016).

[10] Li X., Yang Q., Zhao Y., Long S., and Zheng J., “Dual physically crosslinked double network hydrogels with high toughness and self-healing properties,” Soft Matter, 13, 911, (2017).

[11] Rossow, T., Habicht, A., and Seiffert, S., “Relaxation and dynamics in transient polymer model networks,” Macromolecules, 47, 6473–6482 (2014).

[12] Najafi M., Hebels E., Hennink W. E., and Vermonden T., “Poly(N-isopropylacrylamide): Physicochemical Properties and Biomedical Applications,” in Temperature-Responsive Poly-mers: Chemistry, Properties, and Applications (John Wiley & Sons Ltd., 2018).

[13] Koziol M. F., Fischer K., and Seiffert S., “Structural and Gelation Characteristics of Metallo-Supramolecular Polymer Model-Network Hydrogels Probed by Static and Dynamic Light Scattering,” Macromolecules, 54, 4375, (2021).

[14] Kestin J., Sokolov M., and Wakeham W. A., “Viscosity of liquid water in the range − 8 ° C to 150°C,” J. Phys. Chem. Ref. Data, 7, 941, (1978).

[15] Vermonden T., Van Steenbergen M. J., Besseling N. A. M., Marcelis A. T. M., Hennink W. E., Sudho E. J. R , Cohen Stuart M. A., “Linear Rheology of Water-Soluble Reversible Neodymium (III) Coordination Polymers,” J. Am. Chem. Soc., 126, 15802, (2004).

[16] Van De Manakker F., Vermonden T., el Morabit N., Van Nostrum C. F., and Hennink W. E., “Rheological Behavior of Self-Assembling PEG-Cyclodextrin / PEG-Cholesterol Hydrogels,” Langmuir, 24, 12559, (2008).

[17] Karvinen J., Ihalainen T. O., Calejo M. T., Jönkkäri I., and Kellomäki M., “Characterization of the microstructure of hydrazone crosslinked polysaccharide-based hydrogels through rheological and diffusion studies,” Mater. Sci. Eng. C, 94, 1056, (2019).

[18] Risica D., Barbetta A., Vischetti L., Cametti C., and Dentini M., “Rheological properties of guar and its methyl, hydroxypropyl and hydroxypropyl-methyl derivatives in semidilute and concentrated aqueous solutions,” Polymer (Guildf)., 51, 1972, (2010).

[19] Jangizehi A., Ahmadi M., and Seiffert S., “Emergence, evidence, and effect of junction clustering in supramolecular polymer materials,” Mater. Adv., 2, 1425, (2021).

[20] Ahmadi M. and Seiffert S., “Thermodynamic control over energy dissipation modes in dual-network hydrogels based on metal-ligand coordination,” Soft Matter, 16, 2332, (2020).

5. Defect-controlled softness, diffusive permeability, and mesh-topology of metallo-supramolecular hydrogels

Paola Nicolella,[a,*] Martha Franziska Koziol,[a,*] Lucas Löser,[b] Kay Saalwächter,[b] Mostafa Ahmadi,[a] and Sebastian Seiffert[a]

Published in: *Soft Matter*, **2022**, 18, 1071-1081

DOI: D1SM01456K

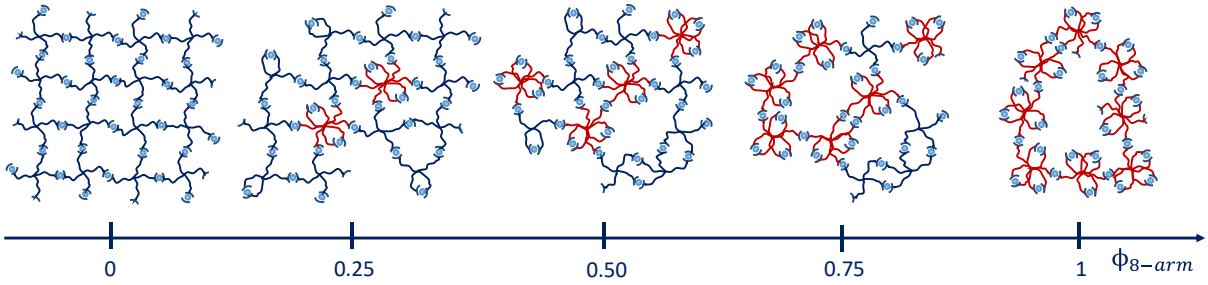

Supplementary information is available in Chapter 10.3.

Author Contributions:

Paola Nicolella: Coordination of the project, synthesis of the polymer precursors together with the student Alena Kuzmina, rheological measurements, preparation of the samples for DQ-NMR, graphics and conceptual design, interpretation of the results, preparation of the manuscript

Martha Franziska Koziol: Synthesis of the dye-labelled polymers, FRAP experiments, relative figures and text, fitting of the curves, revision of the manuscript

Lucas Löser: DQ-NMR experiments, relative figures and text, interpretation of the results

Kay Saalwächter: Supervision of DQ-NMR part, revision of the manuscript

Mostafa Ahmadi: Concept of the work, discussion of the results

Sebastian Seiffert: Supervision of the work, correction of the manuscript

[a]*Johannes Gutenberg-Universität Mainz, Department of Chemistry,*

Duesbergweg 10-14, D-55128 Mainz, Germany

[b]*Institut für Physik-NMR*

Martin-Luther-Universität Halle-Wittenberg,

Betty-Heimann-Str. 7, D-06120 Halle, Germany

**These authors contributed equally*

Summary

In the development of new polymeric materials, the role of defects cannot be underestimated, as imperfections can always naturally occur in polymer networks and their presence strongly influences the macroscopic properties such as the elasticity and permeability. In this context, systematic studies on model supramolecular systems lays the ground for further studies on multi-component systems.

In this collaborative work, the impact of defects on the properties of a supramolecular networks is investigated. This is achieved with the methodological variation of a model system by systematic introduction of known connectivity defects. Therefore, different ratios of a 4-arm terpyridine-functionalized poly(ethylene) glycol (pEG-tpy) are mixed with a 8-arm pEG-tpy of a twofold molar mass and afterwards complexated with Zn(II) metal ions in stochiometric ratio. The interplay between the molar masses and number of arms of the two polymer precursors translates in the same arm length for every pEG and number of potential connections. The increase of the 8-arm pEG-tpy volume fraction in the system determines an increase in the average mesh-size and a decrease in the plateau modulus, as investigated by oscillatory shear rheology. These outcomes are accompanied by an increase of the self-diffusion coefficient of dye-labelled pEG-tpy precursors in the network, as investigated by fluorescence recovery after photobleaching, further denoting a strong interplay with the dynamics of the system.

These results can be explained with the formation of connectivity defects, and in particular loops, as confirmed by DQ-NMR, as the 8-arm pEG-tpy precursor is more prone to form intra-molecular instead of inter-molecular connections due to the higher local density of arms. Therefore, an incremental concentration of this precursor determines an increasing deviation from the properties of the model system, thereby confirming the utility to perform such investigations when engineering new materials.

Acknowledgments

This work was funded from the H2020 Programme (MARIE SKŁODOWSKA-CURIE ACTIONS) of the European Commission's Innovative Training Networks (H2020-MSCA-ITN-2017) under DoDyNet REA Grant Agreement No.765811, as well as through the DFG Research Unit FOR 2811, SA982/14-1 (Project. No. 397384169). Parts of this work were further supported by the German Research Foundation (DFG) under Grant No. SE 1888/7-1 (Project No. 376900084). Microscopy data of this study were acquired with a confocal laser scanning microscope funded in part by the Major Research Instrumentation Program of the German Research Foundation under grant No. INST 247/878-1 FUGG. Paola Nicolella thanks Evelyne Van Ruymbeke and Charles-André Fustin for useful discussions, and Rowanne Lyons and Alena Kuzmina for support with the synthesis. Martha Franziska Koziol kindly thanks Holger Adam for helpful methodological advices concerning FRAP. The authors would like to thank the referees of the peer-review process for their valuable and helpful comments.

1. Introduction

Defect engineering in soft matter is a wide field of research that allows for tuning material properties on multiple levels. [1] In one branch of that discipline, structural inhomogeneities affect the properties of polymer-network gels, specifically the local and global elasticity, [2] fracture mechanism, [3] and the diffusive permeability of guest substances, [4] and since these properties lay the ground for the main applications of gels, the impact and ability of controlling such inhomogeneities is crucial. Prominent examples for inhomogeneities are found in hydrogels, which are three-dimensional polymer networks swollen in water. [5–7] These polymer networks can be formed by connection of polymer strands either by supramolecular or covalent crosslinks. While covalent networks are stable in form and shape, supramolecular networks have the great advantage of being dynamic which means being responsive and recyclable. As a consequence, also the heterogeneities of covalent networks are frozen in time and space, whereas those of supramolecular networks follow spatiotemporal evolutions. The study and modelling of the extent, effect, and evolution of heterogeneities and defects in supramolecular networks require a model platform. One such platform is model transient networks formed by supramolecular crosslinking of multi-arm star-like polymer precursors. In such a network, the network strands denote the chain sections between branching points of two adjacent polymer precursors, and their length determines the network mesh-size ξ, as illustrated in **Figure 1**. During network formation, different types of defects can form. Uneven distribution of the network crosslinks causes global spatial heterogeneities of some tens to hundreds of nanometers in space, and these defects are further pronounced when the polymer network is swollen. [8]

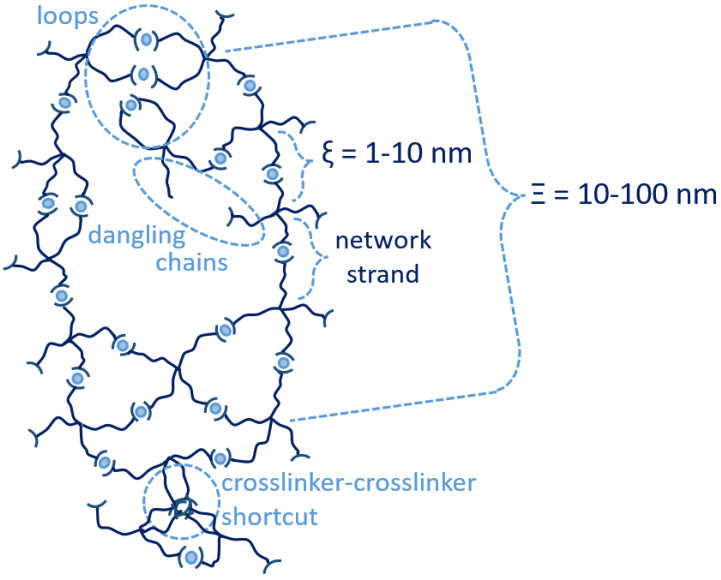

Figure 1. Defects in polymer networks created by interconnection of tetra-arm star supramolecular precursors on different length scales. Local connectivity defects on the order of few nanometers form due to misconnectivities in the network. Global defects on the order of 10–100 nm result due to the inhomogeneous distribution of crosslinking density.

Furthermore, irregularity in the local crosslinking-junction functionality results in local connectivity defects, which are in the magnitude of 1-10 nm, as shown in **Figure 1.** [7,9] These connectivity defects are loops, dangling chains, and crosslinker–crosslinker shortcuts. A loop is formed when several (usually two) arms of the same polymer form intra-molecular connections, or when two adjacent polymers form multiple inter-molecular connections, resulting in higher order loops. [10] A dangling chain is an arm that does not form any connections with another arm. A crosslinker-crosslinker shortcut is formed when two crosslinks interact with each other in form of uncontrolled clusters with varying number of junction functionalities. In view of this picture, we define connectivity as the number of potential inter-molecular connections that a branched polymer macromolecule can form with its arms. Thus, the expected connectivity in a perfectly regular network consisting of only tetra-arm shaped telechelic polymers is four.

For rational material design, it is essential to understand how these different types of defects affect the properties of the hydrogel, such as its viscoelasticity and permeability, to optimize their use in applications. As hydrogels are constituted mainly by water, they are suitable for biomedical applications, such for example in tissue engineering or drug delivery. [11–13] However, to be used in these applications, they need to meet further requirements. In tissue engineering, for example, they need to resemble the mechanical properties of original natural tissues, and this can be challenging, [14,15] as the stiffness of living tissues can vary from a few Pascals to giga-Pascals, and it is even more challenging when considering the diverse functions of tissues. [10,11] In drug delivery, by contrast, not only the stiffness or softness of the tissue is important, but also the diffusive permeability, which is governed by the mesh-size of the hydrogel. [16] If the drug is smaller, similar, or larger than the network mesh-size, then the diffusion would be fast, slow, or even hindered, respectively. [16] Therefore, the control of the diffusion kinetics inside the hydrogel through engineering the mesh-size is crucial for its applications.

There are several approaches to engineer the mesh-size and its distribution in hydrogels. One way is to use precursors of different molecular weights, as suggested by Sakai *et al.* [17] These workers have systematically varied the heterogeneous distribution of the mesh-size in covalent model-network hydrogels formed by tetra-poly(ethylene glycol) (tetra-pEG), by employing precursors of two different molecular weights. [17] Despite they did not characterize the heterogeneities on the nanoscale, their macroscopic findings suggest that these bimodal networks have properties of a hydrogel having a strand size in between the arm length of the two precursors. [17]

Another approach to control the diffusion inside a hydrogel is to add dangling chains to the main network. With this strategy, Grunlan *et al*. controlled the mesh-size of a hydrogel with the introduction of thermoresponsive and charged dangling chains. [18] Their findings show that with negatively charged chains, smaller meshes are possible. [18] In an own previous work, we introduced poly(*N*-isopropylacrylamide) (pNIPAAm) dangling chains into a supramolecular polymer network and were able to similarly hinder the diffusion of small probes upon switching temperature above the lower critical

solution temperature of pNIPAAm. [5] Similarly, we investigated how the network dynamics of gels, constituted by chains carrying sticky side-groups, changes with the introduction of sticky tracers having the same or lower connectivity than the network itself, thereby creating local connectivity defects.[4] Our findings show that the chain dynamics is enhanced in case of the network with connectivity defects, meaning that the probe diffuses faster than expected. [4] The effect of defects on mechanical properties has also been studied by means of simulations. For example, Shibayama *et al.* have introduced random defects in tetra-pEG networks and investigated the influence of the structural inhomogeneity on the mechanical properties. [19] Their findings show that with an increasing defect fraction, the Young modulus of the tetra-pEG networks decreased accordingly. [19]

Targeted mesh mesh-size variations or intentional incorporation of defects in polymer networks allow for a systematic investigation of their impact on the final material properties such as permeability or viscoelasticity. A recent review on defect engineering in soft matter highlights the utmost importance of structure control to implement a novel type of rational material design based on these aforementioned minor structural deviations. [1]

With this work, we aim to contribute to this emerging field of soft matter material design by presenting how to tailor supramolecular hydrogels in a systematic way via connectivity mismatches. We achieve that by systematically introducing different percentages of connectivity defects in a model supramolecular network and investigating the resulting macroscopic elastic response by oscillatory shear rheology, the microscopic self-diffusivity by fluorescence recovery after photobleaching (FRAP), and characterizing and proving the specific type of defects by double-quantum NMR (DQ-NMR).

Our material basis is composed of a supramolecular pEG hydrogel, where each arm of a star-shaped precursor is functionalized with a terpyridine unit that is capable of forming transient bis-complexes with divalent zinc ions. Starting from a regular network that only consists of 4-arm pEG-terpyridine macro-precursors (left network in **Figure 2**), we successively replace a certain percentage of 4-arm pEG building blocks by 8-arm pEG-terpyridine polymers. To ensure a constant total terpyridine concentration, coming along with a constant number of arms, we select the molar mass of the 8-arm pEG to be a twofold of that of a 4-arm pEG. In other words, replacement of two macromolecules with four arms by one macromolecule with eight arms yields the same number of overall terpyridine units but a different degree of connectivity, keeping the same number of network strands per total volume constant (**Figure 2**). With increasing amount of connectivity defects, the hydrogel becomes softer and the self-diffusivity inside increases, as demonstrated by complementary oscillatory shear rheology and FRAP experiments. These findings are associated with the emergence of various defect types, which are quantified by double quantum-NMR. Our results suggest a new paradigm for tuning properties of supramolecular hydrogels in a rational manner that might be transferable to other transient systems.

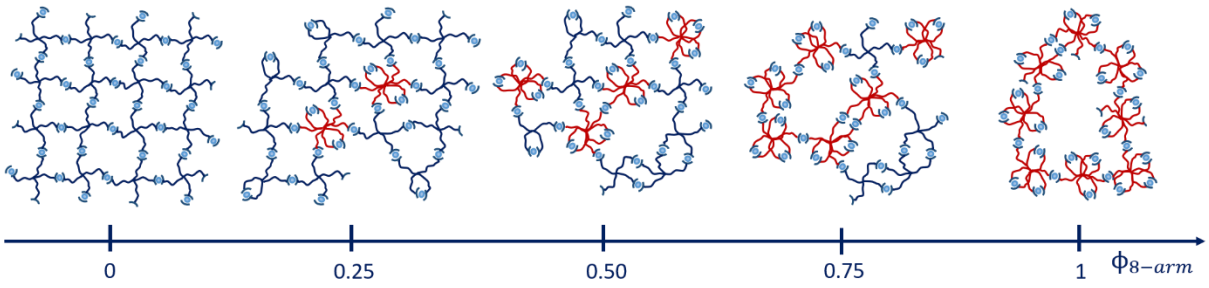

Figure 2. Concept of this work. Metallo-supramolecular polymer-network gels composed of 4-arm pEG-terpyridine (M_w = 20 kg mol^{-1}) and 8-arm pEG-terpyridine (M_w = 40 kg mol^{-1}), combined in different ratios, thereby increasing the amount of connectivity defects in a controlled way. The impact of connectivity defects on macroscopic elastic and microscopic permeability properties are then investigated.

2. Experimental

2.1 Sample syntheses

The list of materials and the synthesis procedure can be found in the ESI. In short, the hydroxyl termini of the star-shaped commercially available 4-arm 20K and 8-arm 40K pEG polymers were converted to terpyridine units by a Williamson type ether synthesis (**Figure SI1, ESI**).

3. Methods

3.1 Oscillatory shear rheology

To prove the effect of defects on the elastic properties of the supramolecular hydrogels, oscillatory shear rheology experiments were performed. For this purpose, stock solutions of 4-arm 20K and 8-arm 40K pEG-terpyridine with a concentration of 70 g L^{-1} were prepared by dissolving the appropriate amount of each polymer in Milli-Q water. This concentration was chosen to obtain gels in a regime well above the overlap concentration of a 4-arm 20K pEG-terpyridine (c* = 35 g L^{-1}). [20] Another aqueous stock solution of zinc nitrate hexahydrate was prepared and a ratio of terpyridine to metal of 2 : 1 was ensured. In a glass vial, the polymer solution was inserted and then subsequently, the metal ion solution was added quickly. For hydrogels consisting of two precursor polymers (4-arm 20K and 8-arm 40K), both polymer stock solutions were mixed in a glass vial before adding the metal ion stock solution. All mixtures were then vigorously vortexed until complete gel formation. In total, five samples were prepared and characterized, with 8-arm pEG-terpyridine volume fractions $\phi_{8\text{-arm}}$ being respectively 0, 0.25, 0.5, 0.75 and 1. Finally, the gels were allowed to equilibrate overnight on a plate shaker at room temperature, to remove all air bubbles.

Oscillatory shear rheology experiments were carried out on an Anton Paar rheometer of the type MCR 302 (Anton Paar, Graz, Austria), equipped with a solvent trap to avoid dehydration and a parallel plate geometry PP-25. After equilibration, amplitude sweeps were recorded in order to determine the linear viscoelastic regime. These were done at a temperature of 25 °C, a constant shear frequency of ω = 1 rad s^{-1} and an increasing amplitude of γ = 0.1–100%. Afterwards, the sample was allowed to equilibrate

again and then frequency sweeps were obtained at 25 °C, at a constant shear rate of $\gamma = 0.1\%$ and a frequency range of $\omega = 0.01–100$ rad s^{-1}.

3.2 Fluorescence recovery after photobleaching

Fluorescence recovery after photobleaching was chosen as a method to microscopically investigate the self-diffusivities of 4-arm pEG-terpyridine macromolecules within the hydrogels depending on the amount of added 8-arm pEG-terpyridine. For this purpose, 3 wt% of a dye-labelled pEG moiety that contains both required functional groups on each arm, a terpyridine unit and a fluorescent NBD group, was integrated into the gels. These polymer tracers were synthesized according to a previously described procedure [21] and are visualized in **Figure SI4 (ESI)**.

The FRAP experiments were carried out on a Leica TCS-SP8 AOBS SMD confocal laser scanning microscope, equipped with a 20x immersion objective (HC PL APO CS2 20x/0.75 IMM, numerical aperture: 0.75) and a PMT detector. Aqueous stock solutions of the 4-arm pEG-terpyridine and the 8-arm pEG-terpyridine (c = 118.5 g L^{-1}, respectively) were prepared, as well as of the NBD-tagged fluorescent 4-arm pEG-terpyridine (c = 14.7 g L^{-1}) and the zinc nitrate hexahydrate (c = 7.28 g L^{-1}). Final gels were prepared by mixing the polymer stock solutions (40 µL total volume: 0%; 25%, 38%, 50%, 63%, 75%, and 100% 8-arm content), adding 10 µL of the dye-labelled polymer stock solution, followed by the addition of 20 µL zinc nitrate solution and subsequent vortexing. With this procedure, the desired stoichiometric ratio of terpyridine to zinc of 2 : 1 was obtained, as well as the overall polymer concentration of 70 g L^{-1}. Due to the twofold molar mass of the 8-arm pEG-terpyridine compared to the 4-arm pEG-terpyridine, the number of terpyridine stickers remains constant in all networks while a sole variation in the overall connectivity is achieved. Samples were gently shaken over night at 39 °C to reach full equilibration. After cooling to room temperature for two hours, the gels were loaded into an eight-well plate (Ibidi®) and sealed to avoid dehydration during the scans. Prior to each measurement, a set of four pre-bleach images is recorded. Permanent irradiation of the fluorophores and therefore creation of a bleached point pattern was achieved by applying a full-power laser beam (10 mW) with a duration of 1 s. A weak reading beam with a wavelength of 488 nm (maximum excitation wavelength of the NBD-dye) was used to excite the dye molecules during the scan series. For the recovery process, it is important to use a remarkable attenuated laser beam to avoid re-bleaching of the region of interest. A series of 250 images was recorded with time intervals of 0.173 s between each scan (bidirectional scan frequency: 400 Hz) to capture the re-emerging of fluorescing macromolecules into the bleached area. Analogous to previous works, [4,22] the FRAP data were analysed using a diffusion model that is based on fitting Gaussian shaped intensity profiles I(r,t) to the time-depending disappearance of the initial bleached spot. [23,24] The bleached area vanishes due to the exchange and diffusive motion of the dye-labelled supramolecular polymers throughout the system until its pre-bleached fluorescence intensity is fully recovered.

3.3 ^{1}H DQ-NMR

Low-field NMR experiments were performed on a Bruker MiniSpec mq20 with a magnetic field of B_0 = 0.47 T. The pulse lengths were between 1.5 and 1.7 µs for 90 ° pulses and between 3.5 and 4.0 µs for 180 ° pulses. A BVT3000 temperature unit was used to keep the samples at a stable temperature of 30 °C ± 1 °C. Samples were synthesized in 10 mm diameter glass tubes according to the synthesis protocol presented in the rheology section and flame-sealed at about 5 cm height to prevent solvent evaporation during the experiments. For the DQ experiments, the Baum-Pines sequence [25] with incremented delays between the pulses and a constant number of two cycles was used. The recycle delay was set to 1.5 s, which is enough to filter out about 90% of the HDO signal (estimating an average longitudinal relaxation time of about $T_{1,\mathrm{HDO}}$ = 12 s), while retaining >95% of the polymer signal (estimation $T_{1,\mathrm{poly}}$ = 0.5 s). This was validated by the first DQ-measurement of the sample consisting of only 4-arm stars ($\phi_{8\text{-arm}}$ = 0) (see DQ-NMR results), where a combined fraction of defects and solvent signal of less than 1% was measured. Therefore, we refrain from the commonly used procedure of quantifying the leftover HDO component after the T_1-filtering by exploiting the large difference in T_1 relaxation times in a saturation recovery experiment, because such a small contribution will be shown to be negligible and the introduced uncertainty significantly larger than the obtained value.

In the following, a concise overview of the obtained data using the DQ experiment and a reasoning for the data treatment is provided. For further information on the derivation and meaning of the measured quantities, the reader is referred to Ref. [10]. After application of the Baum–Pines sequence, two phase cycle-controlled signals are obtained: The first one is the DQ build-up function $I_{\mathrm{DQ}}(t_{\mathrm{DQ}})$, which contains structural information about the sample in the form of residual dipolar coupling (RDC) values and its quantitative distribution. However, it is also modulated by transverse relaxation of the total NMR signal, so the RDC is not easily accessible using only a simple fitting procedure to the $I_{\mathrm{DQ}}(t_{\mathrm{DQ}})$ curve. Thus, a second signal function, sometimes also called reference function $I_{\mathrm{ref}}(t_{\mathrm{DQ}})$ is needed for independent quantification of the relaxational contribution to the signal. Using a specific phase cycle described in Ref. [26], the shape of this signal will only depend on the transverse relaxation times being present in the sample. As shown and already applied on, e.g., the tetra-pEG system of Sakai *et al.* [27] and another terpyridine-based tetra-pEG hydrogel, [28] the following fitting functions (1-3) are used for the two signals:

$$I_{DQ}(\tau_{DQ}) = \sum_{i=1}^{3} a_i \cdot I_{nDQ,i}^{A-l} \cdot \exp[-\left(\frac{\tau_{DQ}}{\tau_i}\right)^{\beta_i}] \quad (1)$$

and

$$I_{\Sigma\mathrm{MQ}}(\tau_{DQ}) = \sum_{i=1}^{3} a_i \exp[-\left(\frac{\tau_{DQ}}{T_{2,i}}\right)^{\beta_i}] + a_{\mathrm{tail}} \exp[-\frac{\tau_{DQ}}{T_{2,\mathrm{tail}}}] \quad (2)$$

Here I_{nDQ} combines the Abragham-Like (A-l)-function that is defined as

$$I_{nDQ}^{A-l}(\tau_{DQ}) = 0.5\left\{1 - \exp\left[-\left(0.378 D_{res}\tau_{DQ}\right)^{1.5}\right] \times cos\left(0.583 D_{res}\tau_{DQ}\right)\right\} \qquad (3)$$

that was firstly derived in Ref. [29]. Both functions are fitted simultaneously to the $I_{\Sigma MQ}$ and I_{DQ} data, with shared parameters for the relaxation part and the respective fractions a_i. In all known cases with tetra-pEG-based systems, including this work, a minimum of 3 A-I functions is needed to sufficiently fit the curves. Each extracted component a_i corresponds to a certain species with molecular mobility and therefore to a certain type of connectivity motif in the network. A fourth, purely exponential function that is exclusive to I_{ref}, is used for characterising sample fractions with unhindered, isotropic motion (e.g., protonated solvent, sol, dangling chains), which reflects in the long tail of the relaxation function, while not contributing to the DQ function. In contrast to Ref. [27] we refrain from explicitly assigning all components a_i to certain connectivities as, admittedly, the simply picture of three easily distinguishable types of connectivities is certainly a simplification in such a complex system. Instead, we only assign the component a_1 to the single link, as the single link can safely be assigned to the component with the highest RDC using the proportionality $D_{res} \sim M_c^{-1}$ and the simple argument of an increased, apparent molecular weight of the crosslinks for higher order connectivities. Analysis of the data shows that a two-component model is not sufficient, thus we still use a 3-component model as the model with the least possible parameters, and therefore, we present results in a 3-parted fashion, however, we suggest to only interpret the sum of the higher order connectivity defects a_2+a_3 or the ratio between the ideal connectivities a_1 and the sum a_2+a_3. This is especially important in the case of samples containing 8-arm stars, as here even more possible connections can be formed which, however, cannot be extracted with our approach due to the strongly increasing number of fitting parameters and the increasing fitting ambiguity.

4. Results and discussion

Our material basis for systematically studying the effects of connectivity defects on the elastic response and diffusive permeability of supramolecular model hydrogels is composed of 4-arm and 8-arm pEG where each arm was end-capped with terpyridine units that are capable of forming bis-complexes with zinc ions. To ensure the same number of terpyridine stickers in each sample, the 8-arm pEG was chosen with a two-fold molar mass compared to the 4-arm pEG, therefore also ensuring the same arm length. To increase the amount of connectivity defects, 8-arm pEG-terpyridine was introduced into the 4-arm model pEG-terpyridine system in different volume fractions $\phi_{8\text{-arm}}$. To investigate the influence of connectivity defects on the properties of supramolecular hydrogels, the macroscopic elastic response of the gels was characterized by oscillatory shear rheology whereas the microscopical diffusive permeability was characterized by FRAP measurements. Finally, the defects were quantified nanoscopically by DQ-NMR. The combination of these three characterization techniques allows us to

obtain information not only on the relaxation dynamics, but also on the structural properties of the system at multiple length-scales.

4.1 Oscillatory shear rheology

The influence of connectivity defects on the macroscopic elastic response of a hydrogel was probed through oscillatory shear rheology experiments. Starting from a network purely composed of 4-arm pEG-terpyridine macromolecules, we successfully replaced different amounts of 4-arm pEG-terpyridine by 8- arm 40K polymers, thereby keeping the number of sticky terpyridine units constant, and an overall polymer concentration of 70 g L^{-1}. The volume fraction of 8-arm pEG-terpyridine $\phi_{8\text{-arm}}$ is then respectively 0, 0.25, 0.5, 0.75 and 1. Frequency-dependent dynamic moduli were investigated at 25 °C. The frequency-dependent dynamic moduli of all networks can be described by a single Maxwell element, as demonstrated in **Figure 3 (A)** by the dashed lines.

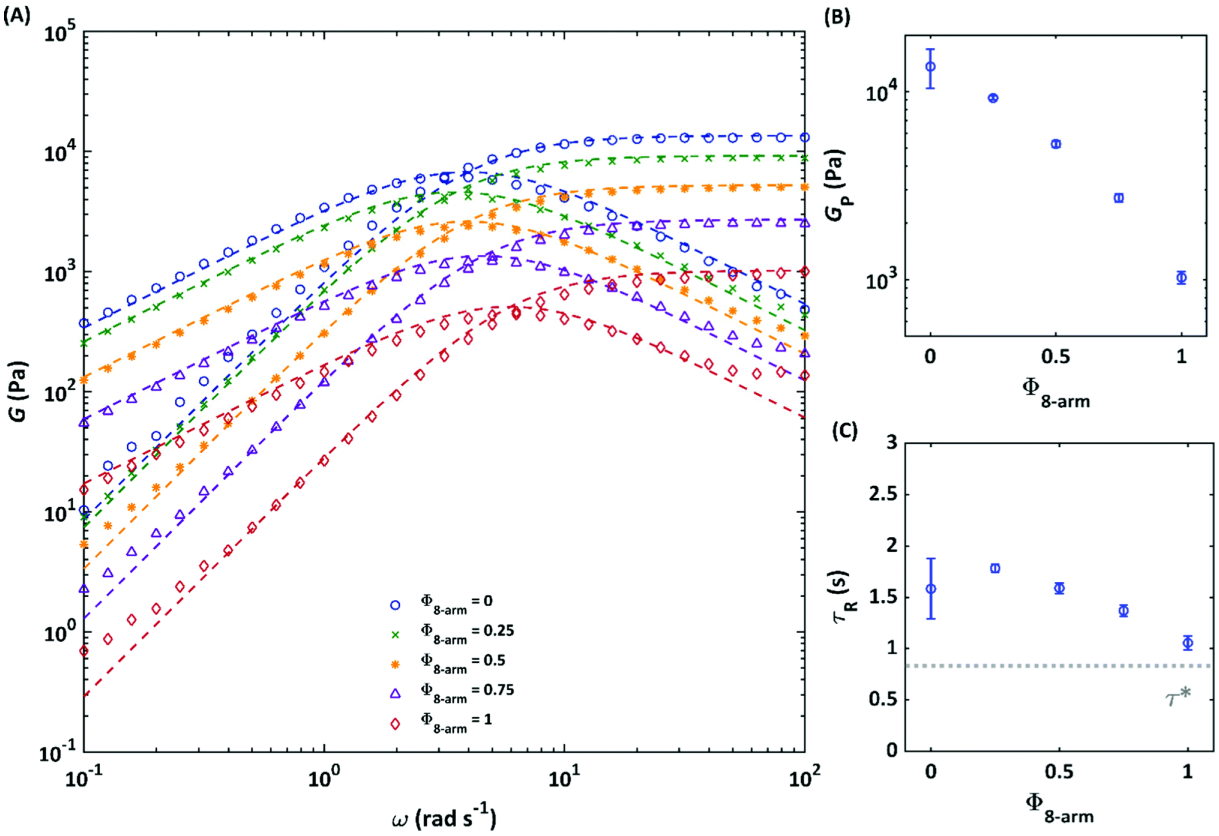

Figure 3. Frequency-dependent elastic and loss modulus of the hydrogels composed by different ratios of 4-arm pEG-terpyridine (M_w = 20 kg mol^{-1}) and 8-arm pEG-terpyridine (M_w = 40 kg mol^{-1}) with zinc in water at a total polymer concentration of 70 g L^{-1} and a temperature of 25 °C, assuring the same terpyridine concentration in all gels. Dashed lines represent fits to the Maxwell model (A). Influence of the 8-arm pEG-terpyridine proportion on the plateau modulus G_p (B) and on the relaxation time τ_R (cross-over frequency of G' and G'') (C). The lifetime τ^* of an isolated zinc-terpyridine complex (taken from Ref. [37]) in dilute aqueous conditions is depicted as dotted grey line. The error bars depict the fit parameters of the Maxwell model within a confidence interval of 95%. The pure 4-arm sample is an outlier.

However, with increasing $\phi_{8\text{-arm}}$, a slight deviation in the moduli at high and low frequencies becomes visible. Such a deviation from the Maxwell model might be an indication of multiple relaxation times. [30] These relaxation times can derive from the relaxation of higher order loops, where two polymer stars share more than one connection or a bigger loop results by connecting several stars in circle. The measured plateau moduli depending on the volume fraction of 8-arm 40K polymers is shown in **Figure 3 (B)**. The pure 4-arm 20K sample exhibits the highest elastic modulus corresponding to $G_{\text{P,4-arm 20K}}$ = 13 kPa, whereas the lowest elastic modulus is obtained in the pure 8-arm 40K gel, corresponding to $G_{\text{P,8-arm 40K}}$ = 1 kPa. The plateau storage moduli of the samples at intermediate compositions systematically decrease with increasing the volume fraction $\phi_{8\text{-arm}}$. Based on the affine network model theory, we expected all samples to show the same plateau modulus, as the number of network strands per volume (corresponding to ν) is kept constant in all gels. In this model, the plateau modulus G_N^0 is given by

$$G_N^0 = \nu RT \tag{4}$$

where ν is the number of network strands per volume, R is the universal gas constant, and T denotes the temperature. ν can be calculated from the molar concentration of pEG precursors and it corresponds to

$$\nu = \frac{f\mu}{2} \tag{5}$$

with f the functionality of the precursor and μ the density of network crosslinks. [31] Hence, the theoretical plateau modulus for both pure 8-arm 40K and 4-arm 20K networks is calculated to be roughly G_N^0 = 17 kPa. This value is valid for a fully percolated and defect-free theoretical polymer network. However, experimental polymer networks always show intrinsic topological defects that determine a deviation from the theoretical value. [31] In this context, the measured plateau modulus of the pure 4-arm network ($G_{\text{P,4-arm 20K}}$ = 13 kPa) is not significantly lower than the calculated theoretical one. Since this is the system with the highest modulus, it will be further taken as reference when compared to the other samples. If the plateau modulus is considered as a quantification of the elastically active network strands, [5] the continuous decrease of G_P depending on an increasing amount of 8-arm in the networks, indicates a decreasing degree of network connectivity. As the matter of fact, with a higher density of arms per each molecule, the 8-arm is more likely to form intra-molecular instead of inter-molecular associations. [32] Alternatively to the affine model, one could use the phantom model, which would consider the functionality of the stars, instead of the total number of strands. In this case, the plateau modulus of the 8-arm pEG is predicted to be higher than the 4-arm pEG. In addition, the phantom model would need to define a functionality for the mixed system, which has not been taken into account so far. Up to now, it is still a matter of debate which of both models is more suitable to describe the rheological spectrum of supramolecular polymer networks, whereas a concentration-dependent transition between the two has been found for chemically crosslinked tetra-arm pEG. [33] The concentration used in this study (2c*), would fall at the boundary between these two models. However, the initial hypotheses of

our studies are in line with the affine model, since we designed our study such to have the same number of network strands in each sample.

The fact that the 8-arm 40K pEG network exhibits a lower plateau modulus can be explained by connectivity defects occurring due to a higher local density of arms. With such overcrowding of arms, it is more likely that two neighbouring arms of the same macromolecule find each other thereby creating loops of different orders. These loops cause a loss in modulus, because they do not actively store energy. Therefore, going from 100% 4-arm pEG-terpyridine ($\phi_{8\text{-arm}} = 0$) to 100% 8-arm pEG-terpyridine ($\phi_{8\text{-arm}} = 1$), the network becomes locally more heterogeneous.

In addition to the elastic modulus, the terminal relaxation times (inverse of the crossover frequency of G' and G'') of the networks slightly decrease with increasing $\phi_{8\text{-arm}}$ (**Figure 3 (C)**). This can be explained by the fact that the 8-arm pEG has a higher functionality and therefore each terpyridine exchanges faster because it is easier to find another free ligand of another 8-arm polymer in close proximity. Even though, for crowded systems there is usually a prolongation of the effective lifetime of the bonds due to the constraint of other chains, this usually occurs in the melt state or at high concentrated regime, while we are still in the semi-dilute regime. In addition, it was already observed in other pEG-terpyridine telechelic systems that the dynamic of the complex in the polymer in enhanced when compared to the one of the terpyridine and metal complex alone. [34] This is in line with previous observations for associative networks with cluster forming end groups, for which it was shown that terminal flow is indeed mediated by the relaxation of single chains. [35,36] Moreover, as it can be seen from **Figure 3 (C)**, with increasing $\phi_{8\text{-arm}}$, the dissociation times of the gels approaches the dissociation time τ^* of an isolated zinc-terpyridine complex in dilute conditions (dotted grey line), taken from Ref. [37] as $1/k_{diss}$. The macroscopic network relaxation time measured by rheology is influenced by the complex dissociation time, as the applied shear stress is released by chain motion and subsequent breaking of the transient crosslink. However, a direct comparison between both times should be considered carefully. First, the lifetime of the isolated complex has been determined in aqueous dilute conditions whereas our network relaxation time is obtained in a semi-dilute regime of 2c*. An earlier work of Olsen *et al.* [38] showed by Forced Rayleigh experiments (FRS) that the complex dissociation time is also strongly influenced by the crowded environment of a network and can therefore deviate from the value obtained in dilute un-percolated conditions. Second, Wilkins et al. [37] used pure terpyridine (2,6-Bis(2-pyridyl)pyridine) for their metal exchange studies whereas in our case, the terpyridine unit is attached to a polymer chain via oxygen atom that influences the electronic properties of the aromatic pyridiyl-ring and therefore also the complex dissociation time. With increasing 8-arm (40K) content, the macroscopic network relaxation time approaches the dissociation time in dilute conditions. In all other networks, the influence of the bond lifetime renormalization (meaning that the complex opens and closes several times before it actually releases the applied shear stress) becomes pronounced. This bond lifetime renormalization vanishes with increased defect fraction.

We further estimate the network mesh- size ξ from the elastic modulus by

$$\xi = \left(\frac{RT}{G_P N_A}\right)^{1/3} \quad (6)$$

with R the universal gas constant, T the temperature, G_P the plateau modulus, and N_A the Avogadro number. [39] According to these calculations, we find an increase in the mesh size with increasing $\phi_{8\text{-arm}}$ in the network (**Figure 4 (A)**). We suggest the 8- arm pEG molecules to significantly contribute to the formation of loops and dangling ends, leading to an increase of the average network mesh size. The mesh-size in a pure 8-arm pEG-terpyridine network is found to be approximately three times larger than the one of the pure 4-arm pEG-terpyridine, suggesting that bigger meshes are formed as a combination of domains with a lower local density of polymers and domains with a higher local density of polymers. A schematic visualization of these higher order loops is shown in **Figure 4**, where **Figure 4 (B)** represents the pure 4-arm 20K network and **Figure 4 (C)** depicts a network with included connectivity defects (pure 8-arm pEG). It is shown that with increasing number of intra-molecular connections (loop formation), the average mesh-size also increases. To prove our hypothesis on the micro- and nano-scale, we further study the diffusive permeability of the networks by FRAP, and the structural properties by DQ-NMR, as follows.

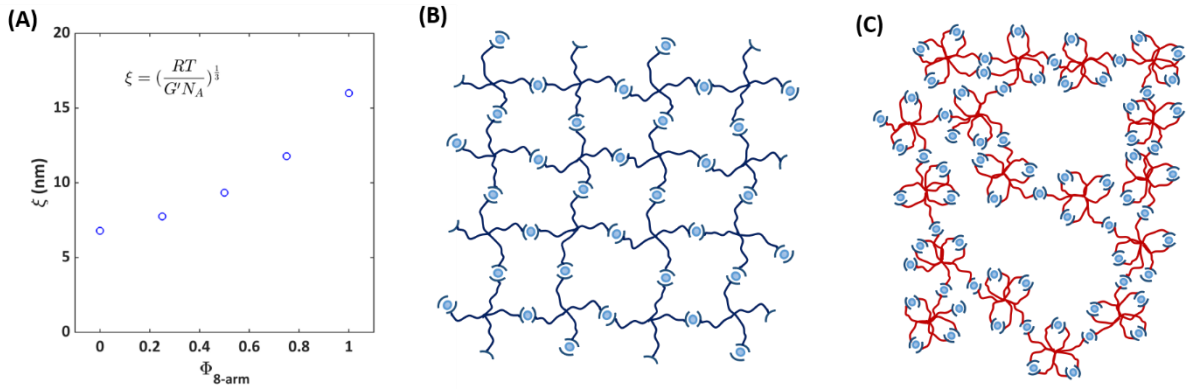

Figure 4. Mesh-size of the network in function of the fraction of 8-arm pEG in the system (A). Ideal 4-arm 20 K network with homogeneous mesh-size distribution (B) and pure 8-arm 40 K network that includes connectivity defects (C). The formation of intra-molecular loops has the consequence to increase the average mesh-size of the network by forming higher order loops.

4.2 Fluorescence Recovery after Photobleaching

To microscopically investigate the influence of connectivity defects on the network structure and the resulting diffusive permeability properties, FRAP measurements were conducted.

For this purpose, a small fraction of a 4-arm polymer 20K (3 wt%) with fluorescing NBD groups attached to each arm in addition to the sticky terpyridine group was integrated into the 4-arm / 8-arm matrix gels. Based on their structural similarity, it was possible to track the intrinsic motion of the 4-arm polymer building blocks within the networks without the ap-plication of any external shear forces

such as those used during rheology experiments. The self-diffusion coefficients of the investigated gels versus $\phi_{8\text{-arm}}$, are shown in **Figure 5**.

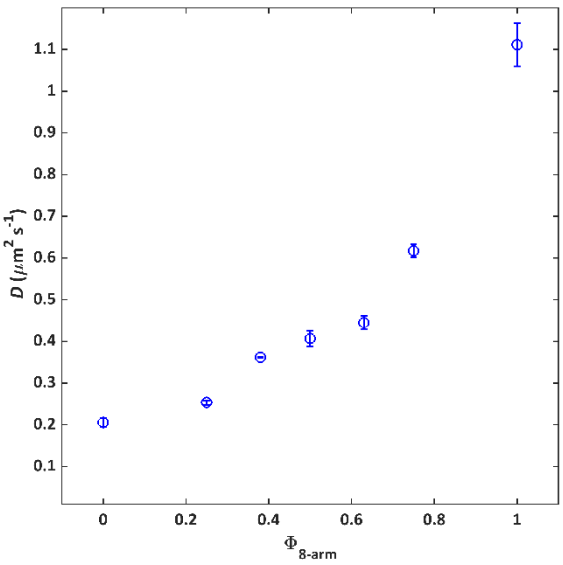

Figure 5. Self-diffusion coefficients of a 4-arm fluorescently dye labelled pEG-terpyridine within the networks consisting of different ratios of 4-arm and 8-arm pEG-terpyridine (c_{total} = 70 g L^{-1}), obtained by FRAP. Errorbars represent standard deviations of measurements at three randomly chosen gel positions.

As a general trend, the diffusion coefficient increases by a factor of 5 from 0.21 μm² s^{-1} to 1.1 μm² s^{-1} between the two composition extremes pure 4-arm 20K and pure 8-arm 40K. This observation is in line with the rheology results, where less elastically active strands were formed upon increasing $\phi_{8\text{-arm}}$. Although all networks contain the same number of terpyridine stickers and therefore theoretically the same probability for a tracer molecule to attach to the network, the diffusivity in a pure 8-arm network is significantly enhanced.

The fact that the diffusion coefficient increases with $\phi_{8\text{-arm}}$, could be rationalized considering that with misconnectivities, the diffusant travels faster without actually forming transient bonds, because the next available terpyridine is farther away. This vision is coherent also with the increasing mesh-sizes calculated through rheology. The trend of the diffusion coefficient follows also the trend of the relaxation time calculated through rheology. As, a faster exchange is strictly connected to a faster diffusion.

4.3 ^{1}H DQ-NMR

To directly evaluate the contribution of 8-arm stars to the formation of local defects and the overall connectivity of the polymer chains in the system, we apply static time-domain ^{1}H DQ-NMR, as described in the experimental part, on a series of networks prepared with different ratios of 4-arm pEG-terpyridine stars and 8-arm pEG-terpyridine stars (see **Figure 6 (A)** for the normalised experimental

data). Starting with a pure tetra-pEG system (4-arm 20K) transiently linked by terpyridine-zinc complexes, two different fitting approaches for the analysis of the DQ data were tried: A two-component approach assuming that two main connectivities in the network are present, being the single link and one type of connectivity defect respectively, and a three-component approach, assuming one additional type of misconnectivity with non-vanishing anisotropic constraints. Although previous experiments on tetra-pEG systems have already shown the necessity of three distinct components in the fitting model, the two-component approach was still tried for the sake of completeness (see **Figure 6 (B)**). It was again shown that the two-component model (although suggested by a first glance at the data) was not sufficient and therefore one additional fit component was introduced. Again, we want to stress the ambiguity of the 3-component model that was already mentioned in the experimental section, meaning that in the final discussion one should not treat a_2 and a_3 as different components, but rather as a combined fraction of higher-order connectivities. With this in mind, we extracted three different types of connectivities, namely the single link and at least two unassigned types of connectivity defects, as well as the fraction of isotropic defects.

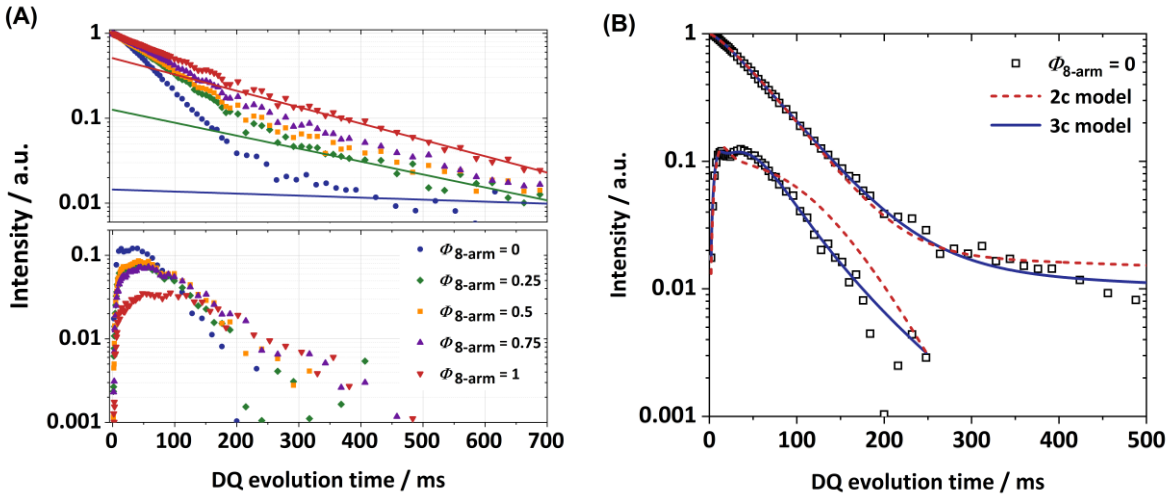

Figure 6. (A) Overview of the measured DQ data with a shared *x*-axis but different $\log_{10}$-*y*-axes. Top: $I_{\Sigma QM}$ curves with exemplary tail fits (fit extrapolated to $t_{DQ} = 0$) for $\phi_{8\text{-arm}} = 0$, 0.5, 1, respectively. Bottom: Corresponding I_{DQ}. The steadily decreasing intensity is caused by the increase in the defects ('long tail') in the $I_{\Sigma MQ}$ data. (B) Exemplary data fit for $\phi_{8\text{-arm}} = 0$. The fit model with 2-components (single links +1 connectivity defect) does not replicate the measured data, whereas the 3-component model does sufficiently fit all maxima.

Firstly, we analyse the amount of isotropic material being present in a sample by quantifying the tail fraction in the relaxation signal of the DQ experiment (see **Figure 6 (A)** for exemplary tail fits). As already mentioned, this is a quantitative sum of protonated solvent and actual isotropic polymer material (defects), where the former constitutes only a small contribution due to the choice of a rather short recycle delay of 1.5 s. Additionally, all samples were prepared by the same preparation protocol and

have the same polymer concentration and roughly the same overall volume. Therefore, we reasonably assume a comparable fraction of protonated D_2O for all samples, being at maximum 1%, as the total isotropic fraction (solvent + defects) in the DQ experiment for the pure 4-arm star system is only 1%. Across the sample series there is a trend of an increasing defect fraction from 1% to 51% with increasing number of 8-arm stars, which we mostly attribute to a steadily increasing number of loops in the 8-arm stars as it can be seen in **Figure 7 (A)**.

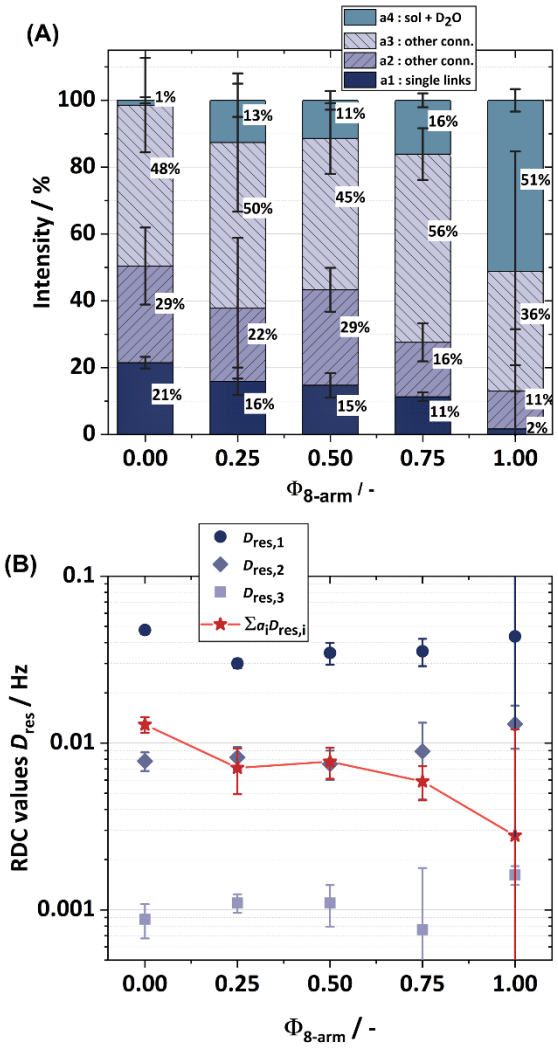

Figure 7. (A) The fractions for each type of connectivities $a_{1–3}$ and a_{tail} as extracted from the fitting procedure are plotted *vs.* the respective samples. Here, $\phi_{8\text{-arm}}$ indicates the volume fraction of 40K 8-arm pEG. A clear relationship between defects and content of 40K 8-arm stars is found. (B) The corresponding residual dipolar coupling (0) values. Within the error bars, no significant change was observed, although the dilution effect induced by the 8-arm stars becomes visible when the weighted RDC is calculated (red star-shaped symbols; connection line as guide for the eye).

This conclusion is supported by the analysis of the corresponding RDC values. As described in the advised literature, [10] the obtained RDC values are an abstract measure of the bulk-averaged anisotropy of motion of the backbone segments under the assumption of fast orientational averaging of the

segmental motion ($T \gg T_G$). Therefore, one can assume that in a network with an increasing and equally distributed number of defects, the RDC values must decrease, as these increase the effective mesh size of the network. With the introduction of the 8-arm stars, as it can be seen in **Figure 7 (B)**, a weak but significant drop of the RDC value of the a1 component (the single links) from 47 Hz ($\phi_{8\text{-arm}} = 0$) to 30 Hz ($\phi_{8\text{-arm}} = 0.25$) can be seen, even though in an ideal network the coupling must slightly increase given the fact that the RDCs are scaling with the phantom factor (f-2)/f, [40] where f is the star functionality, and we now introduced a component with f = 8. We attribute this effect to the increase in the defects from 1% to 13%, having, as mentioned above, a strong influence on the overall network elasticity. [41] An interesting behaviour can be found by looking now at the rest of the sample series with even more 8-arm star content. With increasing $\phi_{8\text{-arm}}$ we now assume even further decreasing RDCs for the single links, while defects in-crease strongly up to 51%. One would expect a vanishing RDC close to 0, as the network is now theoretically transitioning into a liquid (assuming a liquid-gel transition at 50% successful connections between the precursors).

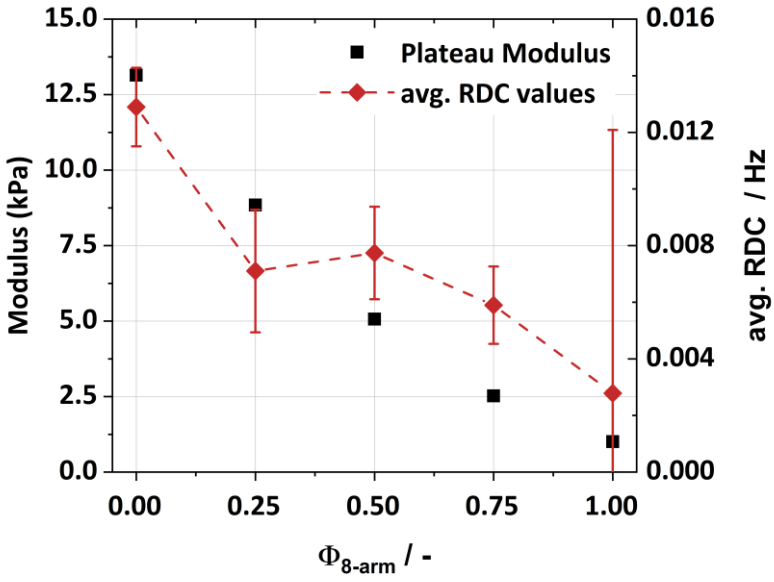

Figure 8. On the left axis, the plateau moduli from rheology are shown and plotted against the volume fraction of 8-arm stars. On the right *y*-axis, the averaged residual dipolar coupling constant (RDC) is plotted against the same molar fractions. Both curves follow the same trend – as expected – although they do not overlap within the error, presumably due to a fit model that does not sufficiently replicate this complex system.

Instead, the RDC value is not changing within the error bars, thus we necessarily must assume that not all defects are equally distributed between the network chains. Given the strong influence of loops on the RDCs, we assume that a majority of the introduced 8-arm stars are creating intra-molecular associations, therefore not or only barely contributing to the network. Thus, with increasing content of 8-arm stars, mostly a dilution effect is observed, which is also reflected in the rheology measurements, especially in the decreasing plateau modulus and increasing network mesh size. A comparison of RDC

values and plateau moduli can be made by calculating the averaged RDC of the sample (weighted by the respective fraction) without further normalisation by the respective defect fraction (because the modulus also accounts for the dilution effect of the defects), as it is proportional to the molar concentration of elastic chains. The comparison can be found in **Figure 8** and both curves show qualitatively the same behaviour, although the data did not overlap within the resulting error bars for the averaged RDC (under the assumption of Gaussian error propagation for a_i and $D_{res,i}$). The quantitative mismatch can mainly be attributed to the complexity of the investigated system.

The same 3-component approach was chosen for all samples, although especially samples with a mixture of 4-arm stars and 8-arm stars may show more types of connectivities and would therefore require a more complex model that distinguishes between them more precisely. However, an increase in the number of fit parameters would also dramatically increase the ambiguity involved in fitting, which we wanted to minimise with our decision of sticking with the model with the least possible parameters. As a final remark, it should be noted that this decision and the resulting mismatch does not influence the conclusions extracted from the experiments, as it can be seen visually, as well as from the fit optimisation, that the individual RDCs roughly stay the same, whereas the defect fraction strongly increases, therefore leading to the stated dilution effect.

A similar non-linear increase of defects is reflected also in the FRAP results, where a non-linear increase in the self-diffusion coefficients is found coming along with the incorporation of 8-arm precursors, and therefore increased defect fraction (compare **Figure 5** and **Figure 7**). The trend of the curves is similar, but mirrored, since at high $\phi_{8\text{-arm}}$, more defects translate in a higher diffusion coefficient.

The DQ-NMR experiments revealed a dilution effect induced by an increasing fraction of 8-arm polymers that have a higher likelihood to form intra-molecular loops. Since loops do generally not contribute to the overall network elasticity, a decrease in the elastic plateau modulus is found, accompanied by an increase in the softness of the hydrogel. At the same time, the mesh mesh-size of the network increases with increasing $\phi_{8\text{-arm}}$, as the number of inter-molecular connections in the network decreases, while the number of intra-molecular connections increases. In addition to that, also the self-diffusion coefficient of a 4-arm 20K macromolecule increases with increasing $\phi_{8\text{-arm}}$, as intra-molecular loops might retard the re-attachment of diffusing dye-labelled polymers.

5. Conclusions

Hydrogels are appealing materials that, due to their high content of water, can be used for biomedical applications such as in tissue engineering and drug delivery. However, due to the amorphous structures that naturally occur in such soft-matter systems, the presence of connectivity defects cannot be ignored. Their influence on the final properties of the hydrogel, such as its softness and diffusivity still remains to be further exploited. Therefore, for a rational material design, it is important to know how these defects affect the final gel properties. In this work, we have investigated the effect of connectivity defects

on the softness and diffusive permeability of supra-molecular pEG-terpyridine hydrogels, on multiple length-scales by systematically introducing 8-arm pEG-terpyridine into a 4-arm pEG-terpyridine model network and characterizing the hydrogels with DQ-NMR, oscillatory shear rheology, and FRAP. As unravelled by DQ-NMR, the pure 8-arm pEG network is more prone to form connectivity defects such as loops. The pronounced loop formation of 8-arm pEG-terpyridine macromolecules is caused by a higher likelihood of forming intra- instead of inter-molecular connections driven by metal-ligand complexation. By increasing the fraction $\phi_{8\text{-arm}}$ of 8-arm pEG-terpyridine, these defects lead to an apparent dilution effect resulting in an increase in the mesh-size of the hydrogels and consequently an increase of the self-diffusivity and the softness of the hydrogels, as probed by oscillatory shear rheology and FRAP. These results give a first insight on the effect of controlled connectivity defects on elastic properties of supramolecular hydrogels and bring awareness when tailoring the diffusive properties of the dynamic hydrogel is to be performed. Future perspectives might include the increase in overall polymer concentration to possibly damp the effect of the incorporated amount of 8-arm pEG (40K), and the variation of the polymer strand size to include further types of defects, as well as taking into account polydisperse building block materials.

References

[1] A. Jangizehi, F. Schmid, P. Besenius, K. Kremer and S. Seiffert, Soft Matter, 2020, 16, 10809–10859.

[2] M. Zhong, R. Wang, K. Kawamoto, B. D. Olsen and J. A. Johnson, Science (80-.)., 2016, 353, 1264–1268.

[3] S. Lin and X. Zhao, Phys. Rev. E, 2020, 102, 052503.

[4] A. Habicht, S. Czarnecki, T. Rossow and S. Seiffert, J. Polym. Sci. Part B Polym. Phys., 2017, 55, 19–29.

[5] P. Nicolella, D. Lauxen, M. Ahmadi and S. Seiffert, Macromol. Chem. Phys., 2021, 222, 2100076.

[6] S. Seiffert, Polym. Chem., 2017, 8, 4472–4487.

[7] F. Di Lorenzo and S. Seiffert, Polym. Chem., 2015, 6, 5515–5528.

[8] S. Mallam, F. Horkay, A. Hecht and E. Geissler, Macromolecules, 1989, 22, 3356–3361.

[9] Y. Gu, J. Zhao and J. A. Johnson, Trends Chem., 2019, 1, 318–334.

[10] K. Saalwächter, in Modern Magnetic Resonance, ed. G. A. Webb, Springer International Publishing, Cham, 2017, pp. 755–781.

[11] N. Sood, A. Bhardwaj, S. Mehta and A. Mehta, Drug Deliv., 2016, 23, 748–770.

[12] S. Mantha, S. Pillai, P. Khayambashi, A. Upadhyay, Y. Zhang, O. Tao, H. M. Pham and S. D. Tran, Materials (Basel)., 2019, 12, 3323.

[13] A. S. Hoffman, Adv. Drug Deliv. Rev., 2012, 64, 18–23.

[14] C. F. Guimarães, L. Gasperini, A. P. Marques and R. L. Reis, Nat. Rev. Mater., 2020, 5, 351–370.

[15] M. A. Haque, T. Kurokawa and J. P. Gong, Polymer (Guildf)., 2012, 53, 1805–1822.

[16] J. Li and D. J. Mooney, Nat. Rev. Mater., 2016, 1, 16071.

[17] S. Kondo, H. Sakurai, U. Il Chung and T. Sakai, Macromolecules, 2013, 46, 7027–7033.

[18] P. Dong, B. J. Schott, A. K. Means and M. A. Grunlan, ACS Appl. Polym. Mater., 2020, 2, 5269–5277.

[19] A. Sugimura, M. Asai, T. Matsunaga, Y. Akagi, T. Sakai, H. Noguchi and M. Shibayama, Polym. J., 2013, 45, 300–306.

[20] M. Koziol, K. Fischer and S. Seiffert, Soft Matter, 2019, 15, 2666–2676.

[21] S. Tang, A. Habicht, S. Li, S. Seiffert and B. D. Olsen, Macromolecules, 2016, 49, 5599–5608.

[22] T. Rossow, A. Habicht and S. Seiffert, Macromolecules, 2014, 47, 6473–6482.

[23] S. Seiffert and W. Oppermann, J. Microsc., 2005, 220, 20–30.

[24] G. I. Hauser, S. Seiffert and W. Oppermann, J. Microsc., 2008, 230, 353–362.

[25] J. Baum, M. Munowitz, A. N. Garroway and A. Pines, J. Chem. Phys., 1985, 83, 2015–2025.

[26] K. Saalwächter, P. Ziegler, O. Spyckerelle, B. Haidar, A. Vidal and J. U. Sommer, J. Chem. Phys., 2003, 119, 3468–3482.

[27] F. Lange, K. Schwenke, M. Kurakazu, Y. Akagi, U. Chung, M. Lang, J.-U. Sommer, T. Sakai and K. Saalwächter, Macromolecules, 2011, 44, 9666–9674.

[28] M. Ahmadi, L. Löser, K. Fischer, K. Saalwächter and S. Seiffert, Macromol. Chem. Phys., 2020, 221, 1900400.

[29] W. Chassé, J. L. Valentín, G. D. Genesky, C. Cohen and K. Saalwächter, J. Chem. Phys., 2011, 134, 044907.

[30] A. Parker and W. Fieber, Soft Matter, 2013, 9, 1203–1213.

[31] M. Ahmadi and S. Seiffert, Soft Matter, 2020, 16, 2332–2341.

[32] R. Wang, M. Geven, P. J. Dijkstra, P. Martens and M. Karperien, Soft Matter, 2014, 10, 7328–7336.

[33] Y. Akagi, J. P. Gong, U. Chung and T. Sakai, Macromolecules, 2013, 46, 1035–1040.

[34] W. Schmolke, M. Ahmadi and S. Seiffert, Phys. Chem. Chem. Phys., 2019, 21, 19623–19638.

[35] A. Mordvinkin, D. Döhler, W. H. Binder, R. H. Colby and K. Saalwächter, Phys. Rev. Lett., 2020, 125, 127801.

[36] A. Mordvinkin, D. Döhler, W. H. Binder, R. H. Colby and K. Saalwächter, Macromolecules, 2021, 54, 5065–5076.

[37] R. H. Holyer, C. D. Hubbard, S. F. A. Kettle and R. G. Wilkins, Inorg. Chem., 1966, 5, 622–625.

[38] S. Tang and B. D. Olsen, Macromolecules, 2016, 49, 9163–9175.

[39] J. Karvinen, T. O. Ihalainen, M. T. Calejo, I. Jönkkäri and M. Kellomäki, Mater. Sci. Eng. C, 2019, 94, 1056–1066.

[40] M. Rubinstein and R. H. Colby, Polymer Physics, Oxford University Press, Oxford, 2003.

[41] M. Lang, ACS Macro Lett., 2018, 7, 536–539.

6. Conclusions and future perspectives

The multiple and diverse applications of hydrogels demand for new multi-responsive materials, whose properties can be tuned on command. To meet this increasing need, a novel dual dynamic network has been synthesised that shows a pH dependent gelation switch, and thermo-responsive network mechanics and permeability. To build a toolkit with this dual dynamic network, the different building blocks have been systematically varied, thereby determining structure–property relationships. Finally, to account for defects inside reversible networks, the effect of connectivity defects on mechanics and permeability has been investigated with a supramolecular model network. The combination of these three studies provides an outstanding overview on the determination of structure–property relationships in supramolecular polymer networks and represent an attractive base for further targeted studies.

The dual dynamic network (DDN) that has been presented in **Chapter 3** and further explored in **Chapter 4**, comprises a main tetra-arm poly(ethylene) glycol (pEG) network where each arm has been functionalized with terpyridine and further with a linear poly(*N*-isopropylacrylamide) (pNIPAAm) chain. On one side, the terpyridine ligand binds in a bivalent fashion with different transition metal ions which offers the possibility to alter the strength and dynamics of the supramolecular crosslinks through the choice of the metal ion. In addition, the terpyridine complexation allows the hydrogel to be degraded and restored upon application of an acid and a base respectively. On the other side, the thermo-responsive pNIPAAm chains undergo a phase-separation when the polymer is heated above its lower critical solution temperature (LCST) in water. In **Chapter 3**, it has been explored how this phase-separation has effects on the mechanics and diffusive permeability of the overall polymer network. In particular, it has been shown how the collective collapse of the pNIPAAm chains leads to a duplication of the elastic plateau modulus, due to the additional connections that the thermo-responsive chains form, as determined *via* oscillatory shear rheology. In addition, this collective collapse, results in a reduction of the mesh-size and therefore, a decrease of the diffusive permeability of small diffusants. This has been assessed with fluorescently labeled diffusants *via* fluorescence recovery after photobleaching.

The mechanical properties of the dual dynamic network have been further explored in **Chapter 4** by presenting the first toolkit for dual dynamic networks. In particular, the molar mass of the two polymer precursors, namely pEG and pNIPAAm, as well as the metal ion has been varied. This way, it was possible to compare different systems and to assess structure–property relationships in a systematic fashion *via* oscillatory shear rheology. Results show that samples with a higher amount of pNIPAAm and longer chains increase their elastic modulus above the LCST more than samples with shorter pNIPAAm chains or higher amount of pEG. This effect probably results from a different collapsing process: long pNIPAAm chains are more likely to meet and collapse together, whereas shorter pNIPAAm chains are more likely to collapse on themselves. Finally, the metal ion has been varied

between zinc(II) and iron(II) and the effect on the mechanical properties was investigated. It was noticed that the plateau moduli (and consequently the mesh-size) of the two samples stays constant up to the LCST and then they increase in a different manner. In the sample with zinc, the plateau modulus increases linearly with the temperature above the LCST, whereas in the sample with iron, the storage modulus reaches a new plateau value above the LCST but then stays constant. These results suggest that for the stronger complexing iron, there might be a configuration of the network below and above the LCST of the polymer, whereas for the sample with zinc, or in general with weaker metal ions, the polymer network might further rearrange with temperature. We hypothesize that above the LCST, the network with zinc forms clusters and with further increase in temperature these clusters break into smaller clusters, thereby, enforcing the hydrogel, as supported by the further increase in the plateau modulus. Finally, in addition to the high-frequency plateau, in the samples with zinc, a second plateau appears at low frequencies at temperatures above the LCST. The emergence of this plateau might be connected to the formation and non-relaxation of the aforementioned clusters, as it increases with higher amount of pNIPAAm and longer chains, showing a behaviour similar to the high-frequency plateau.

Finally, in **Chapter 5**, the structure–property relationships of reversible gels were studied under another perspective, namely the presence of defects. Since natural defects, and in particular connectivity defects, can always occur in supramolecular networks, for a rational materials' engineering it is crucial to be conscious of the effects of these defects on the properties of the hydrogel. However, since for multi-component systems the relationship between structure and properties is not always linear, a thoughtful way to tackle this aspect is to start with single supramolecular network and then scale it up to multi-component systems in future studies. Consequently, in **Chapter 5** different amount of connectivity defects were introduced in a systematic fashion into a well-known a 4-arm terpyridine-functionalised pEG model network. Connectivity defects are introduced systematically by mixing the 4-arm pEG-terpyridine precursor with different ratios of 8-arm pEG-terpyridine precursor, and afterwards adding zinc(II) to form the network. By choosing the 8-arm pEG precursor of a two-fold molar mass compared to the 4-arm pEG precursor, the 4-arm and 8-arm pEG have same arm length. Therefore, the obtained networks potentially possess the same mesh-size and thus same plateau modulus, since the total number of potential connections should be the same. However, the experimental behaviour of the systems deviates from this theoretical prediction. The 4-arm and 8-arm pEG indeed do have the same arm length; however, they bind in a different way and show therefore two dynamics. As investigated by DQ-NMR, by increasing the amount of 8-arm pEG precursors in the samples, the number of defects increases. These defects, that are mainly loops, form because the 8-arm pEG is more prone to form intra-molecular interactions instead of inter-molecular interactions. These connectivity defects reflect themselves in the properties of the network. With a systematic increase of these defects in the network, the plateau modulus of the samples decreases monotonously and then deviates strongly from the theoretical values of the affine network model. At the same time, the self-diffusion coefficient of 4-arm fluorescently-labelled pEG-terpyridine increases with increasing amount of 8-arm pEG in the network. This trend,

that goes together with an increasing mesh-size, can be explained by the fact that due to the terpyridine being busy in intra-molecular loops, the next available free terpyridine is further away. In fact, the experimentally observed effects of an increasing amount of connectivity defects on the mechanics and dynamics substantially differed from the model behavior.

This thesis contributes exceptionally to the rational engineering of new materials on different levels. First of all, it contributes to the field of materials engineering with the development of an innovative multi-responsive dual dynamic network. In addition to the possibility to switch the elasticity, permeability, and recyclability of this polymer network on demand, this material offers the attractive opportunity to further tune these properties by a wise choice of the two polymer precursors as well as the metal ion. In addition, it contributes to the field of defects engineering by providing an exceptional practical demonstration of the utility of systematic structure–property relationships investigations in dynamic networks and in particular the role of defects. To study such dynamics on model systems allows a greater applicability and later a wider implementation to more complex systems. The evaluation of the effect of defects is crucial in the development of new polymer networks and can be even wisely used as a tool for accordingly finely tune the properties of materials in defects engineering. The combination of these three studies offers therefore an excellent complementary platform for the engineering of multi-responsive hydrogels and thereby enlarge their applicability.

7. Publications

1) **Reversible hydrogels with switchable diffusive permeability**
   Paola Nicolella, Daniel Lauxen, Mostafa Ahmadi, Sebastian Seiffert
   Published in: Macromolecular Chemistry and Physics, 2021, 222: 2100076
   DOI: 10.1002/macp.202100076

2) **Mechanical switching of a comb-like dual dynamic polymer network**
   Paola Nicolella and Sebastian Seiffert
   Accepted in: Journal of Rheology, 2022, Special Issue for Double Dynamics Polymeric Networks
   DOI: 10.1122/8.0000388

3) **Defect-controlled softness, diffusive permeability, and mesh-topology of metallo-supramolecular hydrogels**
   Paola Nicolella, Martha Franziska Koziol, Lucas Löser, Kay Saalwächter, Mostafa Ahmadi, Sebastian Seiffert
   Published in: Soft Matter, 2022, 18, 1071-1081
   DOI: D1SM01456K

4) **Effect of block length and polydispersity on the network connectivity and temperature resistance of model, soft thermoplastic elastomers**
   Simone Sbrescia, Paola Nicolella, Tom Engels, Michelle Seitz
   Published in: Journal of Rheology, 2022, 66, 177
   DOI: 10.1122/8.0000373

5) **Metal-ligand complexation, collective assembly, and clustering of nitro-catechol-iron ions in model supramolecular hydrogels with a side-chain structural platform**
   Amir Jangizehi, Sarah Pschierer, Paola Nicolella, Mostafa Ahmadi, and Sebastian Seiffert
   Manuscript in preparation

6) **Dynamics of model transient polymer networks with temporal hierarchy of energy dissipation**
   Mostafa Ahmadi, Paola Nicolella, Sebastian Seiffert
   Manuscript in preparation

8. Conference contributions

8.1 Presentations

1) Structure and diffusion in DDNs at the nano- to micro- scale

DoDyNet Project Meeting FORTH - Heraklion, Greece, September 2018

2) Structure and diffusion in DDNs at the nano- to micro- scale

DSM industrial workshop – Maastricht and Venlo, The Netherlands, January 2019

3) Synthesis of a Double Dynamic Network with thermoresponsive polymer and metal ion complex

DoDyNet Project Meeting DTU – Copenhagen, Denmark, May 2019

4) Structure–property relationships in double dynamic networks at the nano- to micro- scale

DoDyNet Project Meeting - Online, September 2020

5) Structure–property relationships in dual dynamic networks

TESA industrial workshop - Online, February 2021

6) Connectivity-tailored properties in dual dynamic networks

DoDyNet Project Meeting – Montpellier, France, October 2021

8.2 Posters

1) Design of a double dynamic model network with terpyridine complex and thermoresponsive polymer crosslinking motifs

Summer School on "Transient and complex polymer networks" – Capri, Italy, July 2019

Paola Nicolella and Sebastian Seiffert

2) Design of a double dynamic model network with terpyridine complex and thermoresponsive polymer crosslinking motifs

Spring School – Soft Matter Characterization – Mainz, Germany, February 2020

Paola Nicolella and Sebastian Seiffert

9. List of abbreviations and symbols

9.1 Abbreviations

D_2O	Deuterium oxide
DCM	Dichloromethane
DDN	Dual dynamic network
DMF	Dimethylformamide
DMSO	Dimethyl sulfoxide
DN	Double network
DOSY	Diffusion-ordered spectroscopy
DQ	Double quantum
DSN	Double supramolecular network
e. g.	Exempli gratia
FRAP	Fluorescence recovery after photobleaching
GPC	Gel permeation chromatography
HCl	Hydrogen chloride
HDO	Partially back-protonated water
i. e.	Id est
KOH	Potassium hydroxide
LCST	Lower critical solution temperature
NaCl	Sodium chloride
NaOH	Sodium hydroxide
NBD	Nitrobenzoxadiazole
NHS	*N*-hydroxysuccinimidyl
NMR	Nuclear magnetic resonance
PAM	Polyacrylamide
PAMPS	Poly(2-acrylamide-2-methylpropane sulfonic acid)
pEG	Poly (ethylene glycol)
pNIPAAm	Poly (*N*-isopropylacrylamide)
PVA	Poly (vinyl alcohol)
RDC	Residual dipolar coupling
Ref.	Reference
THF	Tetrahydrofuran
tpy	terpyridine
UCST	Upper critical solution temperature
UV-vis	Ultraviolet-visible spectroscopy

9.2 Symbols

γ	Shear amplitude
ε	Strain or deformation
η	Viscosity
μ	Density of network density
ν	Number of network strands per volume
ξ	Mesh-size
Ξ	Spatial distribution of crosslinking density
σ	Stress
τ_{DQ}	DQ evolution time
τ_r, τ_{rel}	Relaxation time
ϕ	Volume fraction
ω	Angular frequency
A	Pre-exponential factor
a_i	Fraction
A-l	Abragham-like
Ar	Argon
B_0	Magnetic field
c*	Overlap concentration
C, c	Concentration
d	dimensionality
D	Diffusion coefficient
$D_{res,i}$	Residual dipolar coupling
eq.	equivalents
f	Functionality
F	Friction
Fe	Iron
G_P°, G_N°	Plateau modulus
G'	Storage or elastic modulus
G''	Loss modulus
He	Helium
Hz	Hertz
$I_{DQ(tDQ)}$	DQ build-up function
I_{imm}	Intensity of the immobile fraction
I_{mob}	Intensity of the mobile fraction
$I_{ref(tDQ)}$	Reference function
k_B	Boltzmann constant
M	Amount of diffusive species or bleached fluorophores
M_c, M_w	Molecular weight
N_A	Avogadro constant
Ne	Neon
Ni	Nickel
p	Reaction probability
pH	Potential of hydrogen
r	Radial coordinate
R	Universal gas constant
R_H	Hydrodynamic radius
t	Time
T	Absolute temperature
t_0	Time zero
$T_{1,HDO}$	Longitudinal relaxation time
$T_{1,pol}$	Longitudinal relaxation time polymer
tan δ	Loss factor
w	Standard deviation
wt%	Weight percent
Zn	Zinc

10. Appendix

10.1 Appendix Chapter 3

Supporting Information

Reversible hydrogels with switchable diffusive permeability

***Paola Nicolella**, Daniel Lauxen, Mostafa Ahmadi, Sebastian Seiffert*

Macromolecular Chemistry Physics, **2021**, 222: 2100076 (DOI: 10.1002/macp.202100076)

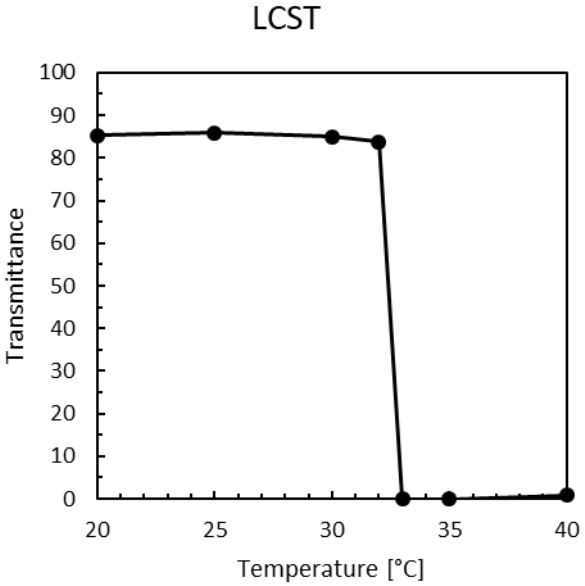

Figure S1. Determination of the cloud point with UV-VIS. The could point can be taken as an indication of the LCST. In this case, the transition temperature is 32.5 °C.

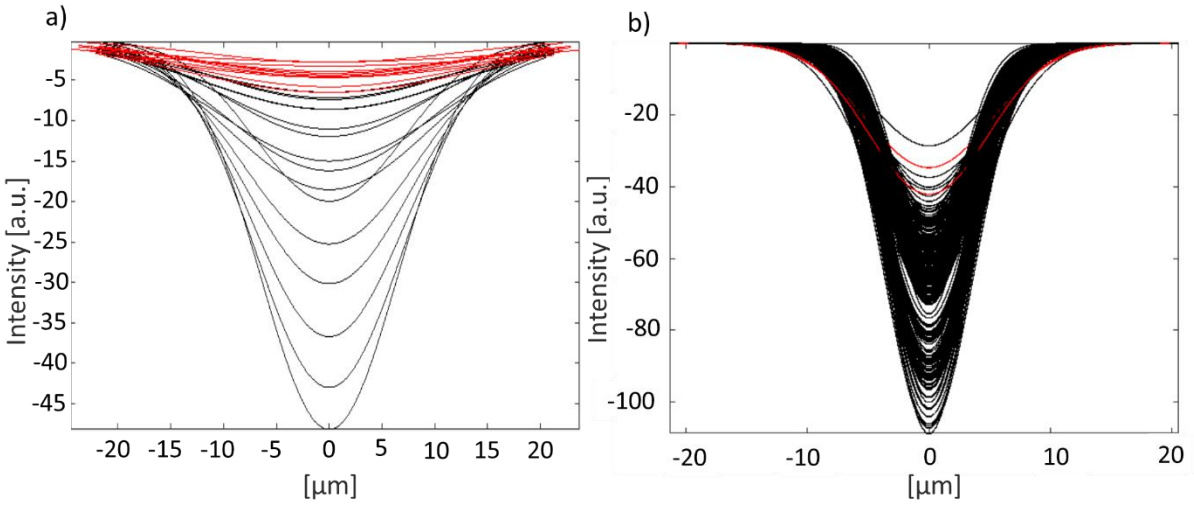

Figure S2. Gaussian distribution of the intensity in the FRAP measurements at 25 °C a) and at 35 °C b). At 36°C there are more Gaussian curves because the bleaching spot did not disappear.

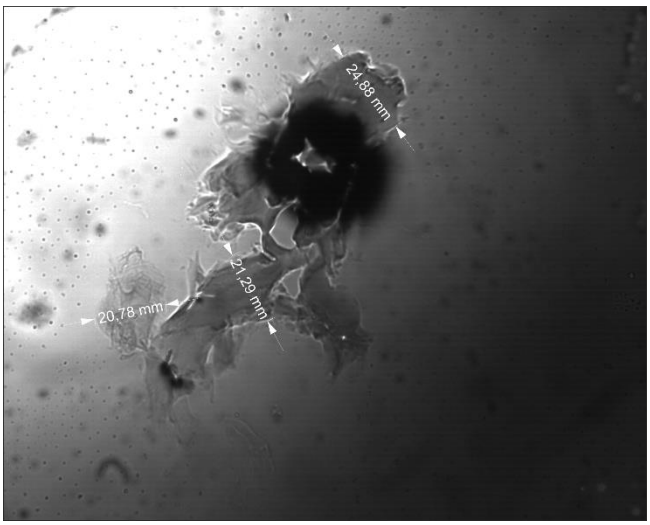

Figure S3. To check if the hydrogel shrinks with temperature, it was put in oil in order to avoid evaporation of the solvent, and pictures were taken with temperature. This picture refers to 25 °C.

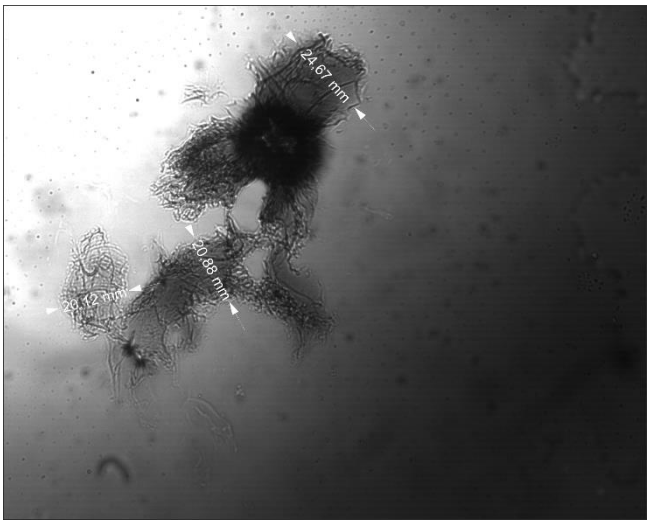

Figure S4. To check if the hydrogel shrinks with temperature, it was put in oil in order to avoid evaporation of the solvent, and pictures were taken with temperature. This picture refers to 35 °C.

As it can be seen by comparison of the **Figures S2-S3**, the hydrogel did retain its original volume.

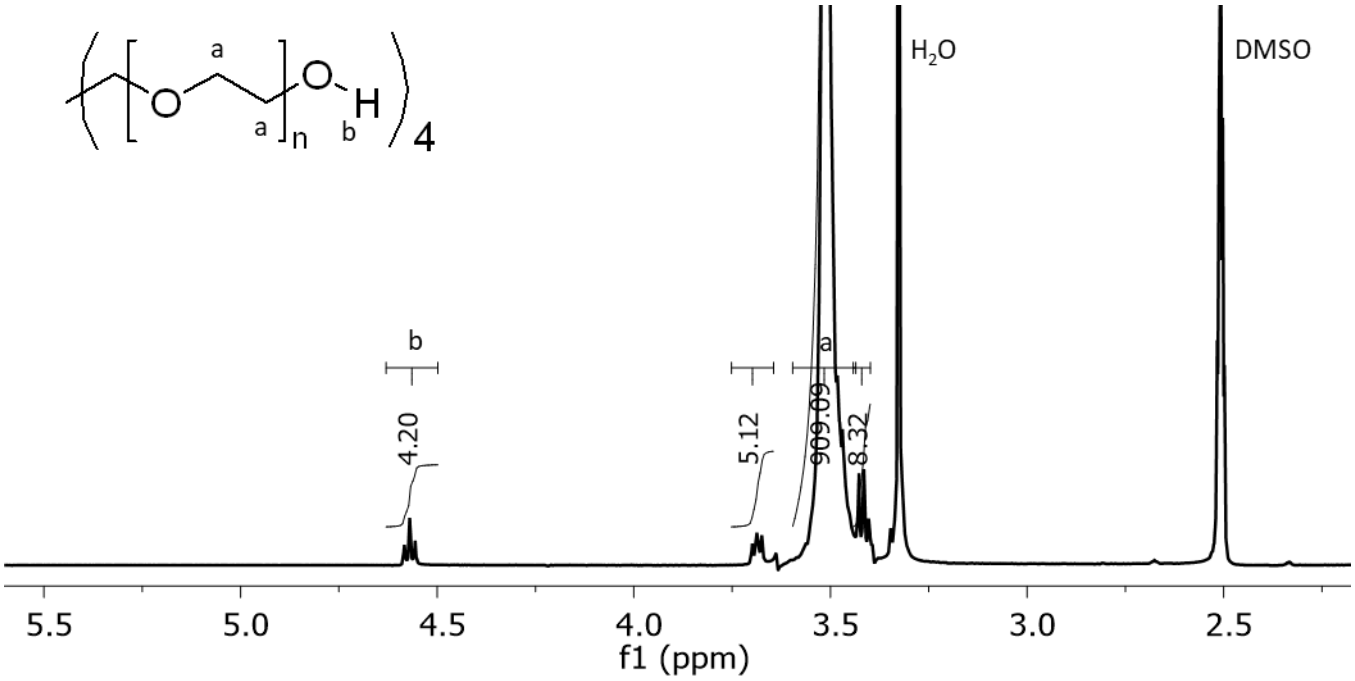

Figure S5. [1]H-NMR of tetra-pEG-OH 10 000 g/mol in DMSO: 4.57 (t, 4H), 3.70 (m, 5H), 3.51 (m, 909H, pEG backbone), 3.42 (m, 8H).

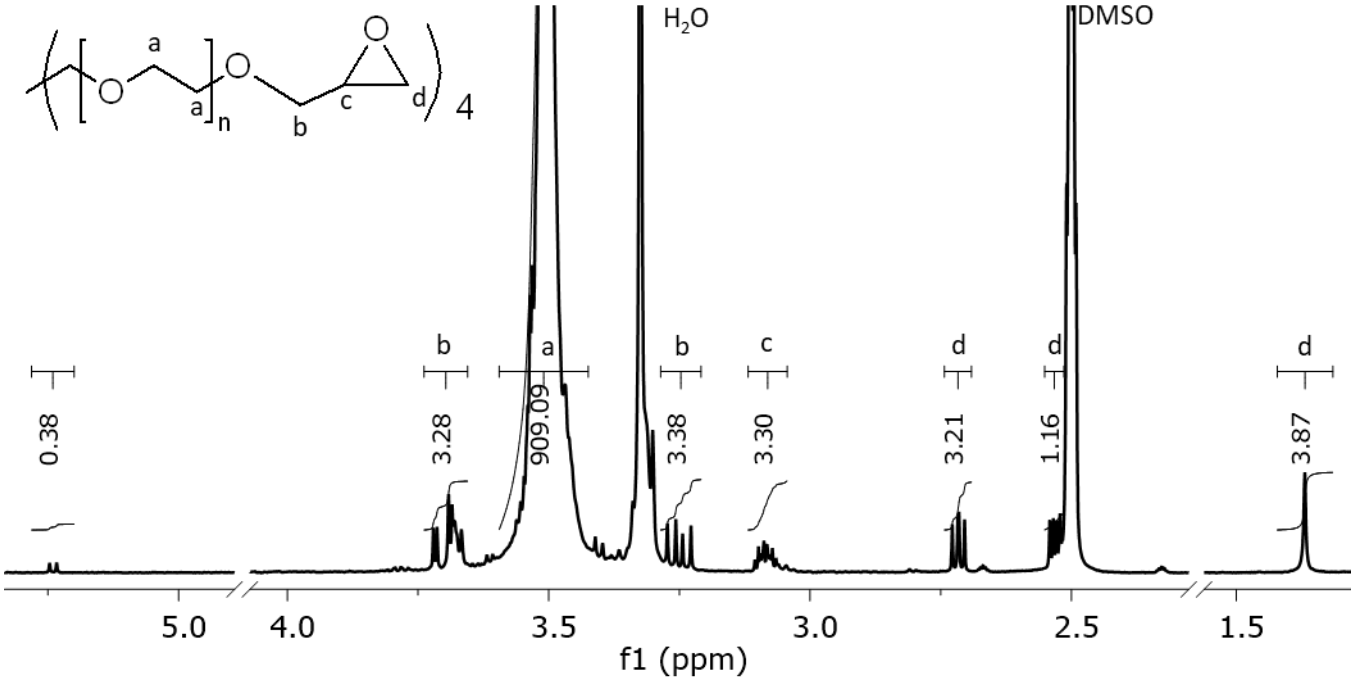

Figure S6. [1]H-NMR of tetra-pEG-epoxide in DMSO: 3.70 (m, 3H), 3.51 (m, 909H, pEG backbone), 3.25 (m, 3H), 3.09 (m, 3H), 2.72 (m, 3H), 2.52 (s, 1H), 3.87 (s, 4H).

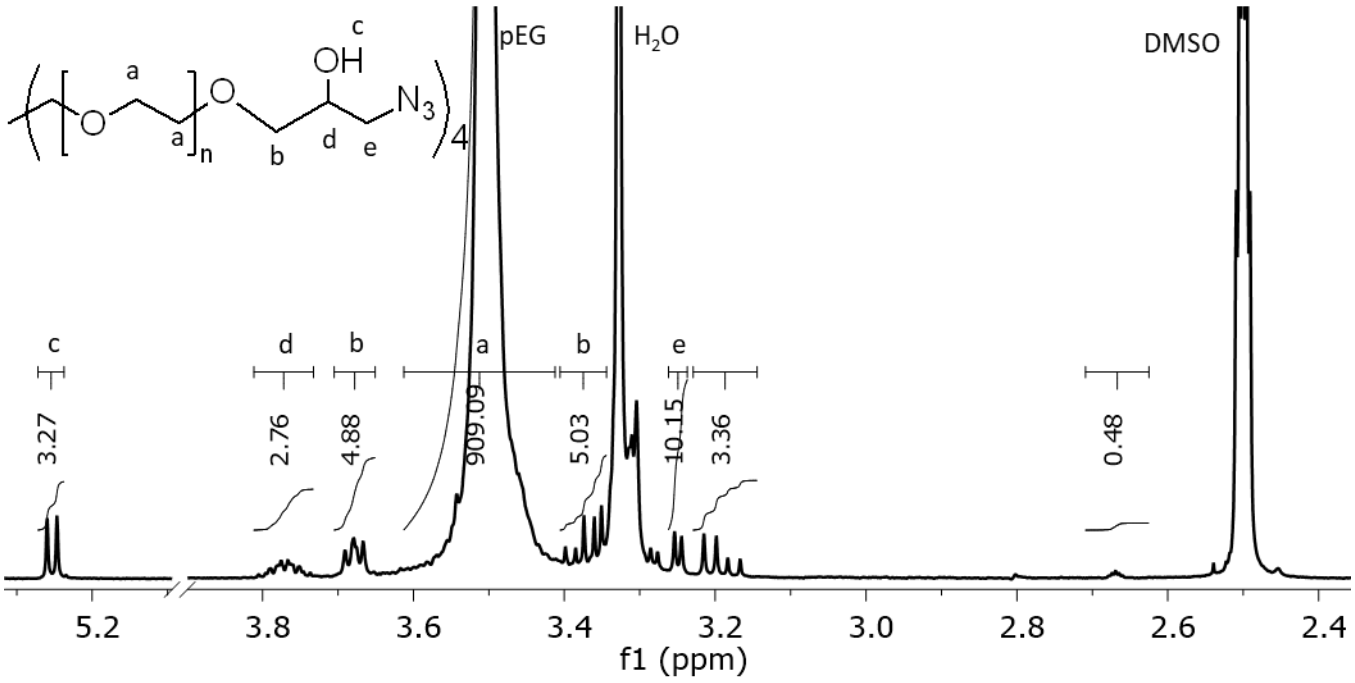

Figure S7. [1]H-NMR of tetra-pEG-hydroxy-azide in DMSO: 5.25 (d, 3H), 3.77 (m, 3H), 3.68 (m, 5H), 3.51 (m, 909H, pEG backbone), 3.37 (m, 5H), 3.25 (d, 10H), 3.19 (m, 3H).

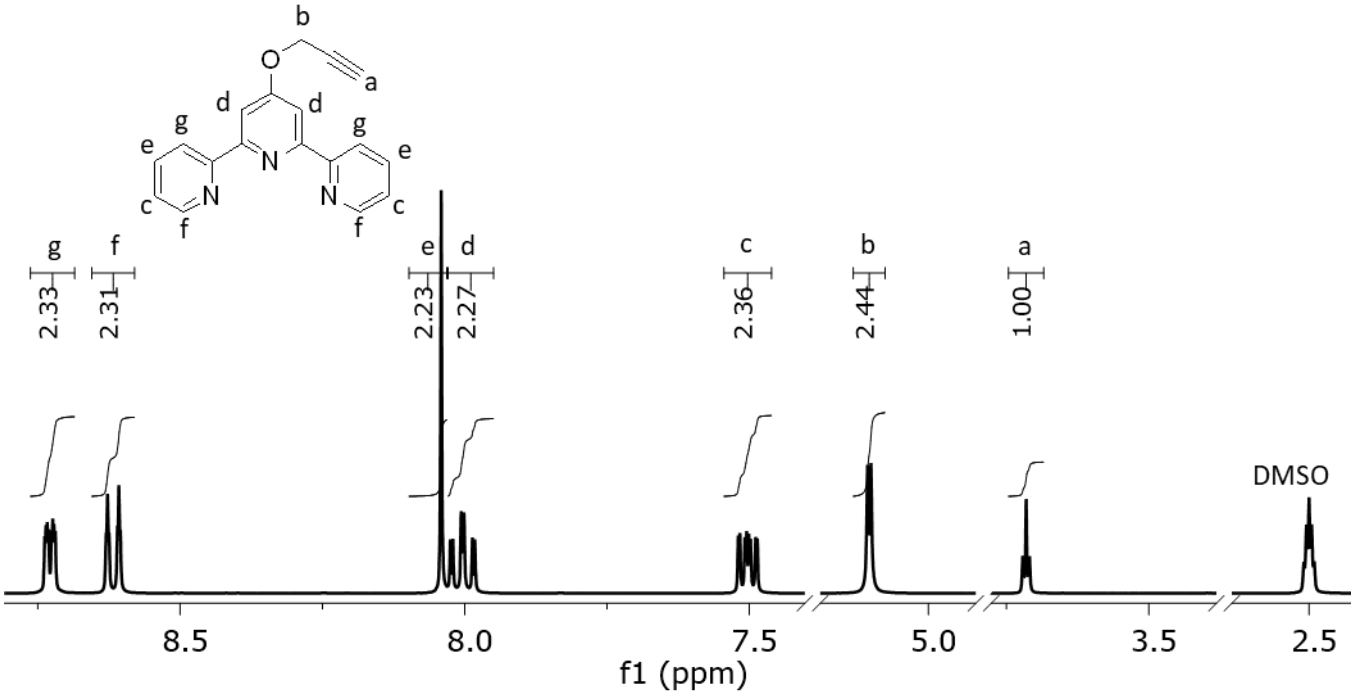

Figure S8. [1]H-NMR of propargyl-terpyridine in DMSO: 8.74 (ddd, 2H), 8.62 (dt, 2H), 8.05 (s, 2H), 8.01 (td, 2H), 7.51 (ddd, 2H), 5.11 (d, 2H), 3.72 (t, 1H).

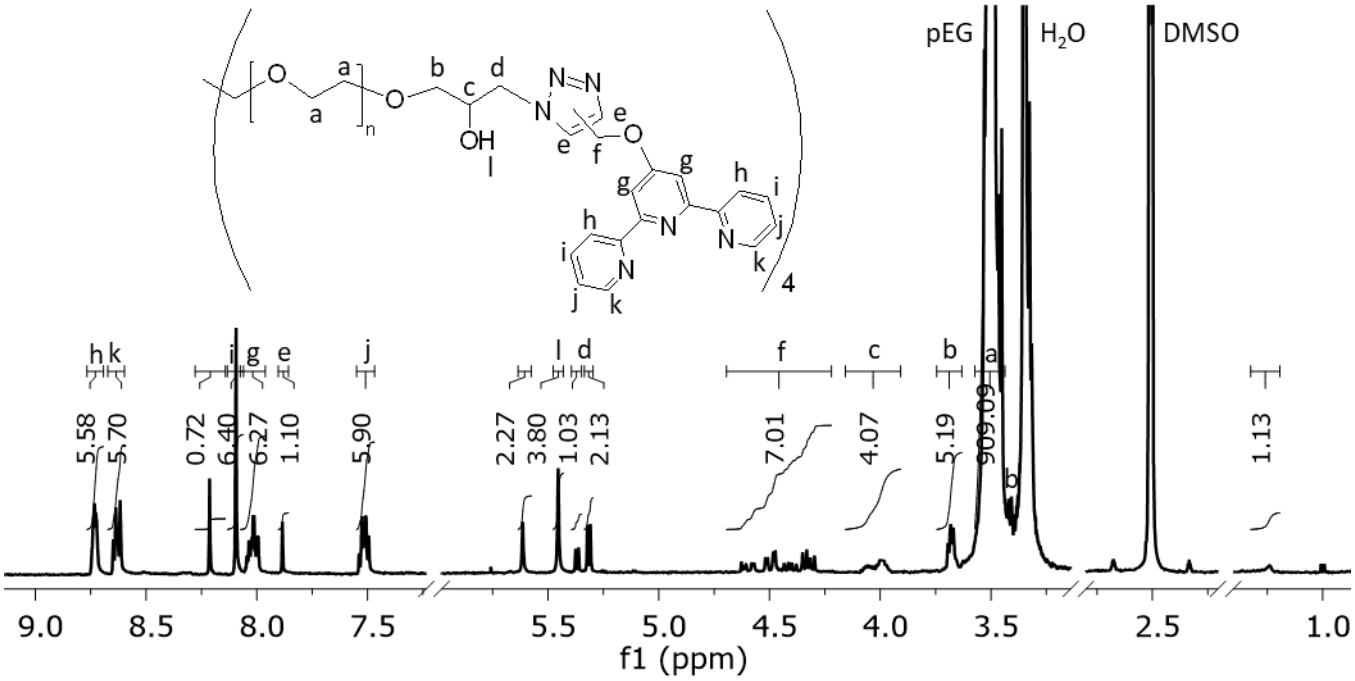

Figure S9. [1]H-NMR of tetra-pEG-hydroxy-terpyridine in DMSO: 8.73 (m, 6H), 8.63 (m, 6H), 8.21 (s, 1H), 8.10 (d, 6H), 8.02 (m, 6H), 7.88 (s, 1H), 7.51 (m, 6H), 5.61 (s, 2H), 5.45 (s, 4H), 5.37 (d, 1H), 5.32 (d, 2H), 4.45 (m, 7H), 4.00 (m, 4H), 3.68 (t, 5H), 3.47 (m, 909H, pEG backbone), 1.24 (s, 1H).

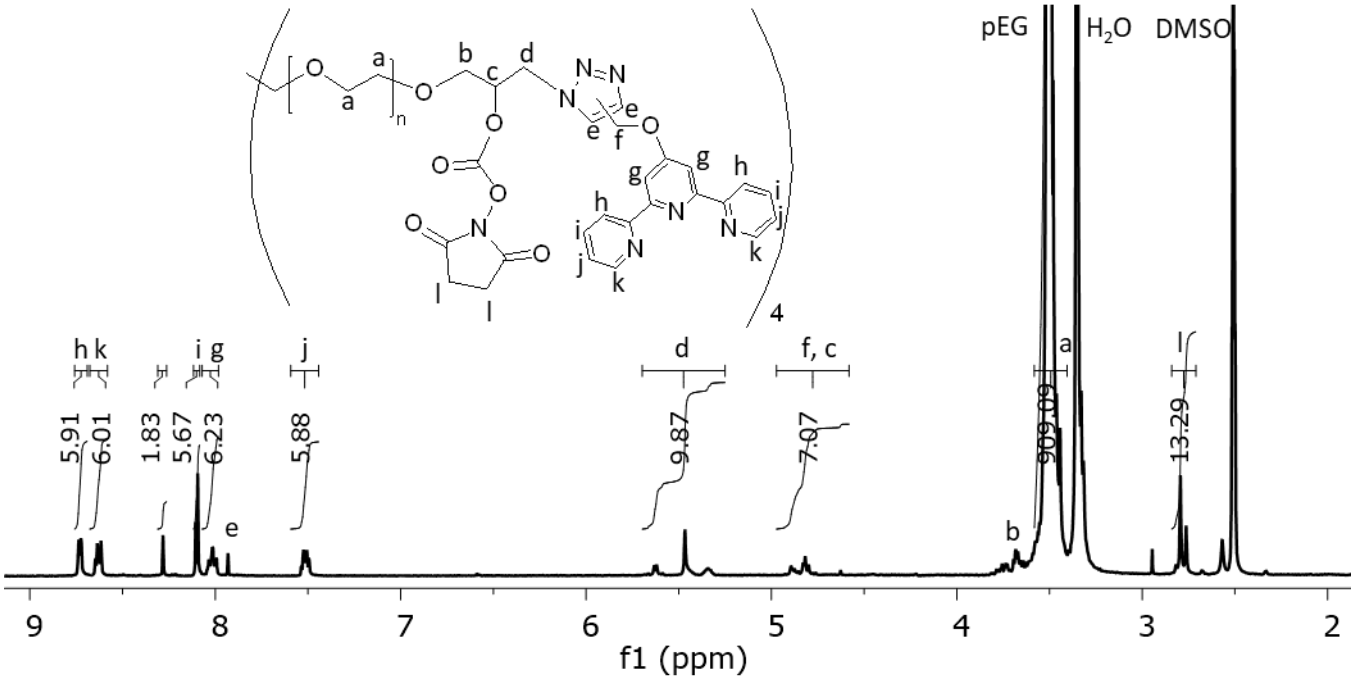

Figure S10. [1]H-NMR of tetra-pEG-N-hydroxysuccinimide-terpyridine in DMSO: 8.73 (d, 6H), 8.63 (m, 6H), 8.28 (s, 2H), 8.10 (m,6H), 8.02 (m, 6H), 7.52 (m, 6H), 5.47 (m, 10H), 4.77 (m, 7H), 3.47 (m, 909H, pEG backbone), 2.78 (m, 13H).

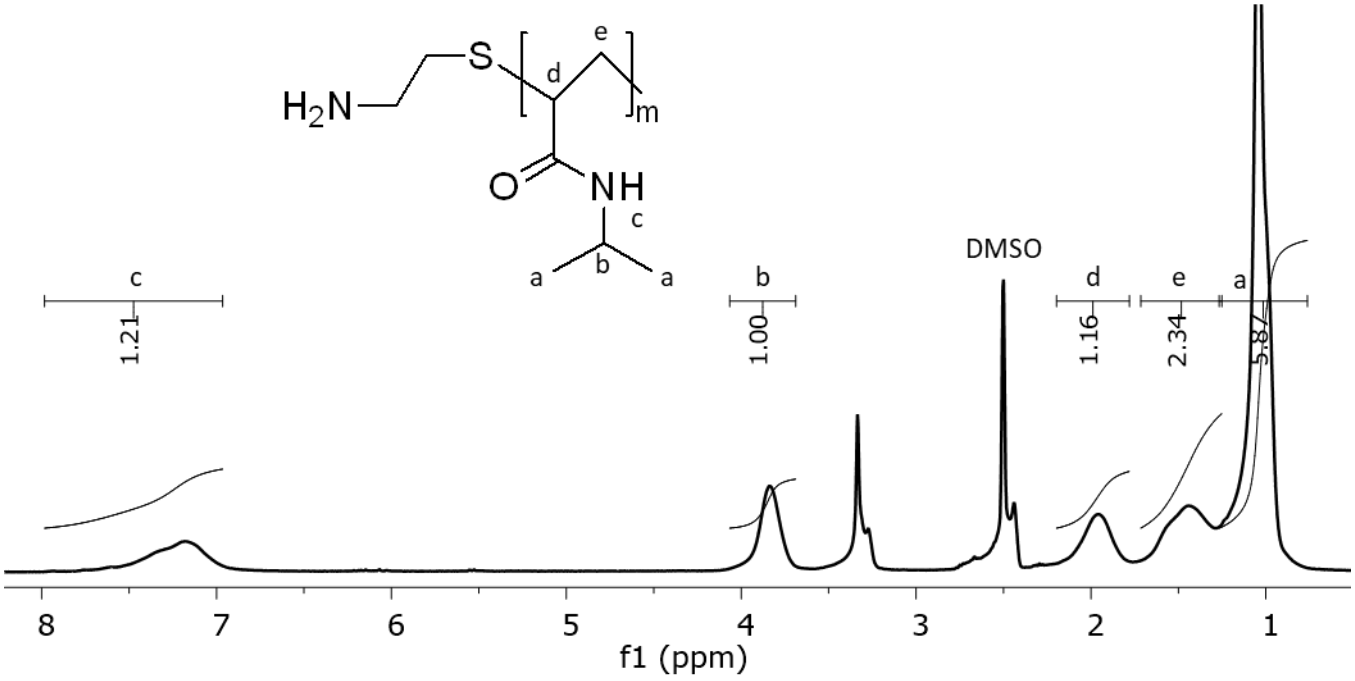

Figure S11. [1]H-NMR of pNIPAAm-NH_2 in DMSO: 7.43 (m, 1H), 3.87 (m,1H), 2.2 (m, 1H), 1.45 (m, 2H), 1.03 (m, 6H).

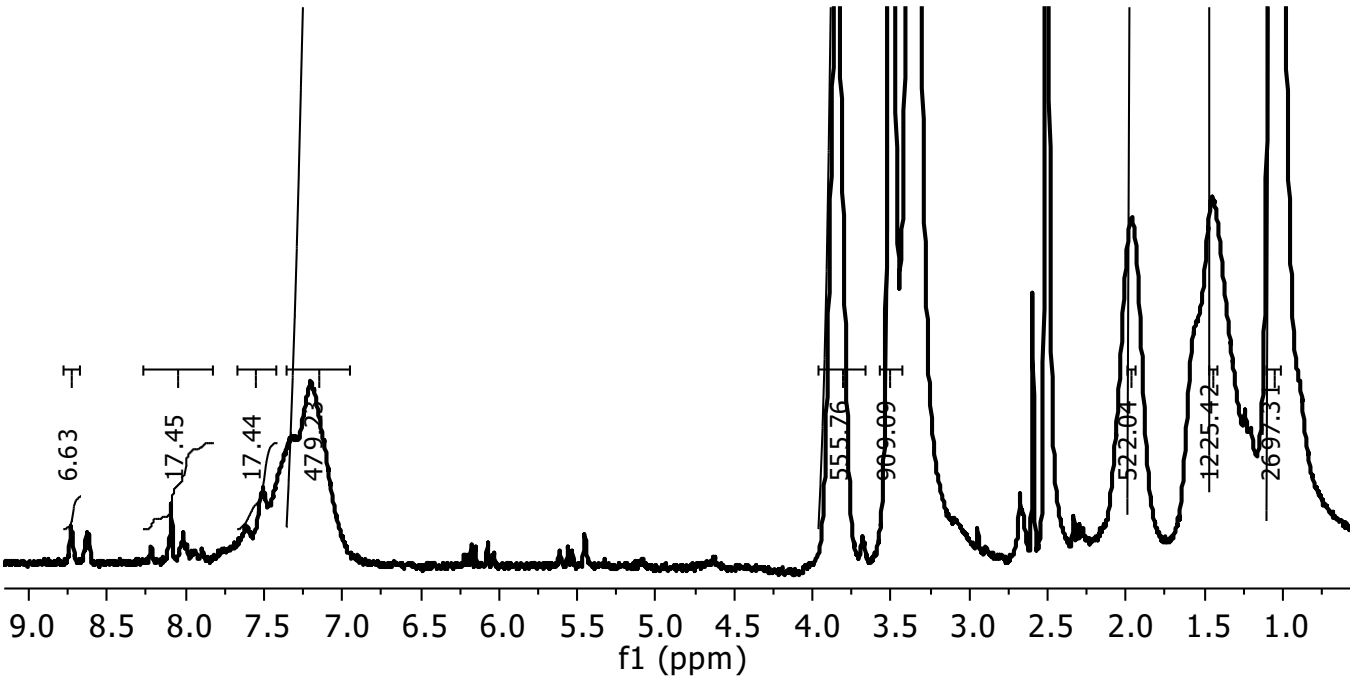

Figure S12. [1]H-NMR of tetra-pEG-pNIPAAm-terpyridine in DMSO before dialysis: 8.72 (m, 7H), 8.62 (m, 8H), 8.21 (s, 2H), 8.04 (m, 17H), 7.54 (m, 17H), 7.18 (m, 479H), 6.15 (m, 6H), 5.67 – 5.49 (m, 11H), 4.62 (s, 6H), 3.84 (s, 556H, pNIPAAm), 3.50 (s, 909H, pEG), 1.96 (s, 522H, pNIPAAm), 1.45 (m, 1225H, pNIPAAm), 1.04 (s, 2697H, pNIPAAm).

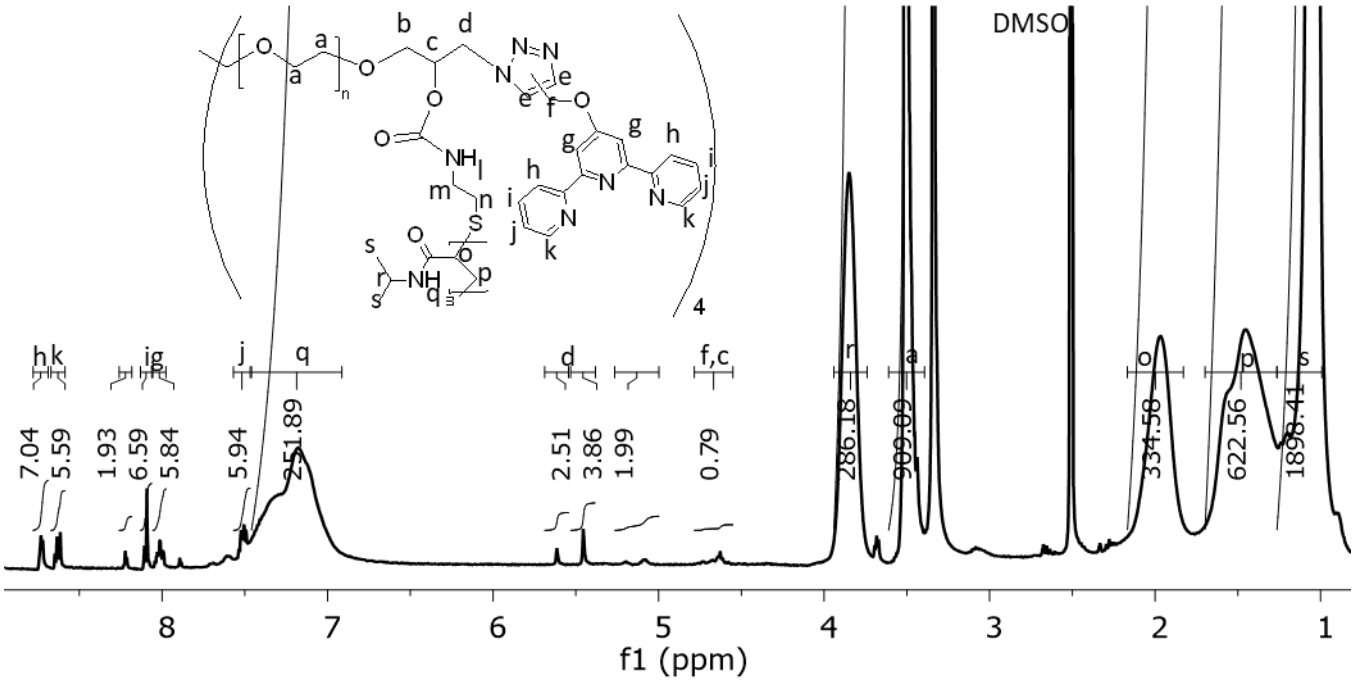

Figure S13. [1]H-NMR of tetra-pEG-pNIPAAm-terpyridine in DMSO after dialysis: 8.73 (m, 7H), 8.63 (m, 6H), 8.22 (d, 2H), 8.10 (m,7H), 8.01 (m, 6H), 7.52 (m, 6H), 7.16 (m, 252H pNIPAAm), 5.61 (s, 3H), 5.45 (s, 4H), 5.08 (m, 2H), 4.67 (m, 1H), 3.85 (m, 286H, pNIPAAm), 3.49 (m, 909H, pEG backbone), 1.98 (s, 335H, pNIPAAm), 1.46 (m, 623H, pNIPAAm), 1.12 (m, 1898H, pNIPAAm).

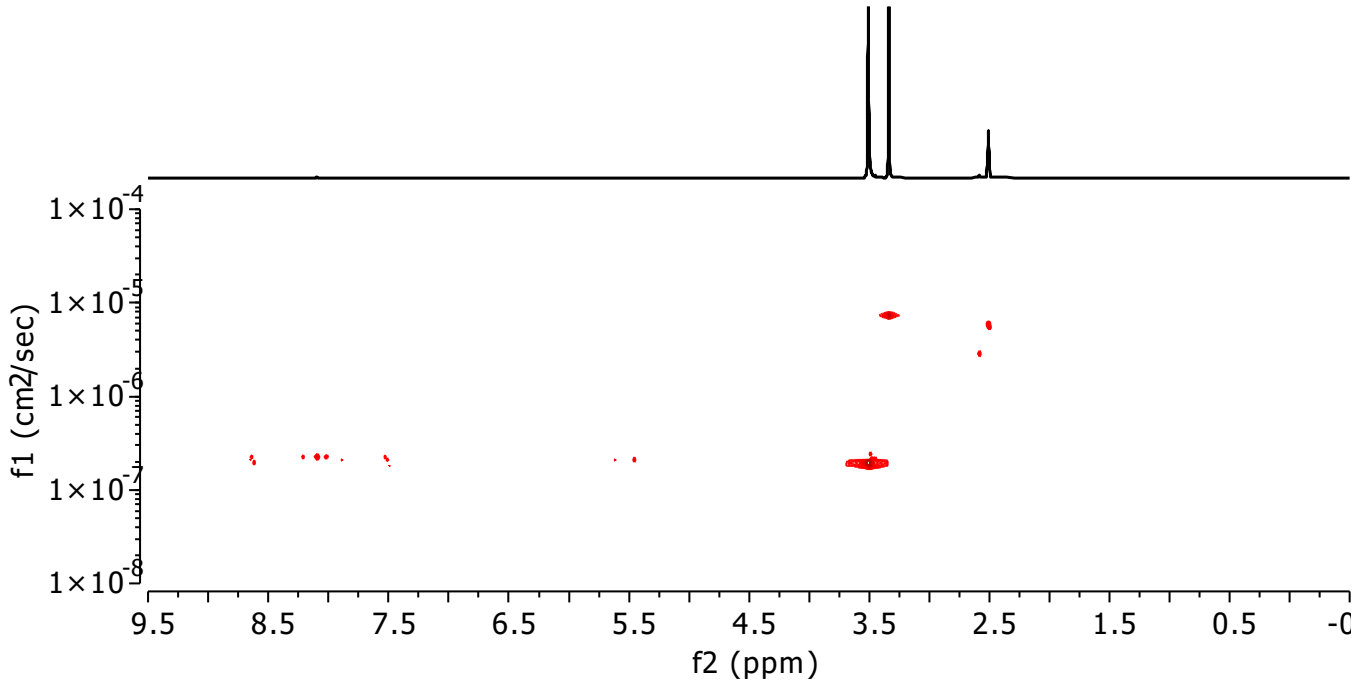

Figure S14. DOSY-NMR of tetra-pEG-NHS-terpyridine in DMSO: 8.65-7.51 ppm terpyridine, 3.51 ppm pEG.

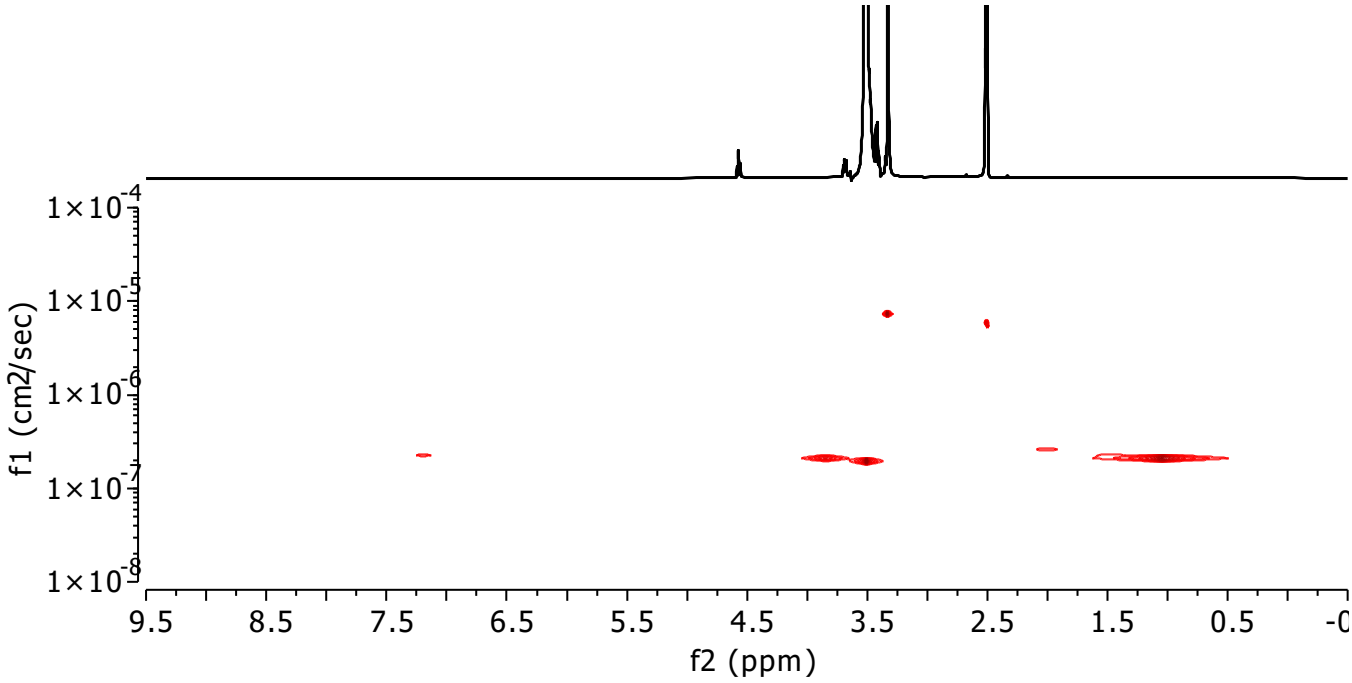

Figure S15. DOSY-NMR of tetra-pEG-pNIPAAm-terpyridine in DMSO: 7.20 ppm pNIPAAm, 3.87 ppm pNIPAAm, 3.51 ppm pEG, 2.02 ppm pNIPAAm, 1.04 ppm pNIPAAm.

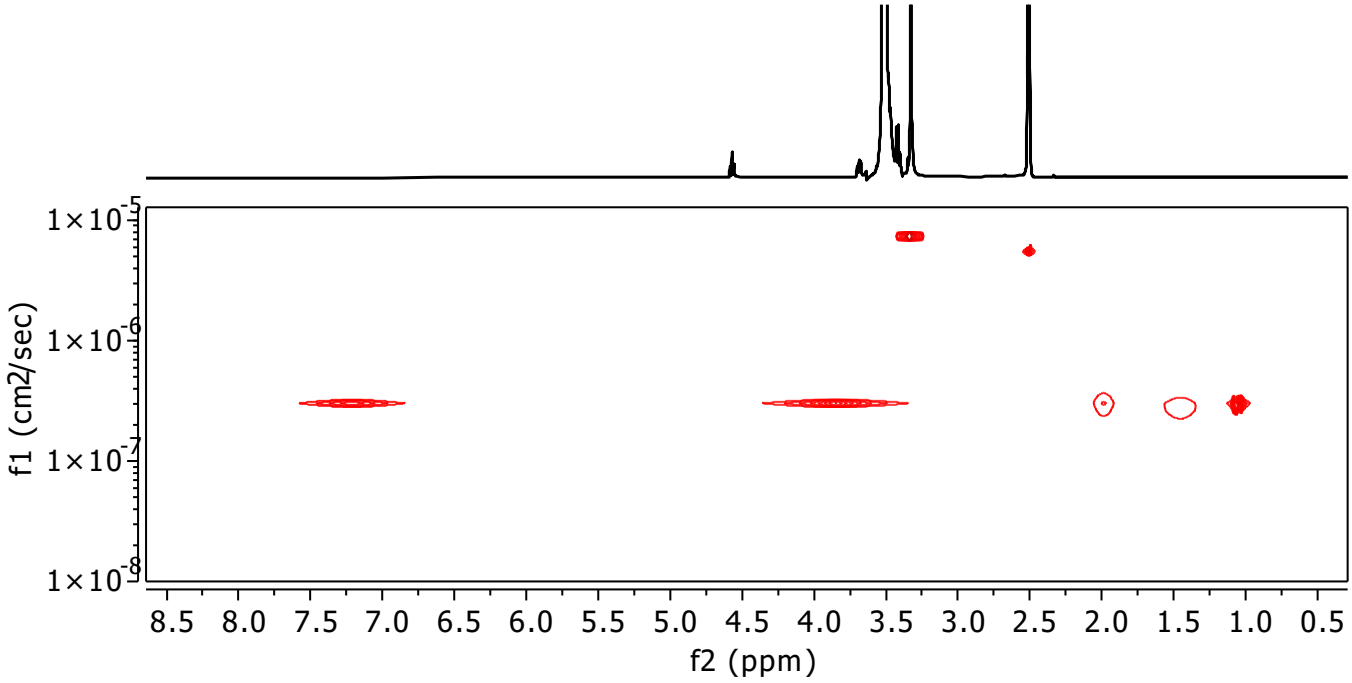

Figure S16. DOSY-NMR of pNIPAAm-NH_2 in DMSO: 7.25 ppm, 3.88 ppm, 2 ppm, 1.46 ppm and 1.04 ppm pNIPAAm.

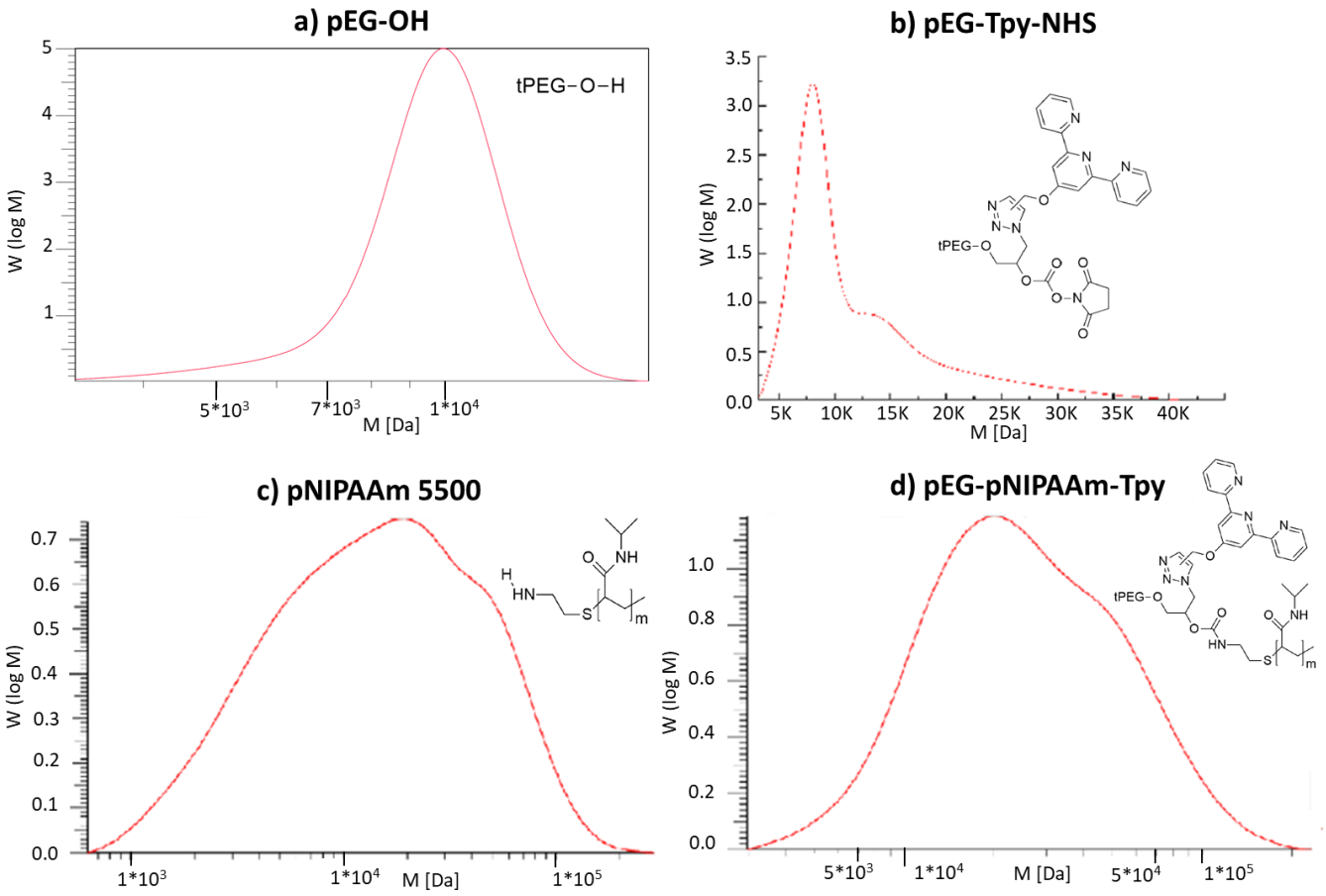

Figure S17. GPC results in DMF of a) tetra-pEG-OH, b) tetra-pEG-N-hydroxysuccinimide-terpyridine, c) amine functionalized pNIPAAm 5500 g/mol and d) tetra-pEG-pNIPAAm-terpyridine.

10.2 Appendix Chapter 4

Supplementary Material

Mechanical switching of a comb-like dual dynamic polymer network

Paola Nicolella *and Sebastian Seiffert*

Journal of Rheology, 2022 (DOI: 10.1122/8.0000388)

S1. Synthesis

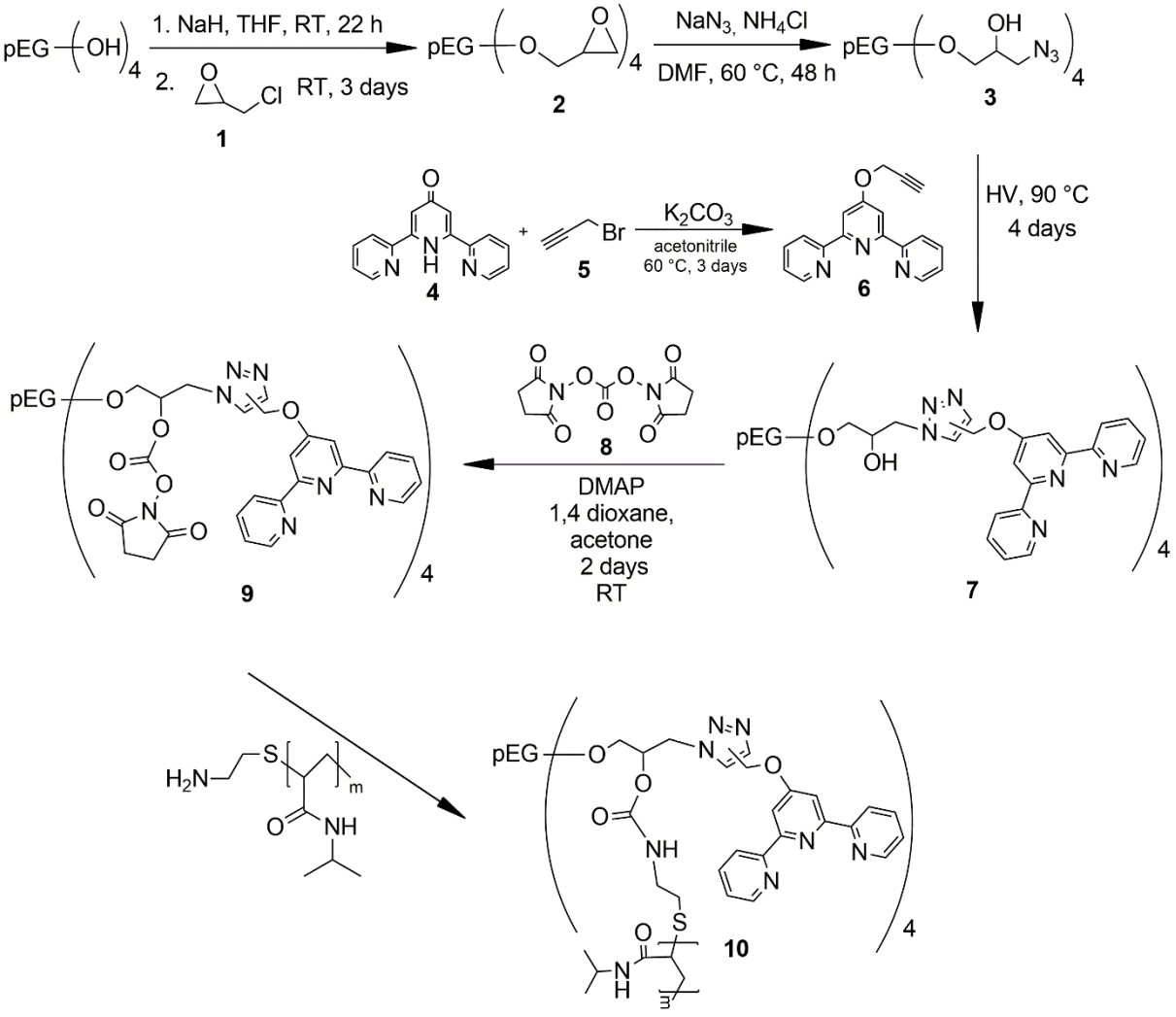

Scheme S1. Synthesis route of the tetra-pEG-terpyridine-pNIPAAm dual dynamic network. Further details on the synthesis procedure can be found in Ref. [1], whereas quantities and characterization are to be found below.

S1.1 Tetra-pEG-epoxide (2)

Table SI. Synthesis details of the tetra-pEG-epoxide (**2**)

		10K tetra-pEG-OH				20K tetra-pEG-OH			
	Mw [g mol^{-1}]	m [g]	V [mL]	n [mmol]	Eq.	m [g]	V [mL]	n [mmol]	Eq.
Tetra-pEG-OH	-	13.06	-	1.3	1	13.98	-	0.7	1
Tetrahydro-furan	-	-	320	-	-	-	180	-	-
Sodium hydride (60% in mineral oil)	23.99	1.67	-	41.8	32	0.91	-	27.6	33
Epichloro-hydrin (**1**)	92.53	9.67	8.2	104.5	80	5.24	4.5	56.6	81

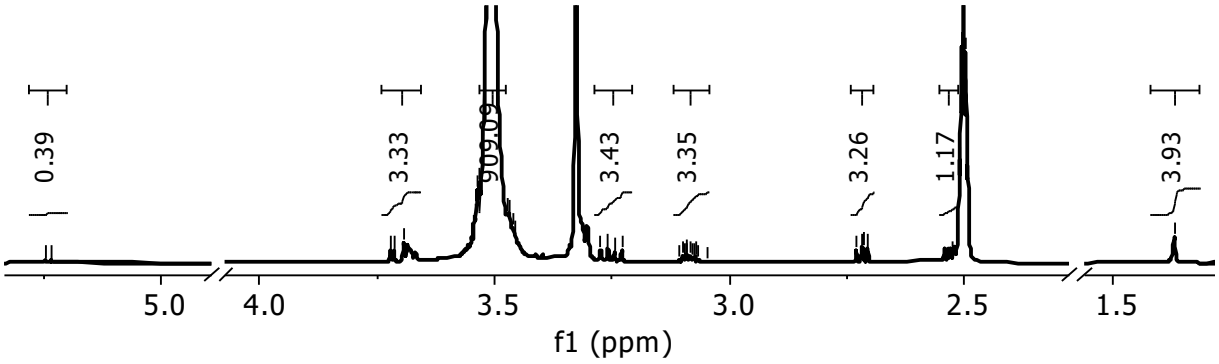

Figure S1. ^{1}H-NMR (DMSO-d$_6$, 400 MHz) 10K-Tetra-pEG-epoxide (**2**)

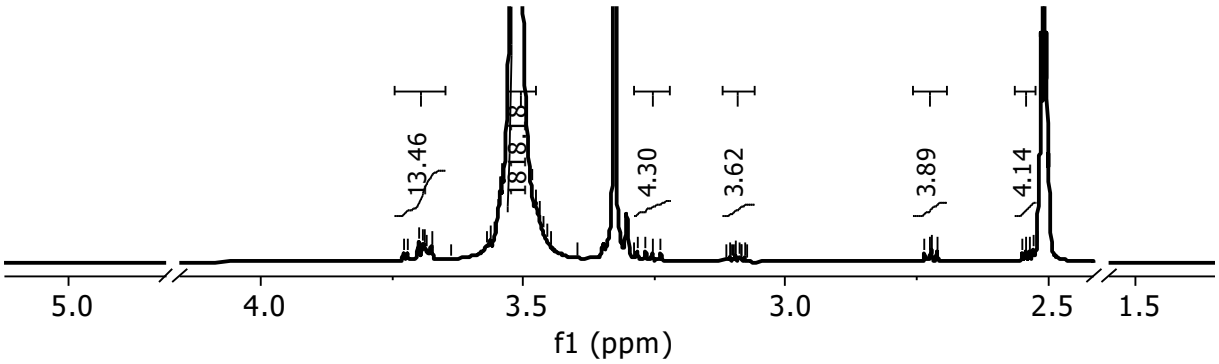

Figure S2. ^{1}H-NMR (DMSO-d$_6$, 400 MHz) 20K-Tetra-pEG-epoxide (**2**)

S1.2 Tetra-pEG-hydroxy-azide (3)

Table SII. Synthesis details of the tetra-pEG-hydroxy-azide (**3**)

		10K tetra-pEG-epoxide				20K tetra-pEG-epoxide			
	Mw [g mol^{-1}]	m [g]	V [mL]	n [mmol]	Eq.	m [g]	V [mL]	n [mmol]	Eq.
Tetra-pEG-epoxide (**2**)	-	10.63	-	1	1	11.79	-	0.58	1
Dimethyl-formamide	-	-	110	-	-	-	110	-	-
Sodium azide	65.01	2.77		42.65	42.65	1.54	-	23.7	41
Ammonium chloride	53.49	4.54	-	84.88	84.88	2.51	-	46.9	81

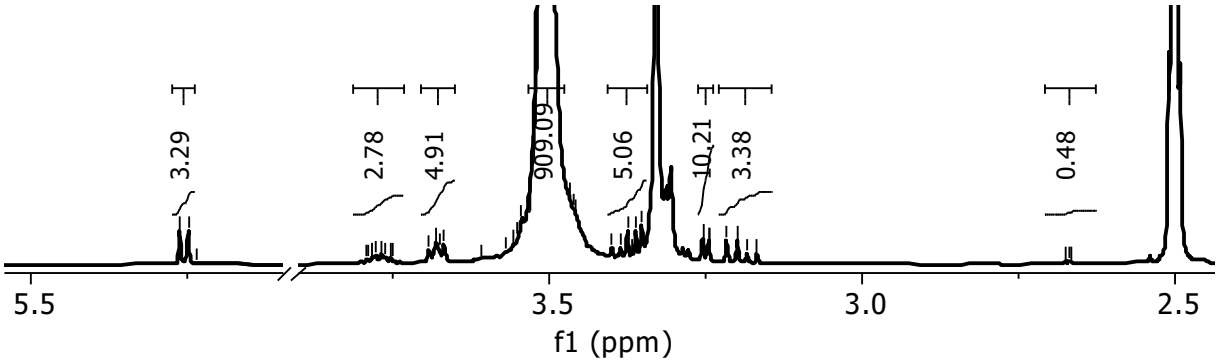

Figure S3. ^{1}H-NMR (DMSO-d$_6$, 400 MHz) 10K-Tetra-pEG-hydroxy-azide (**3**)

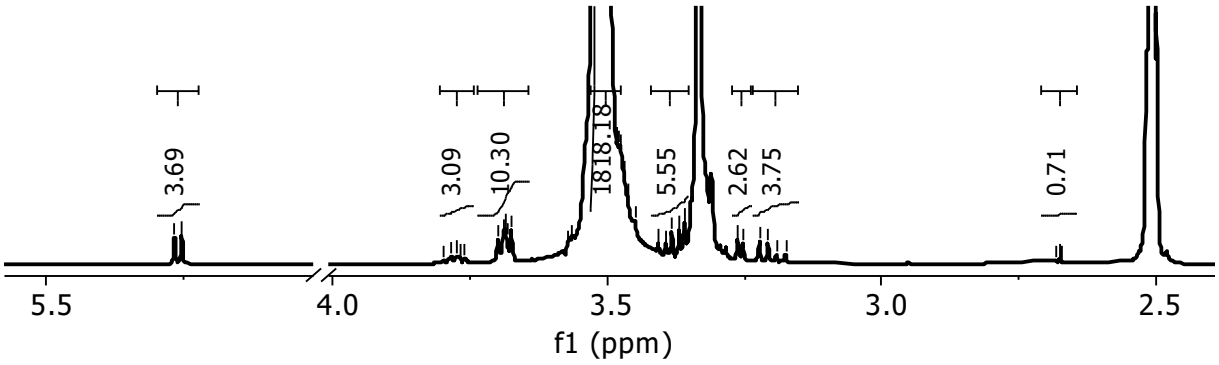

Figure S4. ^{1}H-NMR (DMSO-d$_6$, 400 MHz) 20K-Tetra-pEG-hydroxy-azide (**3**)

S1.3 Propargyl-terpyridine (6)

Table SIII. Synthesis details of the propargyl-terpyridine (**6**)

	Mw [g mol^{-1}]	m [g]	V [mL]	n [mmol]	Eq.
2,6-Bis(2-pyridyl)-4(1H)-pyridone (**4**)	249.27	5	-	20.05	1
Acetonitrile (dry)	-	-	200	-	-
Potassium carbonate	138.20	16.82	-	121.7	6
Propargyl bromide (**5**) (9.2 M in toluene)	118.98	-	2.7	22.7	1.13

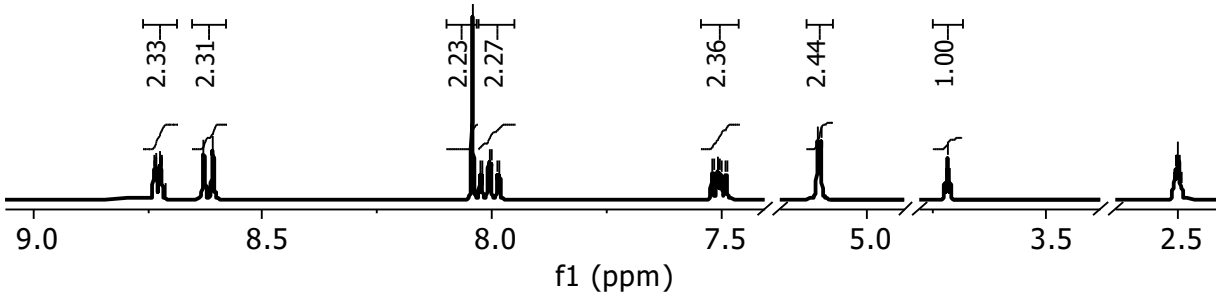

Figure S5. ^{1}H-NMR (DMSO-d_6, 400 MHz) Propargyl-terpyridine (**6**)

S1.4 Tetra-pEG-hydroxy-terpyridine (7)

Table SIV. Synthesis details of the tetra-pEG-hydroxy-terpyridine (**7**)

		10K tetra-pEG-hydroxy-azide				20K tetra-pEG-hydroxy-azide			
	Mw [g mol^{-1}]	m [g]	V [mL]	n [mmol]	Eq.	m [g]	V [mL]	n [mmol]	Eq.
Tetra-pEG-hydroxy-azide (**3**)	-	7.15	-	0.68	1	6.15	-	0.3	1
Propargyl terpyridine (**6**)	287.31	1.64	-	5.7	8.3	0.74	-	2.56	8.5

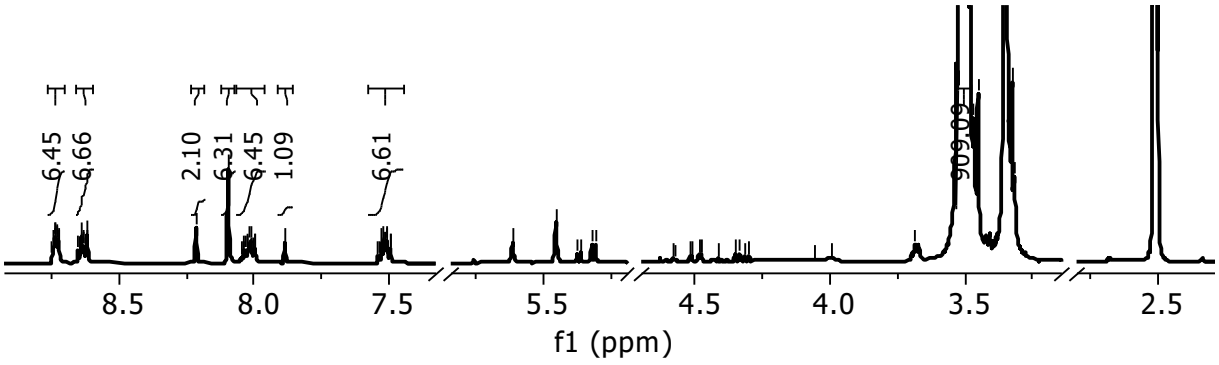

Figure S6. ^{1}H-NMR (DMSO-d_6, 400 MHz) 10K-Tetra-pEG-hydroxy-terpyridine (**7**)

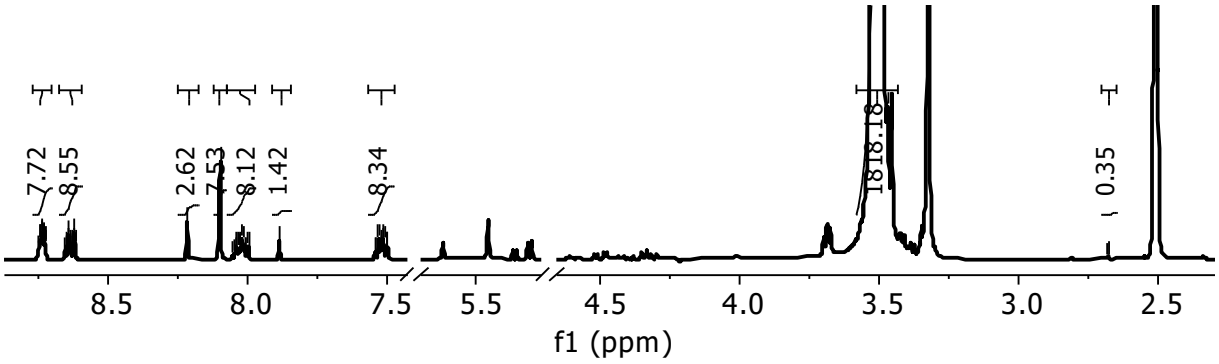

Figure S7. ^{1}H-NMR (DMSO-d_6, 400 MHz) 20K-Tetra-pEG-hydroxy-terpyridine (**7**)

S1.5 Tetra-pEG-*N*-hydroxysuccinimide-terpyridine (9)

Table SV. Synthesis details of the tetra-pEG-*N*-hydroxysuccinimide-terpyridine (**9**)

		10K tetra-pEG-hydroxy-terpyridine				20K tetra-pEG-hydroxy-terpyridine			
	Mw [g mol^{-1}]	m [g]	V [mL]	n [mmol]	Eq.	m [g]	V [mL]	n [mmol]	Eq.
Tetra-pEG-hydroxy-terpyridine (**7**)	-	6.2	-	0.53	1	6.11	-	0.28	1
N,*N*'-Disuccinimidyl-carbonate	256.17	1.1	-	4.29	8	0.61	-	2.37	8.4
4-(Dimethyl-amino)-pyridine	122.17	0.53	-	4.33	8.1	0.29	-	2.34	8.3
Dioxane (dry)	-	-	30	-	-	-	19.0	-	-
Acetone (dry)	-	-	10	-	-	-	10.4	-	-

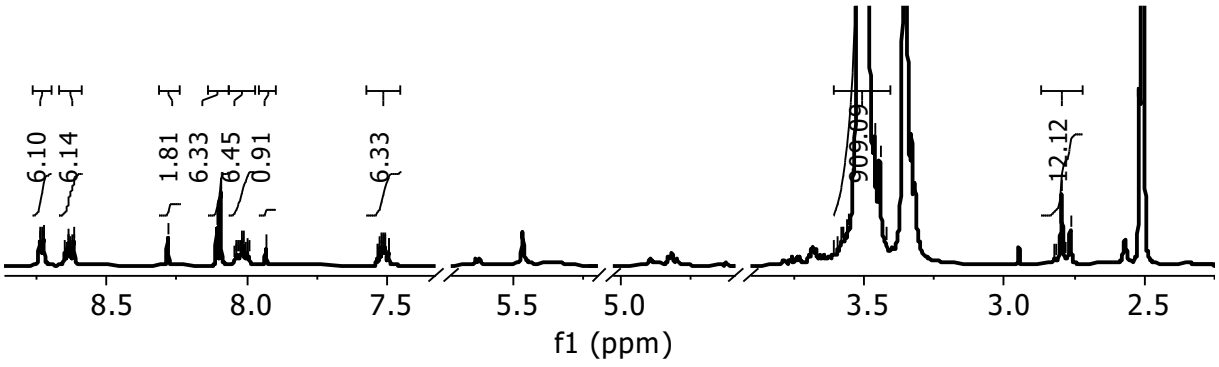

Figure S8. ^{1}H-NMR (DMSO-d_6, 400 MHz) 10K-Tetra-pEG-*N*-hydroxysuccinimide-terpyridine (**9**)

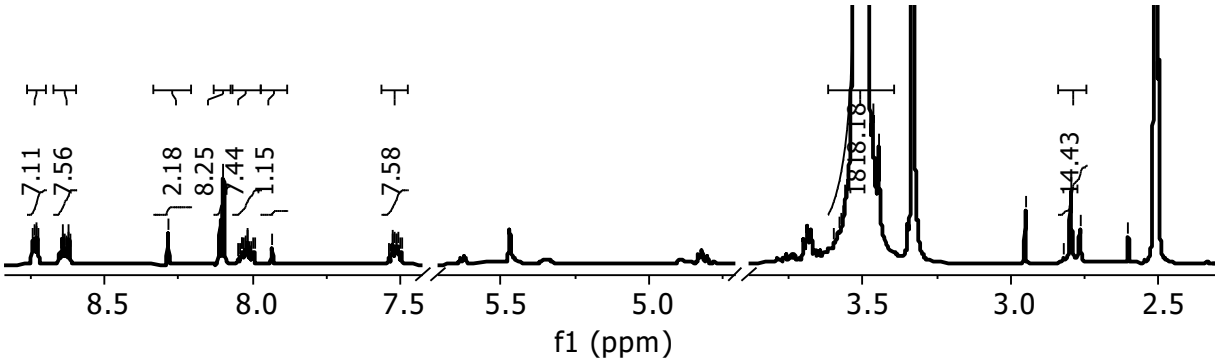

Figure S9. [1]H-NMR (DMSO-d_6, 400 MHz) 20K-Tetra-pEG-*N*-hydroxysuccinimide-terpyridine (**9**)

S1.6 Tetra-pEG-pNIPAAm-terpyridine (10)

Table SVI. Synthesis details of the tetra-pEG-pNIPAAm-terpyridine (**10**)

	1025			1055			2025		
	m [g]	n [mmol]	Eq.	m [g]	n [mmol]	Eq.	m [g]	n [mmol]	Eq.
Tetra-pEG-terpyridine-NHS 10K (**9**)	1.01	0.083	1	1.01	0.083	1	-	-	-
Tetra-pEG-terpyridine-NHS 20K (**9**)	-	-	-	-	-	-	1.01	0.045	1
NH_2-pNIPAAm 2.5 kg mol^{-1}	1.71	0.0684	8.2	-	-	-	1.01	0.408	9
NH_2-pNIPAAm 5.5 kg mol^{-1}	-	-	-	3.93	0.714	8.6	-	-	-
Phosphate buffer (pH 7)	100 mL			100 mL			100 mL		

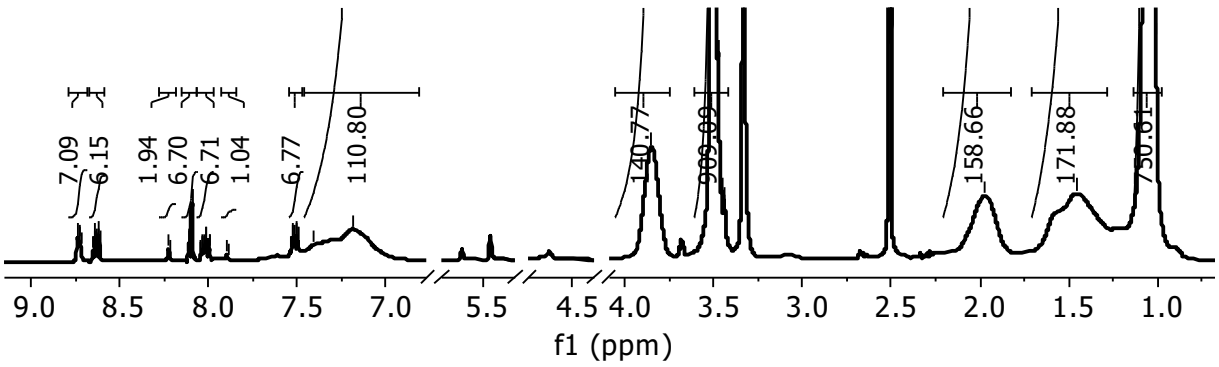

Figure S10. [1]H-NMR (DMSO-d6, 400 MHz) **1025**-Tetra-pEG-pNIPAAm-terpyridine (**10**)

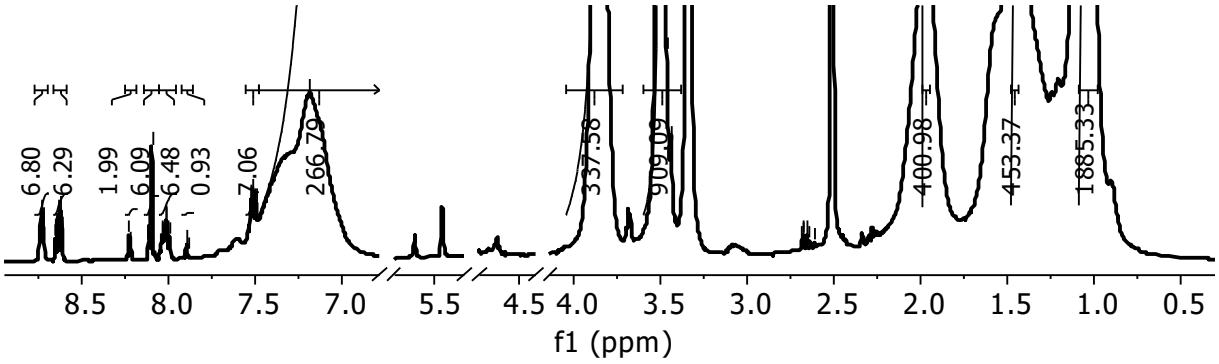

Figure S11. [1]H-NMR (DMSO-d6, 400 MHz) **1055**-Tetra-pEG-pNIPAAm-terpyridine (**10**)

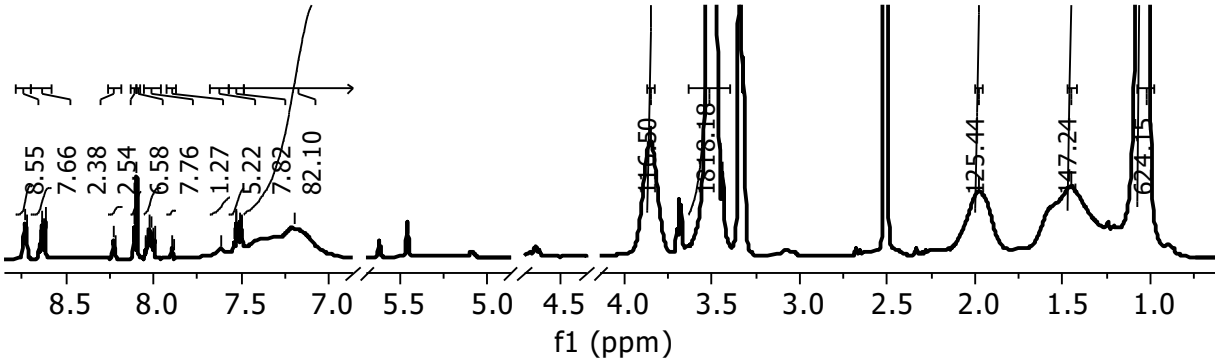

Figure S12. [1]H-NMR (DMSO-d6, 400 MHz) **2025**-Tetra-pEG-pNIPAAm-terpyridine (**10**)

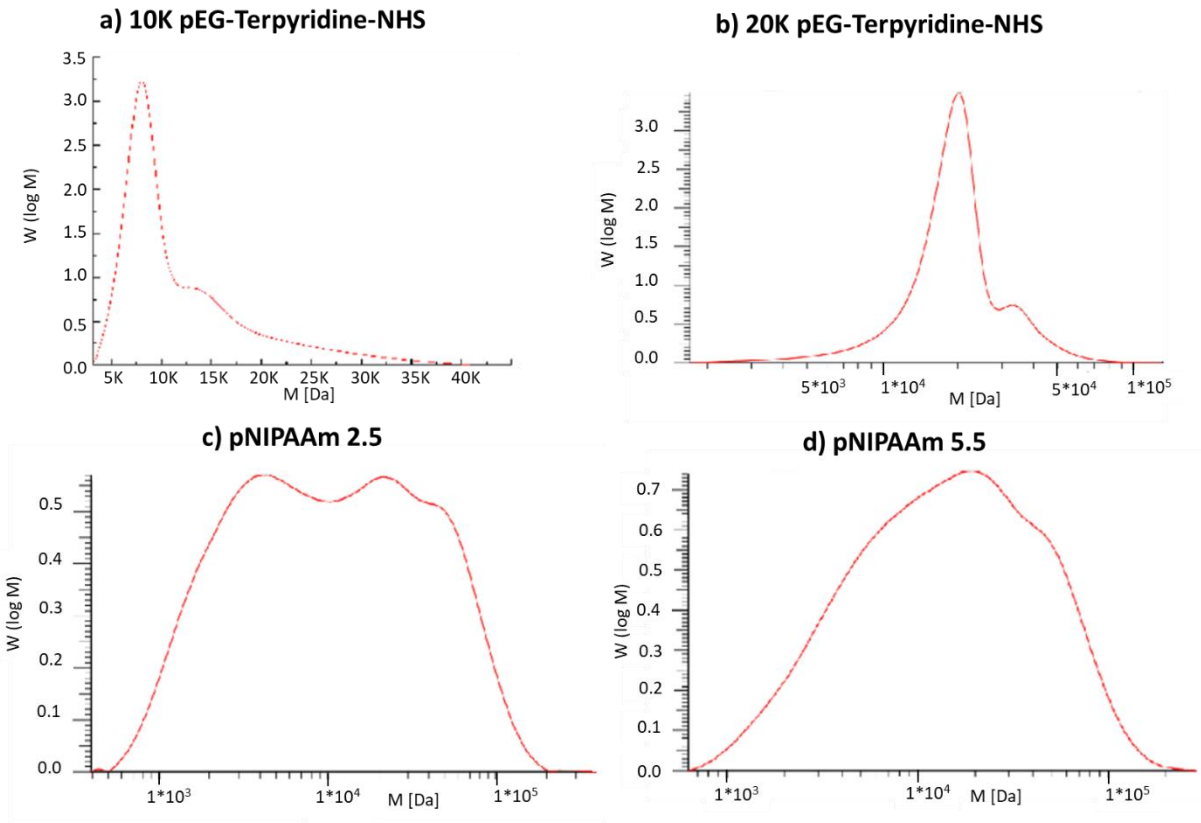

Figure S13. GPC results of the polymer building blocks

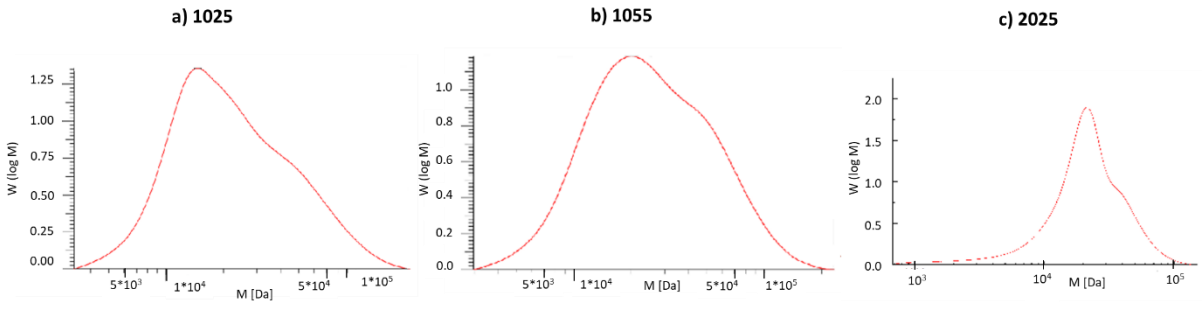

Figure S14. GPC results of the tetra-pEG-terpyridine-pNIPAAm dual dynamic networks

References

[1] Nicolella P., Lauxen D., Ahmadi M., and Seiffert S., "Reversible Hydrogels with Switchable Diffusive Permeability," Macromol. Chem. Phys., 222, 2100076, (**2021**).

10.3 Appendix Chapter 5

Supplementary Information

Defect-controlled softness, diffusive permeability, and mesh-topology of metallo-supramolecular hydrogels

***Paola Nicolella**, Martha Franziska Koziol, Lucas Löser, Kay Saalwächter, Mostafa Ahmadi, and Sebastian Seiffert*

Soft Matter, 2022, 18, 1071-1081 (DOI: D1SM01456K)

Materials

Four-arm hydroxy-terminated poly(ethylene glycol) (pEG), M_w = 20 kg mol^{-1}, further denoted as 4-arm 20K, and 8-arm hydroxy-terminated pEG, M_w = 40 kg mol^{-1}, denoted as 8-arm 40K, were purchased from Creative PEG Works (NC, USA), and re-precipitated in cold diethyl ether before further use. Potassium hydroxide (KOH) flakes (90%) and 4'-Chloro-2,2':6',2''-terpyridine (99%) were purchased from Sigma Aldrich. Extra dry dimethyl sulfoxide (DMSO, + 99.7% over molecular sieve) is purchased from Acros Organics. Sodium chloride (NaCl, ≥ 99.5%), dichloromethane (DCM, ≥ 99.8%), and diethyl ether (≥ 99.5%) were purchased from Fisher Scientific. Zinc nitrate hexahydrate (98%) is purchased from Alfa Aesar.

Syntheses

Terpyridine-functionalized 4-arm and 8-arm polymer precursors.

The hydroxyl termini of the star-shaped pEG polymers were converted to terpyridine units by the following Williamson type ether synthesis (**SI1**).

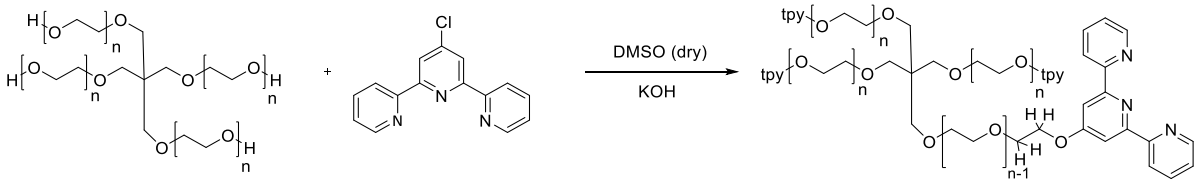

Figure SI1. Reaction route for the synthesis of tetra-arm pEG-terpyridine. The functionalization of 8-arm pEG-terpyridine is analogous.

Before use, the pEG was purified and therefore melted at 60 °C, cooled to 40 °C, dissolved in DCM, precipitated in diethyl ether, and dried under vacuum. KOH (0.056 g, $1 \cdot 10^{-3}$ mol, 20 eq.) was dried in a flask for 1 h under reduced pressure, and dry DMSO (20 mL) was added in inert N_2-atmosphere. To this suspension, 4-arm pEG (M_w = 20 kg mol^{-1}, 1 g, $5 \cdot 10^{-5}$ mol, 1 eq.) was added. The reaction mixture was stirred under nitrogen counter flow at 60 °C for 1 h. Afterwards, 4'-Chloro-2,2':6',2''-terpyridine (0.1340 g, $5 \cdot 10^{-4}$ mol, 10 eq.) was added, and the reaction was stirred at 60 °C for another 48 h. After cooling to room temperature, the reaction mixture was add-ed dropwise to cold water (200 mL) and a small amount of white precipitate was filtered off. To the liquid phase, brine (200 mL) was added, and

the aqueous solution was washed three times with DCM (200 mL). The organic phases were collected, dried with sodium sulphate, and concentrated under vacuum. Afterwards, the polymer was precipitated in ice-cold diethyl ether (500 mL). The white powder was collected and dried under vacuum overnight. The same reaction conditions were applied to functionalize the 8-arm 40K pEG-OH, but the reaction was performed twice to achieve a high degree of terpyridine functionalization. The degree of functionalization of terpyridine was quantified by NMR and was found to be 95% (4-arm 20K) and 90% (8-arm 40K), respectively (**SI2-SI3**).

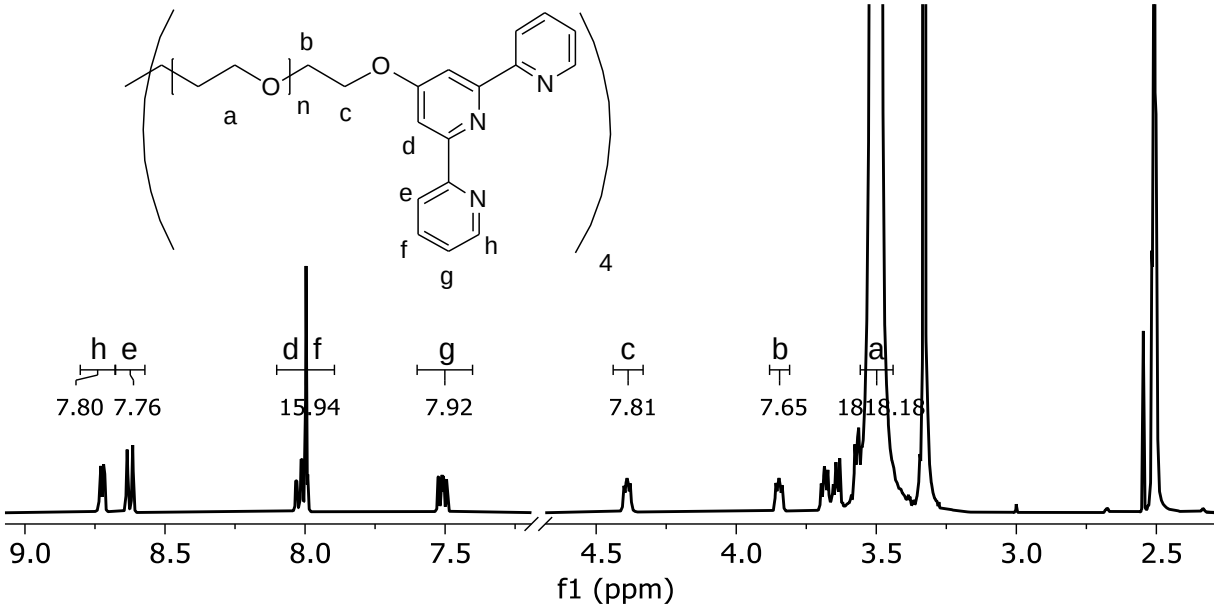

Figure SI2. [1]H-NMR of the 4-arm pEG-terpyridine (20K) in DMSO.

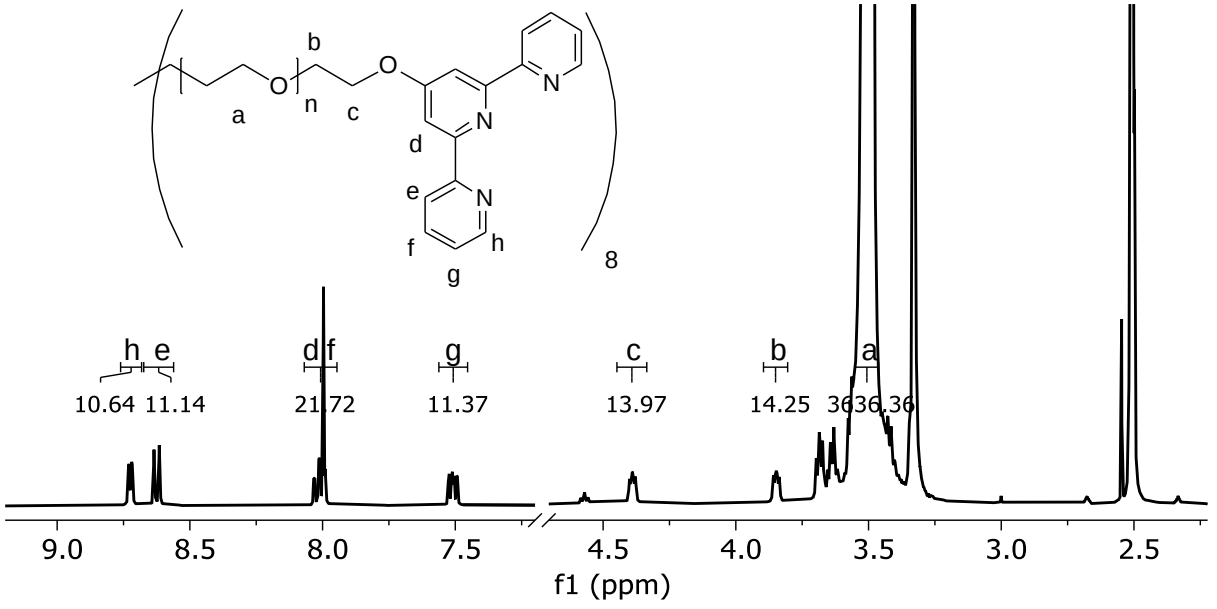

Figure SI3. [1]H-NMR of the 8-arm pEG-terpyridine (40K) in DMSO.

Fluorescence-labelled polymer tracer for FRAP measurements.

To measure polymer self-diffusion coefficients by FRAP experiments, a fluorescently active dye molecule has to be attached to the polymer building blocks of interest. In addition to that, it is of major importance that the dye-labelled 4-arm polymers quantitatively contain terpyridine end-groups on each arm. These polymer tracers were synthesized according to a previously described procedure [1] and are visualized in **SI4**. In summary, hydroxy-terminated tetra-arm pEG-OH with a molar mass of 20 kg mol^{-1} was reacted with epichlorohydrin to obtain epoxy-terminated polymers. The subsequent ring-opening with sodium azide yielded in hydroxyl-azide-pEG that further reacted with propargyl-terpyridine in a copper-free Huisgen click reaction. The remaining hydroxyl groups were activated via reaction with p-nitrophenylchloroformate and through addition of (S)-(+)-4-(3-aminopyrrolidino)-7-nitrobenzofurazan (NBD), the final fluorescence-labelled tracer polymers were obtained. Unreacted excess dye was removed via size exclusion chromatography in methanol using a Sephadex™ LH-20 column. The degree of terpyridine functionalization was determined by NMR to be 89% (**SI5**).

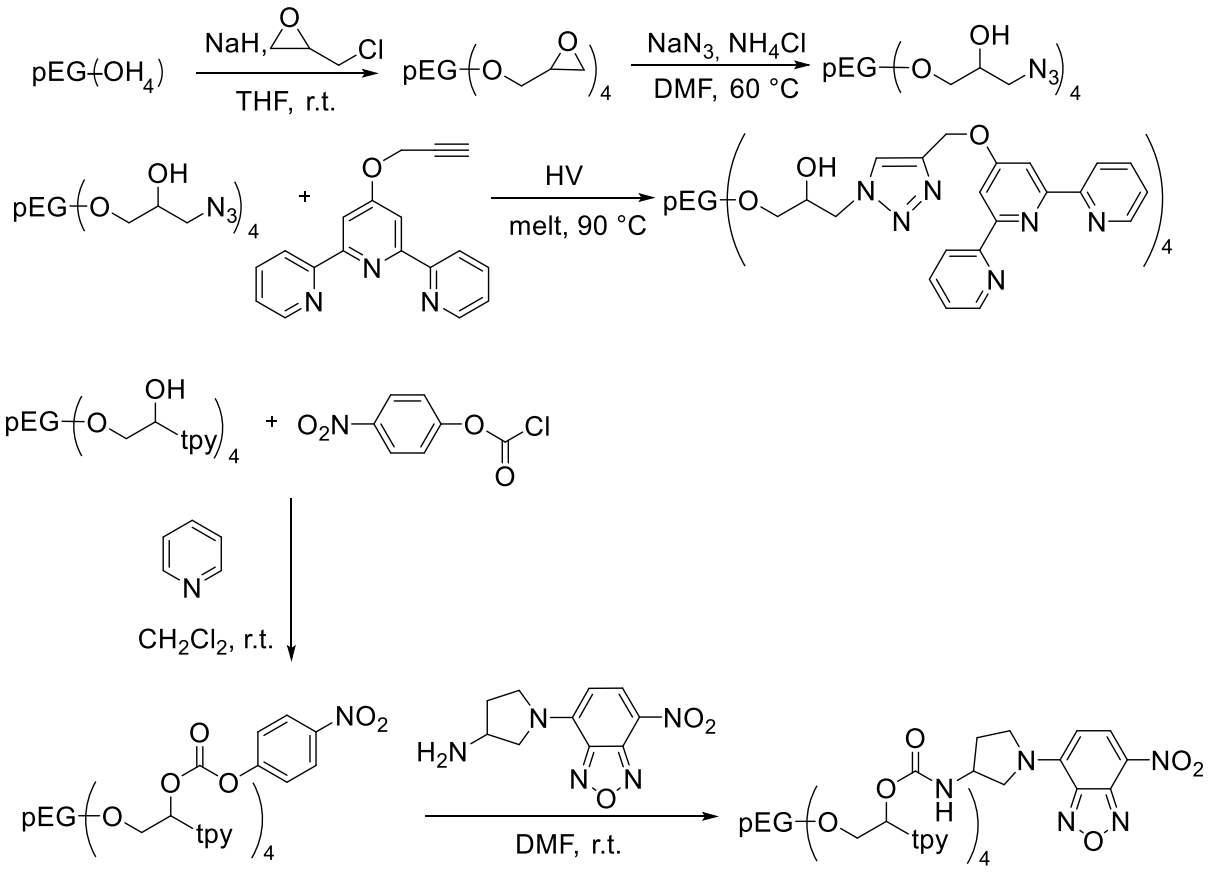

Figure SI4. Reaction route for the dye-labelled tetra-arm pEG-terpyridine (20K) tracer molecules.

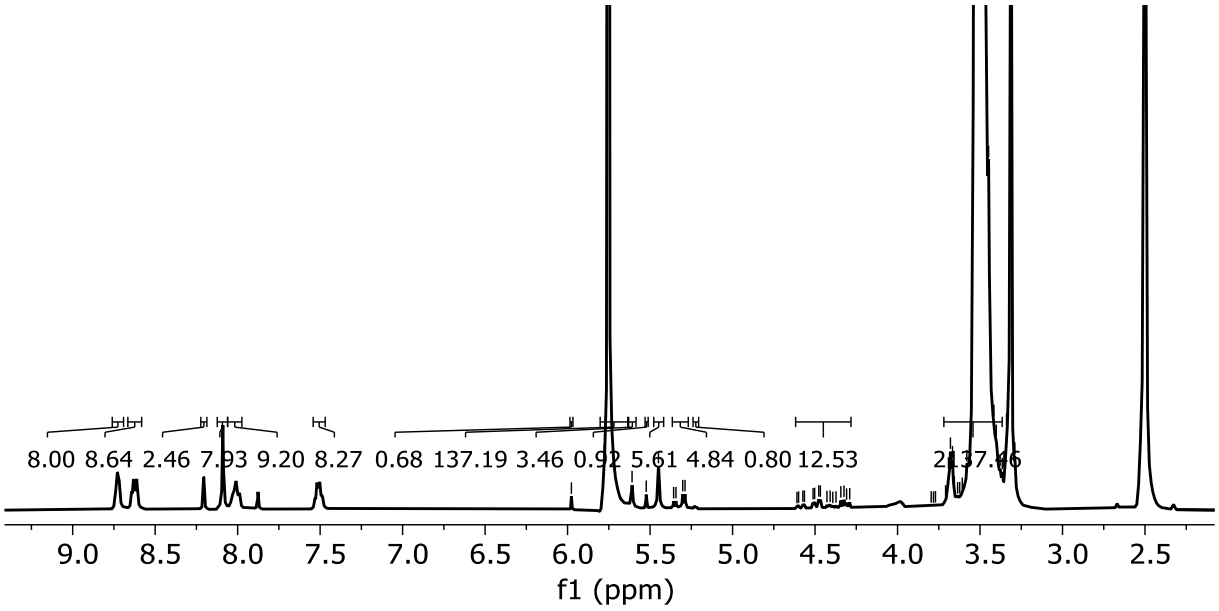

Figure SI5. ^{1}H-NMR of the 4-arm pEG-terpyridine (20K) tracer molecules in DMSO.

References

[1] S. Tang, A. Habicht, S. Li, S. Seiffert and B. D. Olsen, Macromolecules, 2016, 49, 5599–5608.